Louisiana State University
LSU Digital Commons

LSU Doctoral Dissertations | Graduate School

2007

Mass transfer and evolution of compact binary stars

Vayujeet Gokhale
Louisiana State University and Agricultural and Mechanical College, gokhale@phys.lsu.edu

Follow this and additional works at: https://digitalcommons.lsu.edu/gradschool_dissertations

 Part of the Physical Sciences and Mathematics Commons

Recommended Citation
Gokhale, Vayujeet, "Mass transfer and evolution of compact binary stars" (2007). *LSU Doctoral Dissertations*. 2969.
https://digitalcommons.lsu.edu/gradschool_dissertations/2969

This Dissertation is brought to you for free and open access by the Graduate School at LSU Digital Commons. It has been accepted for inclusion in LSU Doctoral Dissertations by an authorized graduate school editor of LSU Digital Commons. For more information, please contactgradetd@lsu.edu.

MASS TRANSFER AND EVOLUTION OF COMPACT BINARY STARS

A Dissertation

Submitted to the Graduate Faculty of the
Louisiana State University and
Agricultural and Mechanical College
in partial fulfillment of the
requirements for the degree of
Doctor of Philosophy

in

The Department of Physics and Astronomy

by
Vayujeet Gokhale
BSc, Bombay University, 1996
M.S., Bombay University, 1998
May 2007

Acknowledgments

I would like to thank my thesis advisor Juhan Frank for his continual support and guidance. I am particularly grateful to him for his patience and understanding. I also would like to thank Joel Tohline for his probing questions and insightful discussions.

I would like to acknowledge and express my gratitude for the positive atmosphere at the physics and astronomy department at LSU by thanking the faculty and staff, in particular Rob Hynes, Brad Schaeffer, Geoff Clayton, Amy Campbell and Arlo Landolt – who has been kind enough to let me increase the entropy in his library by letting me have my office there. Among the staff I would like to acknowledge the ever helpful Arnell Dangerfield, Ophelia Dudley, Beverly Rodriguez and others at the department office. I also would like to appreciate the staff and members of the Highland Road Park Observatory in Baton Rouge for letting me use their wonderful facility – I have spent many a wonderful, clear nights peering through the telescope and taking beautiful pictures.

I would like to thank my colleagues, in particular Mario D'Souza (who also had the misfortune of being my room-mate), Karly Pitman, Ravi Kopparappu, Xiaomeng Peng, Patrick Motl and Shangli Ou. Thanks also to Horst Beyer and Dimitry Uskov for endless sessions of ping-pong and fun – thanks to them I am a much better player now.

I would also like to express my gratitude towards my professors and colleagues with whom I had the privilege of working before I came to LSU. In particular I am indebted to D.C.V. Mallick of the Indian Institute of Astrophysics, Bangalore for truly setting me on an academic path that has brought me this far. I would like to thank Subir Bhattacharya and Sunder Sahayanathan for making me feel at home at the NRL, BARC.

Most of all I would like to thank Manavi Jadhav for not only tolerating me through the years, but for helping me become a better person and without whom, I am lost. Finally, I would like to thank my parents for their support and upbringing. Nothing would have been possible without them.

Table of Contents

List of Tables

List of Figures

Abstract

We present a study of key aspects of the evolution of binary stars with emphasis on binaries consisting of two white dwarf stars. The evolution of such systems is driven by the loss of angular momentum by gravitational wave radiation. Effects like mass transfer and other modes of angular momentum loss and redistribution influence the evolutionary fate of the binary, and can lead to a merger, the tidal disruption of one of the components or its survival as a long-lived AM Canum Venaticorum (AM CVn) type system. Our study takes into account some of these effects; like mass loss, tides, accretion disk formation and direct impact accretion. We find that under some circumstances, the tidal coupling between the spin of the components and the orbit of the binary leads to oscillations in the orbital separation and the mass transfer rate. We also find that as compared to previous studies, a larger fraction of the systems should survive to form AM CVn type systems. We also consider systems in which the mass transfer rate exceeds the critical Eddington rate, leading to mass loss from the system. It is possible that some of the lost mass settles into a disk around the binary to form a circumbinary disk. In the second part of the thesis, we present a toy model for disks in general, and find that the coupling of such a circumbinary disk to the binary has a destabilizing effect on the binary.

Part I: Evolution of Compact Binaries

1. Introduction

1.1 Historical Background

It is now a well known fact that most of the stars in the solar neighborhood are in fact, multiple stars, most of which are binary stars (Kallrath & Milone, 1999). That the 'stars' we observe in the night sky are not always single stars like our Sun has been known for a long time – Father Giovanni Baptista Riccioli being the first to realize on observing ζ Ursae Maioris (Mizar) that in fact it was a 'double star' in 1669. Most of the early discoveries of 'double stars' were serendipitous with no attempt made to explain the proximity of the two components, and it was not until the year 1767 that the Reverend John Michell proposed that these curious objects were indeed objects held together by their mutual gravitation (Kopal, 1977). Despite (or probably due to) his initial skepticism, it was William Herschel who embarked on generating a systematic catalogue of the 'double stars' in 1782 and 1785 which led to further strengthening of the statistical argument that the observed frequency of the 'double stars' far exceeded the chance association of stars uniformly distributed in space. Around the same time, Goodricke identified Algol as (what we would today call) an eclipsing binary in order to explain its periodic changes in brightness. Finally in 1889, Vogel laid to rest any doubts about the true binary nature of Algol (and many other 'double stars' by extension) by identifying it as a spectroscopic binary.

Unlike the pioneering days of Herschel when the theoreticians anticipated the properties of the 'double stars' based primarily on geometry and the laws of gravitation, the trend now has been of new observations leading the way and having theoreticians come up with models to explain the observations. The advent and development of higher power telescopes and light collecting apparatus has revealed a rich diversity in the observational properties of these objects and has led to an equally rich field in modelling the formation and evolution of different classes of binary stars.

1.2 Importance of Binary Systems in Astrophysics

Before we proceed with our study of binary evolution, it is appropriate to underscore the importance of binary systems to astrophysics. By design, binary systems reveal more about themselves than single stars do; like the masses, the radii and the orbital separation. This is especially true in the case of eclipsing binaries, which are binaries for whom our line of sight happens to be in the orbital plane of the binary. Moreover, each component in the binary can be at different stages of its evolution, which itself can be influenced by the presence of the companion as is the case in

interacting binaries. All this information is critical in providing constraints and observational checks on theoretical models of stellar structure and evolution (See Shore et al. (1992) for an excellent overview of the interplay between observations and theory of binary stars).

The sheer richness of the different classes of binaries, and the fact that these objects reveal much information about themselves, in itself, makes binary systems worth studying. Binaries can be classified on the basis of their component stars, for example: Cataclysmic Variables (CVs, main sequence + white dwarf), Low Mass X-Ray Binary (LMXB, main sequence + neutron star/black hole), Algols (main sequence or subgiant pair), RS Canum Venaticorum & BY Draconis stars (F-type stars with strong magnetic activity) and so on (Carroll & Ostlie, 1996). Each of these classes provides unique opportunities for study of stars, sometimes in extreme environments not reproducible in terrestrial laboratories.

Most of the objects and classes listed above, apart from being binary systems also undergo mass transfer at some stage in their evolution. Accretion due to Roche lobe overflow is one of the most important phenomena in stellar astrophysics (Frank et al., 2002)– it alters the fate of the binary systems and results in a dizzying array of observational effects, which help us observe these objects in the first place. An inevitable consequence of accretion is the formation of an accretion disk around the accreting star, unless the accretion stream impacts the surface of the accreting star (see below). Accretion disks are a common phenomena in astrophysics. They are found not only in binary stars, but also in protoplanetary disks and active galactic nuclei (AGN) as well. A large fraction of the effort in understanding astrophysical objects and the corresponding observations entails accretion disk modeling. Since binaries are the most accessible of all objects that contain accretion disks, disks in binaries are of utmost importance to astrophysicists.

Compact binaries (Section 1.4), on the other hand, are useful targets to test the predictions of general relativity. As we shall see later, compact binaries like double white dwarfs (DWDs), AM CVns, and neutron star binaries profusely radiate gravitational wave radiation (GWR), which can be detected by gravitational wave detectors like LIGO (Laser Interferometer Gravitational-Wave Observatory, Abbott et al. (2005)) and LISA (Laser Interferometer Space Antenna, Bender (1998)). The Hulse-Taylor pulsar, PSR 1913+16 (Hulse & Taylor, 1975), provides striking indirect evidence of the same – the rate of orbital decay in this system exactly matches the predicted rate of angular momentum loss by GWR in the quadrupole approximation. With the advent of highly sensitive GWR detectors, modeling of such compact binary systems and their populations has attracted much attention (Nelemans (2001a, b, c)). For efficient detection, one needs accurate templates of the gravitational wave strain and frequency for these systems (Section 5.4).

1.3 The Roche Potential

Binary systems can be classified according to the type of their constituent stars or their observational properties; for example as CVs, LMXBs, and HMXBs and

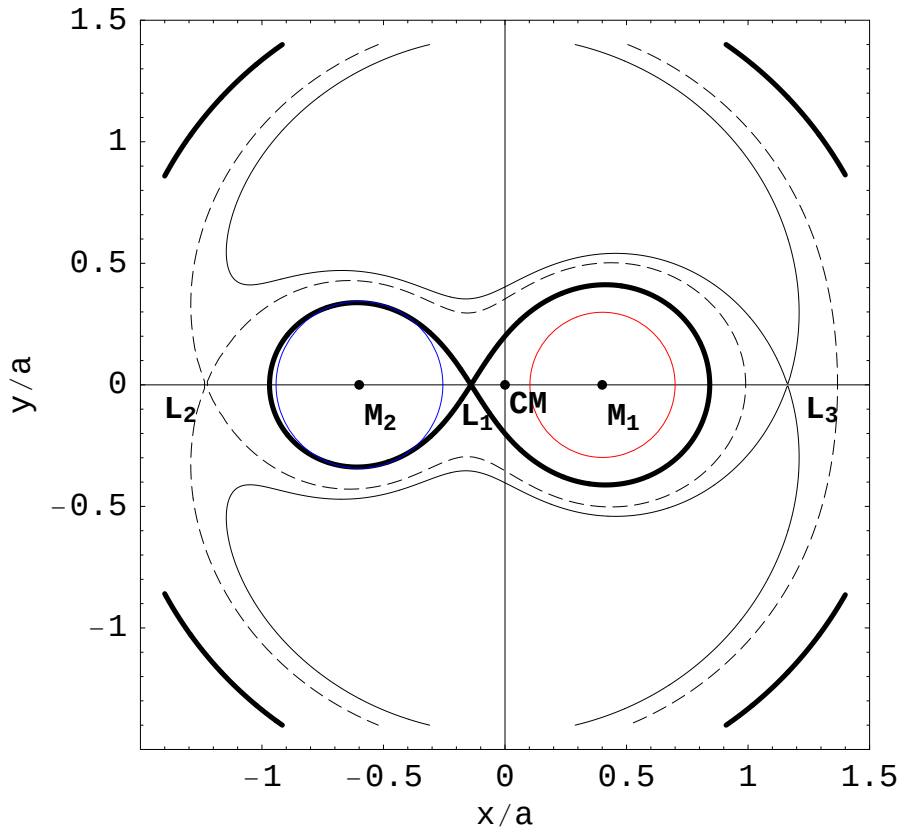

FIGURE 1.1. The Roche equipotentials in the equatorial plane for a mass ratio $q = 2/3$. The Lagrangian points L_1, L_2 & L_3 are also shown along with the center of mass of the system and the centers of the two components. The contours represent equipotential surfaces associated with the Lagrange points. The contour corresponding to the L_1 point is shown in bold, whilst the contour passing through L_2 is shown as a dashed line.

so on (see above). However, we are interested in a more theoretical approach to classifying binaries. In order to do this, we introduce here, the concept of the Roche potential which leads us to a way of classifying binary stars on the basis of their dynamic properties. The French mathematician Edouard Roche introduced a model for stellar configurations as a limiting case of binary objects whose components are centrally condensed. As it turns out, this is quite a good approximation for most stars. Kopal (1955) introduced the concept of Roche potential and Roche equipotential surfaces. In the co-rotating reference frame, for synchronously rotating binary stars with components with masses M_2 and M_2 at r_1 and r_2 respectively, one can write the Roche potential as

$$\Phi(\vec{\mathrm{r}}) = -\frac{GM_1}{|\vec{\mathrm{r}} - \vec{\mathrm{r}_1}|} - \frac{GM_2}{|\vec{\mathrm{r}} - \vec{\mathrm{r}_2}|} - \frac{1}{2}(\vec{\Omega} \times \vec{\mathrm{r}})^2 \tag{1.1}$$

Here, $\Omega = \left(GM/a^3\right)^{1/2}$ is the angular velocity of the binary, pointed perpendicular to the plane of rotation. 'a' is the separation, and 'M' is the total mass of the system. In Fig. 1.1, we plot the equipotential contours in the equatorial plane for the

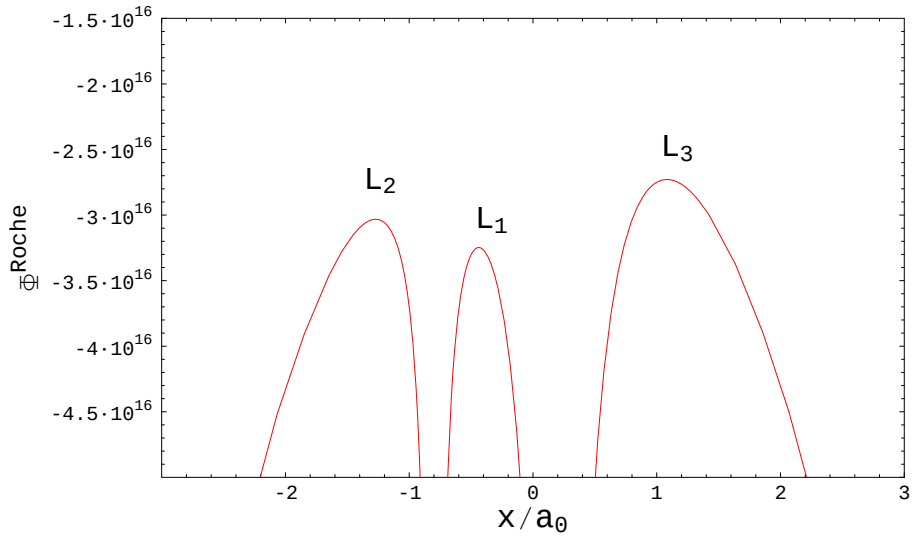

FIGURE 1.2. Roche Potential along the line of centers. The x-axis is normalized to the separation a_0.

Roche potential. At large distances from the binary ($r >> a$), the equipotentials are similar to a point mass of total mass M. Also close to the centers of the component stars, we have spherical contours resulting from the strong gravitational potential of the highly condensed (point mass) stars with minimal perturbations from the other component. The overall shape of the equipotentials is a function of the mass ratio $q = M_2/M_1$ whilst the scale is governed by the binary separation a. The equipotential of most significance is the 8-shaped potential contour (shown in bold in Fig. 1.1) which constitutes a dumbbell shaped *critical surface* for each component – it is called the "Roche lobe" of a given component. The dumbbell is joined at a saddle point (see Fig. 1.2) known as the *inner Lagrange point* L_1. The material within the Roche lobe of each component is bound to that component though it is influenced by the tides generated by the other component. Around the critical L_1 point, the material inside one of the lobes can flow freely onto the other side. This is indeed what happens when one of the stars is big enough to fill up its Roche lobe. As long as the star is within its Roche lobe, hydrostatic equilibrium can be maintained for either component. As soon as one of the components fills up its Roche lobe, material leaks through the L_1 point onto the other side in a phenomenon called Roche Lobe Overflow (RLOF). Two other extremal points lie along the line joining the centers of the two components and the center of mass (CoM) – L_2 (near the less massive component) and L_3 (near the more massive component), which are also points of unstable equilibrium. The equipotential surface corresponding to the L_2 point (shown as dotted contour in Fig. 1.1) is sometimes referred to as the *outer critical surface*. We are now in a position to classify binary stars based on how the components fill up their respective Roche lobes:

1. Detached binary: In these systems, neither of the two components fills up its Roche lobe.

2. Semi-detached binary: In this case, one of the stars fills up its Roche lobe and transfers mass to the other component via RLOF.

3. Contact binary: Both components fill up their respective Roche lobes, and can extend up to a level between the inner and outer critical surfaces (Fig. 1.1).

A given system can evolve from one of these classes to the other – for example, a detached binary can become a semi-detached binary as one of the components comes into contact by loss of orbital angular momentum. Similarly during the course of its evolution a system may become a contact binary after going through a phase of being semi-detached.

In this work, we will primarily be concerned with semi-detached binaries. Many interesting binaries fall into this category – Cataclysmic binaries, AM CVn binaries, Algol-type binaries, Low and High Mass X-ray Binaries (LMXB, HMXB) to name a few. Most of these objects involve one component filling its Roche lobe (the **donor** or secondary), transferring mass to a compact star (the **accretor** or primary). Another interesting facet to this is that the mass leaking out of the L_1 point forms an *accretion disk* around the accretor in most cases, and we shall deal with accretion disk theory in detail in Chapter 6. For now we continue with categorizing different types of binaries on the basis of its geometric or dynamic properties. An individual star evolves as time goes along and usually it expands – from the main sequence to the red giant branch and then off to the asymptotic giant branch. Now, if a star is a member of a binary star system, then it is possible that as the components evolve, one of them (or both) can fill up its Roche lobe. Kippenhahn and Weigert (1967) classify mass transferring binaries on the basis of what state of evolution the donor is in as follows:

- Case A : A normal main-sequence star fills up its Roche lobe as it gradually evolves over the extremely long timescale of nuclear evolution.

- Case B: Mass transfer occurs when the star evolves off the main sequence onto the red giant branch.

- Case C : The donor can fill up its Roche lobe only after expanding sufficiently which occurs when it evolves off to the Asymptotic giant branch.

Another mechanism by which a detached binary can become a semi-detached binary is by losing angular momentum, which results in the shrinking of the orbit, which in turn results in the shrinking of the Roche lobe. As we shall see later, two stars in orbit around one another emit gravitational wave radiation (GWR), which carries with it a small amount of angular momentum. Thus, even if the radii of the component stars are not changing, the respective Roche lobes can gradually shrink until the Roche lobe radius of one of the stars equals its radius, and mass transfer can commence. This is exactly what happens in compact binaries, which we study next.

1.4 Compact Binaries

A binary consisting of two main sequence stars does not remain so forever. If the binary separation is high, one of the stars (the more massive star) will eventually evolve off the main sequence and fill up its Roche lobe to trigger mass transfer to the less massive star. A variety of outcomes await such a binary, depending mostly on the total mass of the system (M), the mass ratio (q) and the separation (a) of the binary (Iben & Tutukov, 1984). We summarize one of these possibilities to illustrate the general outline of this mechanism in which massive, wide, main sequence binaries evolve to low mass, compact, degenerate binaries. In Fig. 1.3, we depict the evolution of a 3.2 $M_{\odot}$ - 3.8 $M_{\odot}$ main sequence binary with an orbital period $P \sim$ a few days to 1 yr. The more massive component evolves to fill up and extend beyond its Roche lobe, which leads to the formation of what is called a 'common envelope'. This is the phase in which the cores of the two components orbit within the expanding envelope of the more massive star. This results in significant mass and angular momentum loss from the system[1]; the first helium white dwarf is formed, and the orbital period decreases to $\lesssim$ 30 days. Eventually the other main sequence star also evolves off the main sequence and another common envelope phase ensues. Mass and angular momentum are again lost from the system, and the degenerate helium core of the latter star is exposed. Thus we are left with a compact binary ($P \sim$ 10 mins - 1 hr) with degenerate components. As mentioned earlier, other combinations of masses and separations lead to different outcomes, such as binaries with components made up of Carbon-Oxygen (CO), Oxygen-Neon-Magnesium (ONeMg) and so on.

In any case, once a compact binary is formed as a result of common envelope evolution, the emission of gravitational wave radiation (GWR) becomes highly efficient, which carries a small but significant amount of angular momentum with it (Landau & Lifshitz, 1975). Loss of angular momentum drives the system closer, which in turn results in the shrinking of the Roche lobe (see Chapter 2) which gradually contracts onto the star. This again, can lead to mass transfer.

AM CVn systems are white dwarf - white dwarf binaries undergoing mass transfer and are objects of particular interest because a) they are observable by traditional observational means since they are undergoing mass transfer and, b) they are the only guaranteed sources of GWR for the space-based gravity wave detector LISA (Laser Interferometer Space Antenna, Bender (1998)). AM CVn systems are a particular sub-class of the wider class of binaries known as Degenerate White Dwarf (DWD, also Double White Dwarf) binaries. They have extremely short periods (a few minutes to an hour) and their spectra are dominated by helium emission lines. Apart from the mechanism outlined above, a number of other theories have been proposed for the formation of the DWD population in the Galaxy: for example, see Iben & Tutukov (1986), Tutukov & Yungelson (1994) and Han (1998).

[1]The exact physical mechanism by which the common envelope achieves this is not accurately known, though traditionally it is widely believed that the common envelope phase does result in loss of angular momentum and mass from the system.

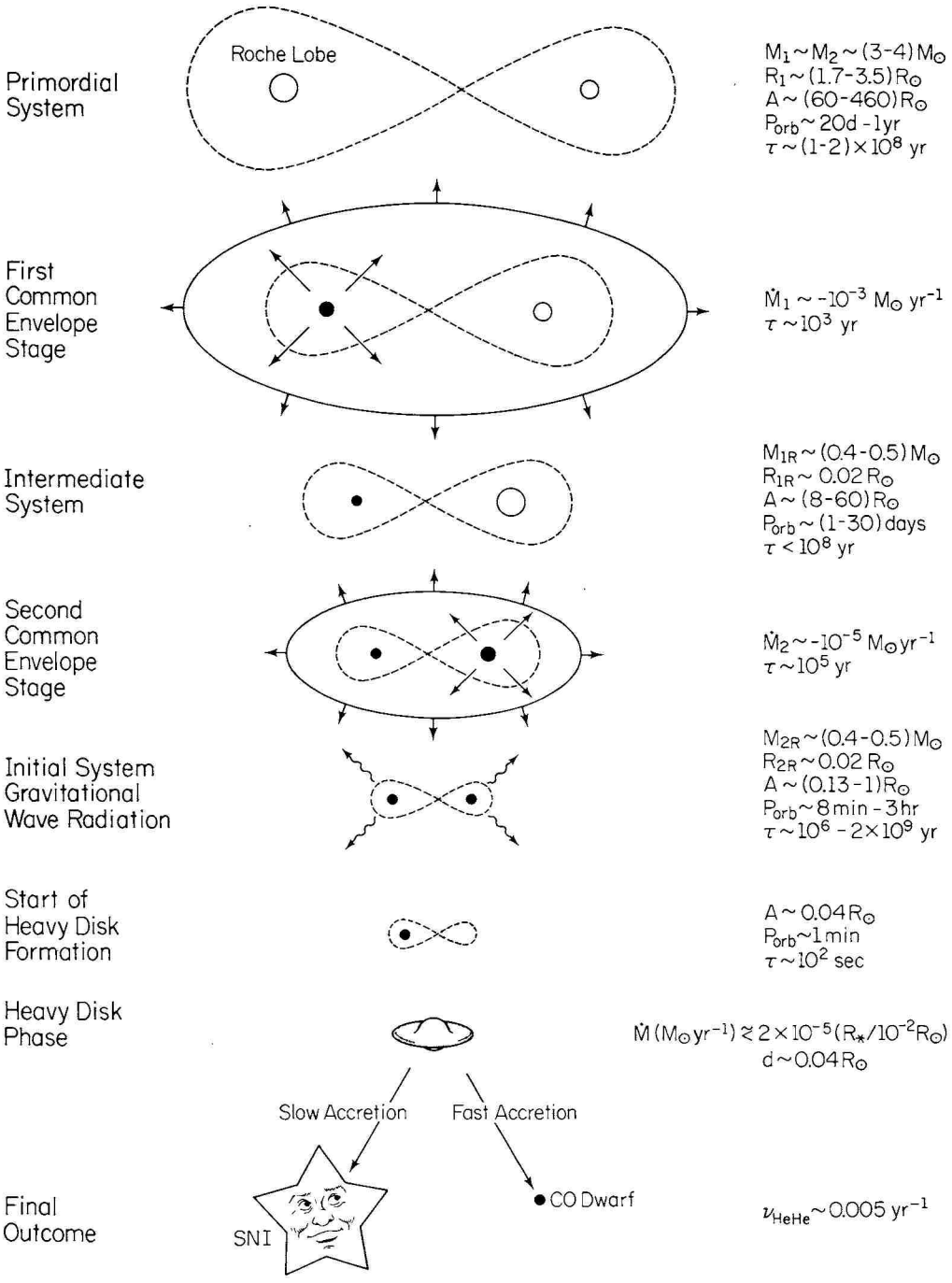

FIGURE 1.3. Formation of a helium-helium white dwarf pair. (Reproduced from Iben & Tutukov (1984)).

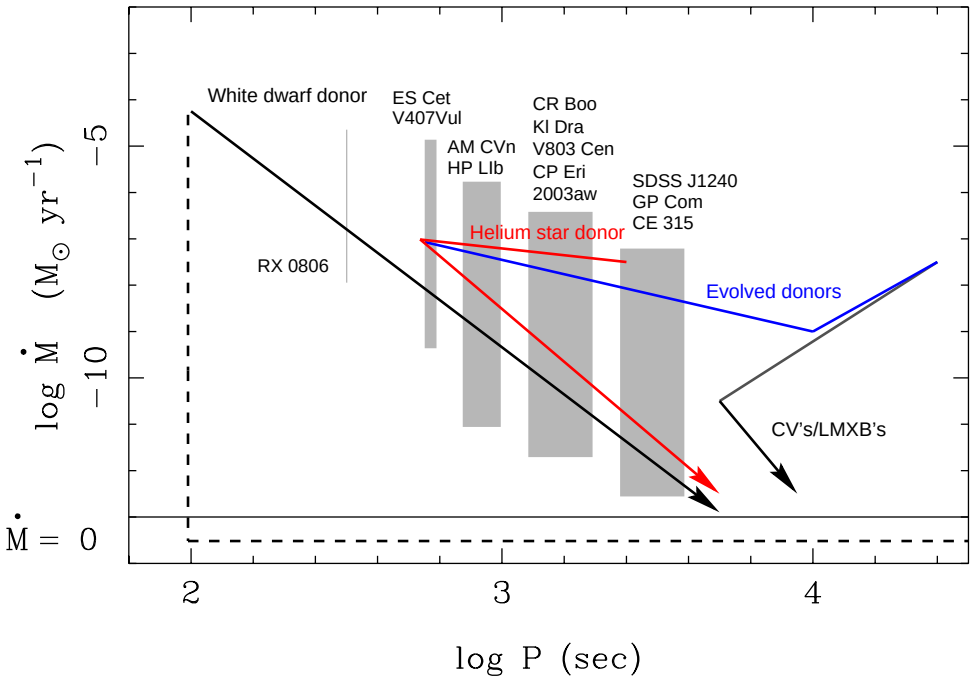

FIGURE 1.4. Formation channels of AM CVn systems (Reproduced from Nelemans (2005)).

DWD systems can consist of He+He WD, CO+CO WD, CO+He WD or He+CO WD pairs. Each of these are outcomes of slightly different evolutions, but each of these involves at least one phase of common envelope evolution and loss of mass and angular momentum from the system (Nelemans et al., 2001) as in the example described above. Detailed calculations to generate the population of compact objects in the galactic disk have been performed by Nelemans et al. (2001) and Yungelson et al. (1994). Nelemans et al. report a detached DWD birth rate of 2.5×10^{-2} and a merger rate of 1.1×10^{-2} per year with a total of 1.1×10^{8} such systems in the galactic disk. On the other hand, the AM CVn formation rate is 3.3×10^{-3} systems per year, with a total of 4.2×10^{7} systems in the galactic disk. The numbers obtained by other investigators are comparable but vary, depending on the details of the models. From their analysis, Nelemans *et al.* estimate that of the $\sim$ 12124 potential detached DWD systems in the galactic disk, about 6000 would be above the noise threshold of LISA sensitivity curve (See Section 5.4).

Returning now to AM CVn systems, which, as mentioned above are a subset of DWD systems, can also form via different channels (Nelemans, 2005):

- From DWD systems, by the loss of angular momentum via GWR. The systems evolve to shorter periods initially, get into contact and then evolve to higher orbital periods once mass transfer commences,

- From a pair consisting of a degenerate WD and non degenerate, Helium rich star which evolves through a period minimum when the latter star becomes

TABLE 1.1. Observational properties of AM CVn systems. The periods are in seconds, distances in parsec and V represents the apparent V-magnitude. Adapted from Nelemans (2005) & Espaillat et al. (2005). *See text for details.*

Name	V	$P_{\rm orb}$ (s)	$P_{\rm sh}$ (s)	q	d (pc)
ES Cet	16.9	621	–	–	
AM CVn	14.1	1029	1051	0.101	235
HP Lib	13.7	1103	1119	0.072	330
CR Boo	13.0-18.0	1471	1487	0.06	> 250
KL Dra	16.8-20.0	1500	1530	–	–
V803 Cen	13.2-17.4	1612	1618	–	250
CP Eri	16.5-19.7	1701	1716	0.04	800
2003aw	16.5-20.3	–	2042	–	–
SDSS J1240-01	–	2242	–	–	–
GP Com	15.7-16.0	2794	–	0.02	70
CE 315	17.6	3906	–	–	77
RX J0806+15	21.1	321	–	–	< 500
V407 Vul	19.7	569	–	–	–

semi-degenerate (analogous to CVs). After this, the system evolves to higher periods with decreasing mass transfer rate,

- From evolved donors in cataclysmic variables, which blow off their envelopes to expose the Helium rich core.

In Fig. 1.4, we have shown the different scenarios for the formation of AM CVn systems and in Table 1.1, we tabulate the observational properties of the known AM CVn systems. The last two systems, RX J0806 and V407 are suspected to be AM CVn progenitors because they are ultra-compact objects in which observations suggest that the orbital period is *decreasing* (Hakala et al. (2003); Strohmayer (2002)). As we shall see in Chapter 4, the orbital period of AM CVn systems is expected to increase once mass transfer commences, even though it loses angular momentum due to GWR. A number of explanations have been sought for this apparent discrepancy, for example it has been proposed that these objects are either double degenerate polars (Cropper et al., 1998), direct impact (DI) accretors (Marsh & Steeghs, 2002) or an 'Electric Star' Wu et al. (2002). Each of these models has its advantages and drawbacks (Cropper et al. (2003); Marsh & Nelemans (2005)) and a series of observations are being carried out to shed more light on the behavior of these systems (Ramsay et al., 2006).

The theoretical understanding of the other systems in Table 1.1 is much more sound and is based on the disk instability model (Tsugawa & Osaki, 1997). The observed systems are categorized into 3 types: high, low and outbursting (intermediate state) systems based on the mass transfer rate in a particular system. The shortest period systems are expected to have a higher mass transfer rate because of

the higher rate of loss of angular momentum due to GWR, whilst the longer period systems have lower mass transfer rates. We summarize the "standard theory" for AM CVn disk systems below:

- "High state" systems: These are the systems with relatively short periods and thus a high mass transfer rate due to the high driving rate. Though the mass transfer rate is high, it is "stable": the depth of contact is proportional to the rate of driving, which itself is secularly falling due to the increasing separation. Of the three objects in this category, AM CVn – the prototype – and HP Lib are known to show a Superhump period ($P_{\rm sh}$, see Table 1.1) along with an orbital period. The superhump period corresponds to the periodic modulation of light from the system, which is a consequence of a precessing eccentric disk. The third object, ES Cet, is sometimes considered to be of the 'atypical variety' of AM CVn's because of uncertainty in the sign of $\dot{P}$, but we consider it to be in a high state because of the high inferred mass transfer rate and short period.

- "Low state" systems: Low state systems are of the longest periods, believed to be systems undergoing stable mass transfer at low rates. The evolution of the system is thus correspondingly slow. Their optical spectra is dominated by strong Helium emission lines, and a weak underlying blackbody radiation emanating from the accreting white dwarf.

- "Outbursting" systems: These are systems of intermediate periods and their optical brightness varies between that of high and low state systems. These are considered to be a result of unstable accretion disks. In the high state, these systems exhibit He absorption lines whilst in the low state they show He emission lines.

As we shall see in Chapter 2 and Section 5.2, for a variety of mass ratios q, DWD systems have a geometry that suggests that the stream does indeed impact the accretor directly. However, for the mass ratios for typical AM CVn systems (Table 1.1), systems tend to be disk accretion systems which is consistent with the observations. Thus, it is possible that the progenitors of AM CVn systems – the DWD systems – are unstable Direct Impact (DI) accretion systems which eventually evolve into stable AM CVn systems.

1.5 Outline of This Dissertation

The study of compact DWD binaries provides useful clues into binary evolution, accretion disks, type Ia supernova progenitors and are important sources of gravitational waves that can be detected by the proposed space based detector LISA. Ideally, one would like our theoretical understanding to be such that given a DWD binary of arbitrary mass and composition, one can reconstruct its previous evolutionary pathway and the subsequent evolution to a merger, tidal disruption or stable mass transfer. A survey of published literature on this subject reveals that

we still lack a uniform theoretical understanding of these binaries for all possible mass ratios and other orbital parameters. One reason for this is that understanding double white dwarf binaries evolution can be quite complex and demanding, necessitating detailed hydrodynamics, nuclear physics, radiative transfer and stellar structure. Therefore it is natural that different assumptions and techniques are used when one attempts to answer a question relevant to different classes of phenomena. For example, the approach adopted in studying the putative progenitors of supernovae of type Ia, or the sources of gravitational waves for LISA, or the progenitors of AM CVn binaries, are all very different. In this work, we do not attempt to cover all the rich physics that may be ultimately necessary to have a uniform and reliable treatment of all possible outcomes of these phenomena, but instead describe them within a single semi-analytic framework.

In the first part of the thesis, we develop analytic and numerical tools to deal with the evolution of binary systems that are undergoing mass transfer. We concentrate on compact DWD binaries, but our model is quite general and as we show in Chapter 4, can be easily extended to other types of binary systems. In Chapter 2, we outline the basic astrophysical mechanisms and phenomena that can influence the evolution of a binary. We then derive the equations for binary evolution, including terms associated with GWR, mass transfer and tides. We discuss the significance of the tidal instability, and show that in the case of semi-detached DWD systems, mass transfer commences before the instability sets in, which leads to the system evolving away from the instability. In Chapter 3, we derive analytic solutions to the evolution equations developed in Chapter 2. These analytic solutions provide physical insight into the evolution equations, and are useful for comparison with the numerical integrations of the equations, which we carry out in Chapter 4. First, we illustrate the differences between the analytic and numerical solutions. Then, we apply the evolution equations to CVs, DWDs and contact binary systems and obtain their evolutionary trajectories. In Chapter 5, we apply the tools developed in the previous chapters to a variety of DWD systems with different initial conditions. We observe 'oscillation cycles' induced by the spin-orbit coupling and obtain stability limits and boundaries for super-Eddington accretion. Then we compare the results obtained in a full 3-D hydro-dynamic code with those predicted by the formalism developed in this work. Finally, the implications of the various phenomena involved in the evolution of DWD binaries for LISA, the space-based GWR detector are outlined.

In the second half of the thesis, we study the behavior of accretion disks, in particular 'circumbinary disks' (CBDs) and their influence on the binary. In Chapter 6 we develop equations for global parameters like the surface density, temperature and viscosity for the steady state and time evolving disks. The formalism we develop, in the form of the torque equation also provides insight into the behavior of the disk boundary layer and the distribution of angular momentum and torques through the disk. Finally, we combine the formalism from Part I with that of Chapter 6 to study the effects of the coupling between a CBD and a DWD binary undergoing super-Eddington mass transfer.

2. Physics of Binary Stars

In this chapter we develop the basic set of equations we will use in later chapters to describe the evolution of a binary system. We use the Roche approximation and assume that the stars are centrally condensed and that Kepler's laws are valid. The equations we derive are "orbit averaged" – for example, the GWR rate we use is averaged over an orbit. Where quantities cannot be derived from first principles or from the geometry of the problem at hand, we assign values based on observations, numerical calculations or treat them as free parameters. In the final section of this chapter, we study the tendency of some binary configurations to be prone to what is called the 'tidal instability'. We realize that semi-detached DWD binaries get into contact well before they reach the minimum separation and thus avoid tidal disruption due to this instability.

2.1 Astrophysical Phenomena Affecting Binary Evolution

As mentioned in Chapter 1, the Roche approximation is valid when we consider centrally condensed components that are synchronized with the orbit. One can then consider the behavior of a parcel of gas which itself has infinitesimal mass as compared to the components, in the sense of a restricted 3-body problem. The centrally condensed stars themselves can be, to a good approximation, treated as point masses orbiting around their common center of mass. Moreover, for most situations Newtonian equations of motion suffice – it is only whilst dealing with neutron stars and black holes that general relativistic effects need to be accounted for. Here, we deal with only white dwarf accretors either in the case of CV's or DWD's. From Kepler's third law, the orbital frequency Ω is given by

$$\Omega^2 = \frac{GM}{a^3} \tag{2.1}$$

where $M = M_1 + M_2$ is the total mass, M_1 and M_2 being the accretor and donor mass respectively[1]. The total angular momentum of the system is given by

$$\begin{aligned} J_{\rm tot} &= J_{\rm orb} + J_1 + J_2 \\ &= \mu a^2 \Omega + k_1 M_1 R_1^2 \omega_1 + k_2 M_2 R_2^2 \omega_2 \end{aligned} \tag{2.2}$$

where k_i are dimensionless constants depending on the internal structure of the components, $\mu = M_1\ M_2/M$ is the reduced mass of the system and ω_i are the angular spin frequencies. The first term in eq. (2.2) represents the orbital angular

[1] the subscript '1' refers to the accretor and '2' to the donor unless otherwise stated.

momentum of the components, and the two other terms represent the spin angular momenta of the stars. The form of the orbital angular momentum term adopted above assumes the binary revolves at the Keplerian frequency Ω, which is a good approximation if the stars are centrally condensed. Before we develop the equations describing the evolution of the binary, let us enumerate the physical mechanisms that influence this evolution.

2.1.1 Gravitational Wave Radiation

The rate at which two bodies in circular orbit lose energy to gravitational waves is given by Landau & Lifshitz (1975)

$$-\frac{d\mathcal{E}}{dt} = I = \frac{32G\mu^2\omega^6 a^4}{5c^5} \tag{2.3}$$

$\mathcal{E}$ is the mechanical energy of the system and I is the orbit-averaged intensity of the GWR. The result of this loss of energy from the system is the secular inspiral of the binary at a radial velocity

$$\dot{a} = a\,\frac{\dot{\mathcal{E}}}{\mathcal{E}} = \frac{2a^2}{GM_1M_2}\frac{d\mathcal{E}}{dt} = -\,\frac{64G^3M_1M_2M}{5c^5a^4} \tag{2.4}$$

Also, for circular orbits, the rate of loss of energy is related to the rate of loss of angular momentum: $\dot{\mathcal{E}} = \dot{J}\Omega$. Using Eqs. 2.1 and 2.3 we have

$$\dot{J}_{\rm tot} = -\,\frac{32G^{7/2}M_1M_2M^{1/2}}{5c^5a^{7/2}} \tag{2.5}$$

From the above equations, one notices that the rate of emission of GWR is a rather strong function of the orbital separation a, and the radial velocity also increases strongly at smaller separations. Thus, the emission of GWR results in the binary moving radially closer in the co-rotating frame and viewed from the inertial frame, the components of the binary spiral into the common center-of-mass at an ever increasing rate. In general, we expect that compact binaries (Section 1.4) to be prodigious emitters of GWR as compared to more extended objects like binaries containing main sequence stars like CV's and LMXB's. Unless some other phenomenon intervenes, the inevitable result of emission of GWR is a merger and that is indeed the case for (say) neutron star - neutron star binaries. However, in the case of CV's and DWD's, mass transfer commences when the Roche lobe radius equals the radius of the donor star which alters the evolution of the binary, sometimes dramatically (Section 2.2). Since AM CVn type binaries can also be detected in other more traditional wavelengths like visible and X-ray, the quality of information that can be extracted from a GWR detection by LISA is significantly enhanced (See Section 5.4).

2.1.2 Mass Transfer Rate

As mentioned in Section 1.3, one of the components of the binary gets into contact with its Roche lobe either due to the expansion of the star (the donor) and/or due

to shrinking of the Roche lobe as a result of angular momentum loss by GWR or other mechanisms. In order to determine exactly when a binary with given total mass and mass ratio q becomes semi-detached, one needs to specify the radii of the component stars and their corresponding Roche lobes. From Roche geometry and following Paczyński (1971), the Roche lobe radius can be crudely approximated as

$$\frac{R_L}{a} \propto \Big(\frac{M_2}{M}\Big)^{1/3} = 0.462\Big(\frac{M_2}{M}\Big)^{1/3} = 0.462\Big(\frac{q}{1+q}\Big)^{1/3} \tag{2.6}$$

A better fit to the Roche lobe radius was determined by Eggleton (1983) and is given by

$$\frac{R_L}{a} = \frac{0.49\ q^{2/3}}{0.6\ q^{2/3} + \ln(1+q^{1/3})} \tag{2.7}$$

The two are plotted for different values of the mass ratio $q = M_2/M_1$ for compar-

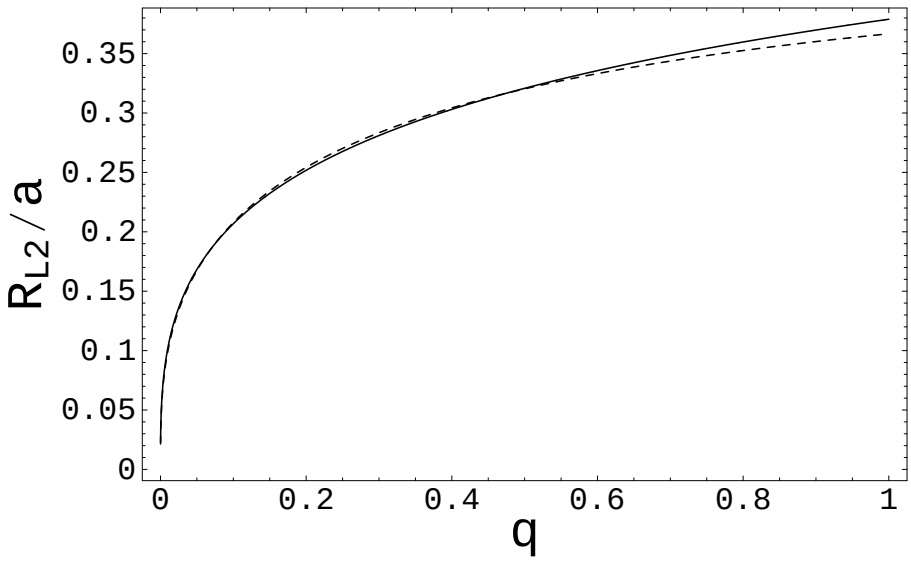

FIGURE 2.1. Comparison of Paczynski (Eq. 2.6, dotted curve) and Eggleton (Eq. 2.7) formulae for the Roche radius, normalized to the binary separation. The simple form of Eq. 2.6 is a reasonable approximation to the more accurate Eggleton formula for mass ratios q $\leq$ 0.6.

ison in Fig. 2.1. Thus we see that the Roche lobe radius is directly proportional to the separation for a fixed mass ratio. Now, the radius of the star can be defined in several ways depending on the problem at hand. For example one can provide a mass-radius relation for the type of donor star we are concerned with. It could be a main sequence star in case we are dealing CV's or a white dwarf in case of DWD's. One can also have a polytrope as the donor – this is especially useful whilst predicting the behavior of 3-D hydrodynamic simulations or comparing the equations of our linear equations with more complicated situations (see Section 5.3). In general, we represent the the logarithmic derivative of the radius with

respect to mass as

$$\zeta_2 = \frac{d \ln R_2}{d \ln M_2} \tag{2.8}$$

which is a measure of how the radius of the donor changes as its mass changes as a result of mass transfer. Strictly, ζ_2 can be interpreted as the mass-radius exponent of the equilibrium mass-radius relationship only when the thermal relaxation timescale $\tau_{th} < \tau_{M_2}$, the mass transfer timescale. This is almost always true for degenerate objects, but in the case of CVs, ζ_2 may vary significantly from the equilibrium value (See discussion following Eq. 2.23 below).

Given Roche geometry and the structure of the star, we can now specify the mass transfer rate. In general, we expect the mass transfer to be a strong function of the 'depth of contact', defined as the amount by which the donor overflows its Roche lobe $\Delta R_2 = R_2 - R_L$ and of the structure of the star, which can be described in different ways depending on the problem at hand. Two of the most commonly used approximations are a) Polytropes and b) Isothermal atmospheres with a characteristic scale height H. Thus, we write (Gokhale et al., 2006)

$$\dot{M}_2 = -\dot{M}_0(M_1, M_2, a) f(\Delta R_2) \tag{2.9}$$

where $\dot{M}_0$ is a relatively gentle function of the binary parameters and f is a strong function of ΔR_2. For example, for polytropic donors with index n, $f = (\Delta R_2/R_2)^{n+3/2}$ (Paczyński & Sienkiewicz, 1972); whilst for a donor with an atmospheric pressure scale height H, $f = \exp(\Delta R_2/H)$ (Ritter, 1988). As we shall see later, the exact value of $\dot{M}_0$ is not very important to determine the overall evolutionary behavior of the binary except in extreme conditions which are usually transient (see below). The depth of contact, on the other hand, is a function of the *driving rate*, i.e., the rate at which angular momentum is lost from the orbit.

2.1.3 Tidal Effects

By design, the component stars in close binaries influence the evolution and observational properties of each other by altering the gravitational potential. Tidal effects play an important role in the circularization and synchronization of the orbit and thus influence the evolution significantly. For example, an initially eccentric orbit is circularized by the action of tides on a characteristic 'circularization timescale'. Though the fact that tidal effects can influence binary evolution has been known for a long time, traditionally, these effects have been largely ignored. Usually, it is common to assume that the spins of the components are synchronized with the orbit throughout the evolution of the binary. This is not always the case, and in fact, following the exchange of spin angular momentum of the individual stars and orbital angular momentum could be critical in determining the fate of the binary.

For our work here, where we are dealing with degenerate white dwarfs, we adopt Campbell's (1984) prescription to calculate the tidal timescales. According

to Campbell, the synchronization timescale is given by

$$\tau_{s_1} \propto \left(\frac{M_1}{M_2}\right)^2 \left(\frac{a}{R_1}\right)^6$$
$$\tau_{s_2} \propto \left(\frac{M_2}{M_1}\right)^2 \left(\frac{a}{R_2}\right)^6 \tag{2.10}$$

The actual timescale is not very well known and consequently we choose a normalization factor (τ_{s_0}) to obtain a desired initial timescale. In any case, in the limit that the timescales are very short, we should have the spins of the stars synchronized with the orbit, just as is assumed usually; whilst when the timescales are long, the asynchronism between the spin and orbit should build up as the system evolves. As we shall see later (Section 5.1), especially after mass transfer commences, there is a possibility of significant asynchronism to be built up in the accretor and then the tidal coupling between the accretor spin and the orbit can influence the evolutionary outcome of the binary significantly.

2.1.4 Other Effects

- **Magnetic Braking (MB)**: Verbunt & Zwaan (1981) proposed a mechanism for explaining the observed mass transfer rates for Cataclysmic Variable stars and low mass X-ray binary stars. They realized that the traditionally accepted mechanism, gravitational wave radiation, was inadequate to explain the observed (high) mass transfer rates. The basic idea behind this mechanism is that "the cool, main-sequence donors in CVs and LMXBs undergo rotational breaking by a magnetically coupled stellar wind, similar to single main-sequence stars" (Verbunt & Zwaan, 1981). The donor star loses angular momentum via winds which is given by:

  $$\frac{dJ_2}{dt} = -0.510^{-18} f^{-2} k^2 M_2 R_2^4 \omega^3 \tag{2.11}$$

  where, f is a numerical factor of order 1. Tides lock the Roche-lobe filling donor to the orbit, and hence there is a net loss of angular momentum from the orbit, which in turn drives the mass transfer. For main sequence donors, Verbunt & Zwaan (1981) note that for typical values of the component masses and orbital periods, the breaking rate (Eq. 2.11) is at least one order of magnitude greater than the GWR rate (Eq. 2.5). Moreover, the MB model also is quite successful in explaining the 'period gap' observed in the distribution of CVs (Verbunt & Zwaan, 1981). To obtain Eq. 2.11, one needs to know the equatorial rotation velocity on the surface of the star, as a function of time. This is known for some (with considerable uncertainty though) main-sequence type stars (Andronov, Pinsonneault & Sills, 2003), but is not known for compact objects. Thus we will not consider this mechanism in our analysis of compact binary evolution, noting however, that in principle whilst dealing with CVs for example, one can replace the GWR driving rate ν_L by a MB rate $\nu_{\rm mb}$ given by Eq. 2.11 in our evolution equations (Section 2.2).

- **Mass Loss**: As mentioned above, single main-sequence stars as well as white dwarfs lose mass at a slow rate via stellar winds. This is evident from the P Cygni profiles that are observed in such objects, which is a characteristic of radiation driven winds. Mass loss can occur in stars as a result of winds emanating from the stars surface because of 'heating' due to incident energetic photons (**Systemic mass loss**); or mass loss can occur as a result of "super-Eddington mass transfer" (**Consequential mass loss**, See section 4.2). Systemic mass loss effectively represents an additional driving term in the evolution equations, analogous to the GWR and MB terms. On the other hand, the consequential mass loss terms influence the stability properties of the binary (see Section 2.2 and Chapter 4).

- **Circumbinary disks (CBD)**: Material can accumulate around a binary as a result of mass loss via winds or mass outflows due to mass transfer, or the remnants of a common envelope which tends to accumulate in the orbital plane of the binary. This can lead to formation of a 'circumbinary disk' (CBD). If this CBD is tidally coupled to the binary, then the resulting tidal torques will alter the angular momentum distribution in the binary and thus, influence the binary evolution. We shall study the properties of CBDs and their influence on binary evolution in Section 7.1.

2.2 Evolution Equations

Now that we have enumerated some of the physical mechanisms that can influence the evolution of a binary, we can proceed to derive mathematical expressions in order to quantify these effects. To reiterate, we work under the following assumptions: i) Roche potential describes the gravitational field, ii) Kepler's laws are valid, and that the stars orbit around their common center of mass in circular orbits, iii) the spin and orbit axes are all parallel to one another and, iv) tidal effects are included even though we ignore the effects of the distortion of the stars, i.e., we assume spherically symmetric stars.

Now, rearranging Eq. 2.2 we have

$$J_{\rm orb} = J_{\rm tot} - (J_1 + J_2) \Rightarrow \dot{J}_{\rm orb} = \dot{J}_{\rm tot} - (\dot{J}_1 + \dot{J}_2) \tag{2.12}$$

where J_1 and J_2 are the spins of the accretor and donor respectively. $\dot{J}_{\rm tot}$ represents the systemic angular momentum loss ($= \dot{J}_{\rm sys}$) whilst $\dot{J}_i$ represents the rate of change of the components (i=1,2). As can be verified, this form allows for the possibility of spin-orbit coupling of the angular momenta. Furthermore, the rate of change of the spin momenta can be given as the sum of an advective or a *consequential* angular momentum term and a tidal term as (Gokhale et al., 2006)

$$\dot{J}_i = \dot{M}_i j_i + \dot{J}_{i,\rm tid} \tag{2.13}$$

where, j_1 and j_2 indicate the specific angular momenta of the matter *arriving* at the accretor and the matter *leaving* the donor respectively. In a conservative

system, these will refer to the specific angular momentum of the *same* material with respect to the center of mass of each star, but at *different* times. The second term in the equation above represents the tidal term, which is a function of the degree of asynchronism $(\Omega - \omega_i)$ and the tidal timescale (τ_{s_i}). We write the tidal torque as

$$\dot{J}_{i,\rm tid} = \frac{k_i M_i R_i^2}{\tau_{s_i}}(\Omega - \omega_i) \tag{2.14}$$

Substituting Eq. 2.13 and Eq. 2.14 into Eq. 2.12 we obtain

$$\dot{J}_{\rm orb} = \dot{J}_{\rm sys} + \dot{M}_2(j_1 - j_2) - \frac{k_1 M_1 R_1^2}{\tau_{\rm s_1}}(\Omega - \omega_1) - \frac{k_2 M_2 R_2^2}{\tau_{\rm s_2}}(\Omega - \omega_2) \tag{2.15}$$

Now, from the functional form of the orbital angular momentum ($J_{\rm orb} = M_1 M_2 (Ga/M)^{1/2}$) we have

$$\left(\frac{\dot{J}}{J}\right)_{\rm orb} = \frac{\dot{M}_2}{M_2}(1-q) + \frac{1}{2}\frac{\dot{a}}{a}.$$

which we compare with Eq. 2.15 to obtain an expression for the rate of change of the orbital separation

$$\frac{\dot{a}}{2a} = \frac{\dot{J}_{\rm sys}}{J_{\rm orb}} - \frac{\dot{M}_2}{M_2}\Big[1 - q - M_2\frac{j_1 - j_2}{J_{\rm orb}}\Big] - \frac{k_1 M_1 R_1^2}{J_{\rm orb}\tau_{\rm s_1}}(\Omega - \omega_1) - \frac{k_2 M_2 R_2^2}{J_{\rm orb}\tau_{\rm s_2}}(\Omega - \omega_2) \tag{2.16}$$

which we rewrite for convenience as

$$\frac{\dot{a}}{2a} = \frac{\dot{J}_{\rm sys}}{J_{\rm orb}} - \frac{\dot{J}_{1,\rm tid} + \dot{J}_{2,\rm tid}}{J_{\rm orb}} - \frac{\dot{M}_2}{M_2}[q_a - q] \tag{2.17}$$

$$q_a = 1 - M_2\frac{j_1 - j_2}{J_{\rm orb}}, \tag{2.18}$$

The sign of the terms on the right hand side of Eq. 2.17 determines if the orbit is shrinking or expanding. q_a represents the net effect of the consequential (advective) transfer of angular momentum. Ignoring the tidal terms for the moment, in the absence of mass transfer, the orbit shrinks as a result of the systemic angular momentum loss, for example, via GWR. But once mass transfer commences, the sign of the quantity in square brackets in Eq. 2.17 comes into play as well – if $q > q_a$ then the binary continues to shrink which as we shall see later (Chapters 4 & 5), is a sign of increased instability. On the other hand, for systems with $q < q_a$, mass transfer leads to the orbit expanding or least not shrinking as rapidly as it would in the absence of mass transfer.

The tidal terms have a more complicated behavior because the sign of the tidal torque $J_{i,\rm tid}$ is a function of the difference in the spin frequencies and the orbital frequency, $\Omega - \omega_i$. In general though, if the spin frequency of a given component is

higher than the orbital frequency, then tides will tend to pump angular momentum into the orbit and thus help increase the separation. Conversely, if the orbital frequency is higher than the spins, it can lead to a runaway instability since the tides will tend to suck more angular momentum out from the orbit which in turn will increase the orbital frequency even more. It is even possible, as we shall see later (Section 5.1), to have a system alternate between a phase where the spin is higher or lower than the orbital frequency, in which case the system can undergo oscillations – this has interesting observational consequences for both traditional astronomy and GWR detectors.

We now determine how the depth of contact evolves to complete the set of equations we need to specify the evolution of the binary system. From Eq. 2.7, we can write

$$\frac{\dot{R}_{\rm L}}{R_{\rm L}} = \zeta_{r_{\rm L}} \frac{\dot{M}_2}{M_2} + \frac{\dot{a}}{a},$$

where $\zeta_{r_{\rm L}} \approx 1/3$ is the logarithmic derivative of $r_{\rm L}$ with respect to M_2[2]. Thus we have

$$\frac{\dot{R}_{\rm L}}{R_{\rm L}} = \frac{2\dot{J}_{\rm sys}}{J_{\rm orb}} - 2\frac{\dot{J}_{1,\rm tid} + \dot{J}_{2,\rm tid}}{J_{\rm orb}} - \frac{2\dot{M}_2}{M_2}[q_a - \frac{\zeta_{r_{\rm L}}}{2} - q] \tag{2.19}$$

Symbolically, generalizing the meaning of the symbols introduced by Webbink & Iben (1987)

$$\frac{\dot{R}_{\rm L}}{R_{\rm L}} = \nu_{\rm L} + \zeta_{\rm L}\frac{\dot{M}_2}{M_2} \tag{2.20}$$

$$\nu_{\rm L} = \frac{2\dot{J}_{\rm sys}}{J_{\rm orb}} - 2\frac{\dot{J}_{1,\rm tid} + \dot{J}_{2,\rm tid}}{J_{\rm orb}} \tag{2.21}$$

$$\zeta_{\rm L} = \zeta_{r_{\rm L}} + 2(q - q_a), \tag{2.22}$$

where the symbol ν stands for *driving terms* and ζ denotes logarithmic derivatives with respect to donor mass. In the same spirit, we write the logarithmic time derivative of the donor radius $R_2 \equiv R_2(M_2, t)$ as:

$$\frac{\dot{R}_2}{R_2} = \nu_2 + \zeta_2\frac{\dot{M}_2}{M_2} \tag{2.23}$$

where ν_2 represents the rate of change of the donor radius due to intrinsic processes such as thermal relaxation and nuclear evolution, whereas ζ_2 usually describes changes resulting from adiabatic variations of M_2 as described above. We derive here a simple analytic approximation to the effective mass-radius exponent

[2]In the range $0 < q \leq 1$, the function $\zeta_{r_{\rm L}}$ takes values between 0.32 and 0.46, and is well approximated by $\zeta_{r_{\rm L}} \approx 0.30 + 0.16q$ for $0.1 \leq q \leq 1$

when the response of the donor is a combination of the adiabatic and thermal adjustments to mass loss. Our starting point is Eq. (2.23)

$$\frac{\dot{R}_2}{R_2} = \zeta_2 \frac{\dot{M}_2}{M_2} = \nu_2 + \zeta_s \frac{\dot{M}_2}{M_2}$$

where ζ_2 is the effective mass-radius exponent we seek, ν_2 stands for the thermal radial reaction rate, and ζ_s is here the purely adiabatic mass-radius exponent. As a consequence of mass loss, the donor's radius R_2 will differ from the equilibrium radius corresponding to its instantaneous mass $R_{\rm eq}(M_2)$. With these definitions we write

$$\frac{\dot{R}_2}{R_2} = \frac{R_{\rm eq}(M_2) - R_2}{R_2 \tau} + \zeta_s \frac{\dot{M}_2}{M_2} \tag{2.24}$$

where we have adopted a simple linear approximation for the thermal adjustment term. The secular evolution of the binary takes place on a mass-transfer timescale $\tau_{M_2} = -M_2/\dot{M}_2$. Differentiating Eq. (2.24) with respect to time, we get

$$\frac{{\rm d}^2 \ln R_2}{{\rm d}t^2} = \frac{1}{\tau} \frac{R_{\rm eq}}{R_2} \left(\frac{\zeta_{\rm eq}}{\tau_{M_2}} - \frac{\zeta_2}{\tau_{M_2}} \right) - \frac{\zeta_s}{\tau_{M_2}^2} \tag{2.25}$$

If the effective mass-radius exponent is to have any meaning, it must not change much over the evolutionary phase one is considering. Thus, we require

$$\frac{{\rm d}^2 \ln R_2}{{\rm d}t^2} = -\zeta_2 / \tau_{M_2}^2 \,. \tag{2.26}$$

Finally, setting $R_{\rm eq} = R_2$ in Eq. (2.25), and solving for ζ_2, we obtain

$$\zeta_2 = \frac{\zeta_{\rm eq} + \zeta_s \tau / \tau_{M_2}}{1 + \tau / \tau_{M_2}}. \tag{2.27}$$

This expression shows that if the evolution is much slower than the thermal relaxation ($\tau \ll \tau_{M_2}$), the donor radius follows the equilibrium radius closely, whereas if mass transfer occurs rapidly, the donor reacts adiabatically.

Eqs. 2.9, 2.14, 2.16, 2.19 and 2.23 (referred to as 'the evolution equations' from now on) completely specify the evolution of the binary and can be integrated numerically which we shall discuss in detail in Chapters 4 and 5. Before we proceed though, we firstly provide semi-analytic expressions for the advective terms that depend primarily on the geometry of mass transfer. We also obtain expressions for the evolution of the spins of the two components. We then proceed to derive analytic solutions by simplifying the above equations for certain special cases.

2.2.1 The Advective Terms and Spin Evolution

Though the evolution equations defined above form a complete set of equations which define the evolution of the binary system, we still need to specify the exact form of the advective terms j_1 and j_2 in order to follow the evolutionary outcome

of a given binary. Defining these terms will also allow us to study the evolution of the spin angular momenta of the individual components. As mentioned above, we shall parameterize the advective terms in terms of geometry (dynamics) of the mass transfer stream on the basis of the Roche approximation.

The Stream Trajectory: The material spilling over the L_1 point as a result of RLOF has a high specific angular momentum relative to the accretor and hence it cannot fall directly on the accretor. Instead, in most cases, the material misses the accretor and goes through a rossette patterned trajectory. The stream then interacts with itself, eventually settling down in a ring in circular orbit around the accretor – thus leading to formation of an accretion disk due to viscous dissipation. We shall discuss disks in detail in Chapter 6 – here we only follow the stream trajectory in order to specify the amount of angular momentum it carries with it, the torques it encounters and the amount of angular momentum that is supplied or sucked out of the orbit and the individual stars as a result. Firstly, we note that the stream spilling over the L_1 point is supersonic. Let $v_\perp$ represent the velocity of the stream perpendicular to the lines of centers of the stars in a frame comoving with the accretor. We have, $v_\perp \sim b_1\omega$ where, $b_1 = (0.500 - 0.227\log q)a$ is the distance of the L_1 point from the center of the primary (Plavec & Kratochvil, 1964). For typical values of q and ω, $v_\perp$ turns out to be a few hundred Km/sec. As the stream is further accelerated by the gravitational force of the accretor almost always $v_\perp > c_s$, the sound speed. As a result, we can treat the stream as a ballistic trajectory, since the pressure forces on the stream can be ignored. In Fig. 2.2, we show the trajectory of a test particle as it oozes out of the L_1 point. As can be seen, the particle follows a rossette shaped trajectory, and a continuous stream would indeed interact with itself, resulting in dissipation of energy due to shocks. On the other hand, the gas cannot easily get rid of its angular momentum, and as a consequence the stream settles into a circular orbit around the accretor at some characteristic radius $R_{\rm circ}$. The velocity of the gas is then given by

$$v_\phi(R_{\rm circ}) = \Big(\frac{GM_1}{R_{\rm circ}}\Big)^{1/2} \tag{2.28}$$

From angular momentum conservation, assuming no torques act between the stream and the orbit or spins of the stars, the angular momentum of the gas at the L_1 point must equal the angular momentum at $R_{\rm circ}$ –

$$R_{\rm circ}v_\phi(R_{\rm circ}) = b_1^2\omega$$

Substituting for b_1 and using the above equations, we can write

$$\frac{R_{\rm circ}}{a} = (1+q)[0.500 - 0.227\log q]^4 \tag{2.29}$$

Thus the specific angular momentum carried by the stream as it approaches the accretor is given by

$$j_1 \equiv j_{\rm circ} = (GM_1R_{\rm circ})^{1/2} \sim [(1+q)r_h]^{1/2}\frac{J_{\rm orb}}{M_2} \tag{2.30}$$

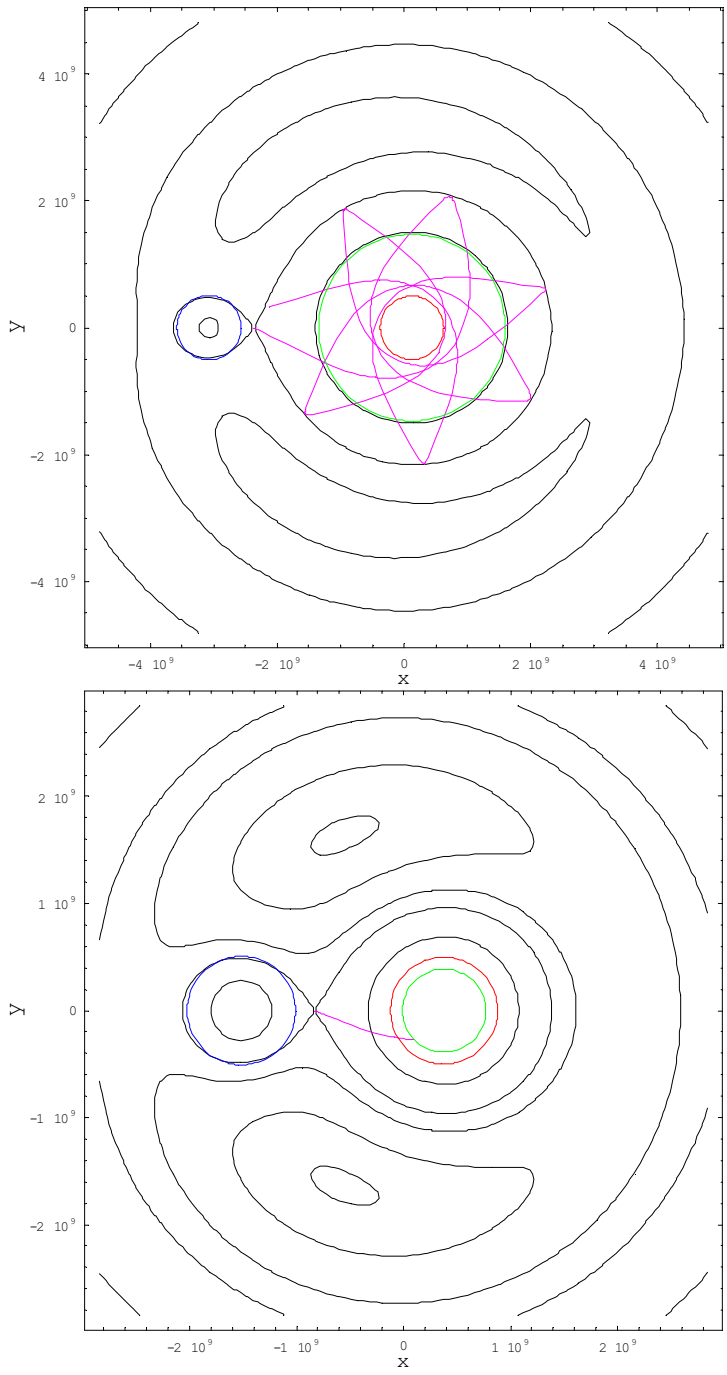

FIGURE 2.2. Stream trajectory for 2 different mass ratios; q = 0.05 (top panel) and q = 0.25 (bottom panel). The blue and red circles represent the radii of the donor and accretor respectively, whilst the green curve denotes the circularization radius. For q = 0.05, the circularization radius is well outside the accretor, and the stream follows a rossette shaped trajectory in the ballistic case. On the other hand, for a mass ratio of 0.25, $R_{\rm circ} < R_1$, and consequently the stream directly impacts the accretor.

Due to the geometry of DWD systems, it is possible for the stream, which follows a ballistic path to a good approximation, to hit the surface of the accretor. We

see from Fig. 2.2 that the point of closest approach for the stream in well within the circularization radius, and much closer to the accretors surface. The closest distance to the surface of the accretor the stream reaches to is given by Lubow & Shu (1975) as

$$\frac{R_{\rm min}}{a} \approx 0.04948 - 0.03815\log(q) + 0.04752\log^2(q) - 0.006973\log^3(q) \quad (2.31)$$

The stream misses the surface of the accretor when $R_{\rm min} > R_1$ and goes on to form a disk, whilst if $R_{\rm min} < R_1$, we have 'direct impact' accretion (DIA). In the latter case, the amount of angular momentum lost from the orbit is the same as the amount carried by the stream – it all goes into spinning up the accretor. If, however, we have an accretion disk, the tidal torques generated between the disk and the orbit lead to efficient return of most of the angular momentum back to the orbit. In that case, we replace $R_{\rm circ}$ with R_1 in Eq. 2.30, since the amount of angular momentum lost at the inner edge of the disk is $(GM_1R_1)^{1/2}$.

The situation with the advective term j_2 is not as obvious. The exact value of j_2 depends on the details of the flow in the vicinity of the L_1 point, which we are not in a position to access. For our purposes, on physical grounds we adopt $j_2 = R_2^2\omega_2$. This term has often been ignored in the analysis of evolution of binaries, but as pointed out by Savonije (1978) and Gokhale et al. (2006), it plays an important role in binary evolution (see Section 5.2). Thus we can write

$$\begin{aligned} q_a &= 1 - \zeta_c = 1 - M_2\frac{j_1 - j_2}{J_{\rm orb}} \\ &= 1 - [(1+q)r_h]^{1/2}(1 - \frac{R_2^2\omega_2}{\sqrt{GM_1R_{\rm circ}}}) \end{aligned} \quad (2.32)$$

where $\zeta_c = d\log J_{\rm orb}/d\log M_2$ represents the consequential angular momentum loss.

The net effect of the consequential redistribution of angular momentum in the binary depends on the sign of $\zeta_{\rm c}$. For DWD binaries, $j_1 > j_2$ during the direct impact stage, and this holds even after the onset of disk accretion, when $j_1 = \sqrt{GM_1R_1}$ and $\zeta_{\rm c}$ becomes smaller but remains positive. In cataclysmic variables and low-mass X-ray binaries, the accretion disk returns via tides most of the angular momentum advected by the stream, the donor is almost synchronous, and the tidal coupling of the accretor to the orbit is very weak. However, in this case $R_1 \ll a$ and thus it is more likely that $j_2 > j_1$. While all the additional terms in eqs. (2.17, 2.18) are relatively small, yielding $q_a \approx 1$, in some cases $\zeta_{\rm c} < 0$, and thus $q_a \geq 1$ making these systems slightly more stable.

2.2.2 Spin Angular Momentum Evolution

We now derive explicit equations to describe the evolution of the spin angular momenta of the two stars. The spin angular momenta of the accretor and donor

can be written in terms of their moment of inertia, $I_i = k_i M_i R_i^2$ and spin frequency (ω_i) as

$$J_1 = k_1 M_1 R_1^2 \omega_1 \tag{2.33a}$$

$$J_2 = k_2 M_2 R_2^2 \omega_2 \tag{2.33b}$$

Taking the logarithmic derivative, and assuming the radii of gyration k_i do not change significantly we can write

$$\frac{\dot{J}_1}{J_1} = \frac{\dot{M}_1}{M_1}(1 + 2\zeta_1) + \frac{\dot{\omega}_1}{\omega_1} \tag{2.34a}$$

$$\frac{\dot{J}_2}{J_2} = \frac{\dot{M}_2}{M_2}(1 + 2\zeta_2) + \frac{\dot{\omega}_2}{\omega_2} \tag{2.34b}$$

The assumption that the k_i's do not change implies that the shape of the stars does not change significantly during the evolution. While this is almost certainly true for stable mass transfer situations, for unstable mass transfer via direct impact accretion, the stars could get significantly distorted (D'Souza et al., 2006). However, we believe that in the unstable case, other effects dominate the evolution of the binary and hence we ignore the distortion of the components for our analysis. Now, using eqs. 2.13, 2.14 & 2.34 along with eq. 2.33, we get on simplification

$$\frac{\dot{\omega}_2}{\omega_2} = \frac{\dot{M}_2}{M_2}(2\zeta_2) + \frac{1}{\tau_{s_2}}\Big(\frac{\omega - \omega_2}{\omega_2}\Big) \tag{2.35a}$$

$$\frac{\dot{\omega}_1}{\omega_1} = -\frac{\dot{M}_2}{M_2}\Big[\frac{j_{\rm circ} M_2}{J_1} - (1 + 2\zeta_1)\ q\Big] + \frac{1}{\tau_{s_1}}\Big(\frac{\omega - \omega_1}{\omega_1}\Big) \tag{2.35b}$$

Eqs. 2.35 describe the evolution of the spin frequency of the components. The first term represents the advective component whilst the second term is the tidal term.

2.3 Stability of Mass Transfer

In Section 2.2 we have described the evolution equations in some detail. We now introduce the concept of the equilibrium mass transfer rate, which is the mass transfer rate that a stable, semi-detached binary undergoes for a given rate of driving. The equilibrium mass transfer rate is a function of the driving rate, the consequential angular momentum loss mechanisms and the value of the mass ratio q. The mass transfer rate can be written quite generally as

$$\dot{M}_2 = -\dot{M}_0(M_1, M_2, a) f(\Delta R_2)$$

Under the assumption that $\dot{M}_0$ is a gentle function of the binary parameters, whilst f is a strong function of the depth of contact ΔR_2, we can write

$$\ddot{M}_2 = -\dot{M}_0 \frac{\partial f}{\partial \Delta R_2}\Big(\frac{\dot{R}_2}{R_2} - \frac{\dot{R}_{\rm L}}{R_{\rm L}}\Big) \tag{2.36}$$

For equilibrium mass transfer, we demand $\ddot{M}_2 = 0$, i.e. the mass transfer rate itself does not evolve very fast. Thus, using the evolution equations and Eq. 2.36 we have

$$\left(\frac{\dot{M}_2}{M_2}\right)_{\rm eq} = \frac{\nu_{\rm L} - \nu_2}{2(q_{\rm stable} - q)} = \frac{\nu_{\rm L} - \nu_2}{\zeta_2 - \zeta_{\rm L}} \tag{2.37}$$

where

$$q_{\rm stable} = q_a - \frac{\zeta_{r_{\rm L}}}{2} + \frac{\zeta_2}{2}, \tag{2.38}$$

is the critical mass ratio for stability of mass transfer. For example, for a polytropic donor with $n = 3/2$ (which is representative of a white dwarf donor) $\zeta_2 \sim -1/3$, $\zeta_{r_L} \sim 1/3$ and so

$$\left(\frac{\dot{M}_2}{M_2}\right)_{\rm eq} = \frac{\dot{J}_{\rm sys}/J_{\rm orb}}{2/3 - \zeta_{\rm c} - q}$$

which is the familiar form in case of direct impact DWD's (Marsh et al., 2004), except that here $\zeta_{\rm c}$ is reduced by the contribution from the donor as given by Eq. 2.32.

On the other hand, for a main sequence donor in the case of CVs, $R_2 \propto M_2$, in which case $\zeta_2 \sim 1$ and so

$$\left(\frac{\dot{M}_2}{M_2}\right)_{\rm eq} = \frac{\dot{J}_{\rm sys}/J_{\rm orb}}{4/3 - \zeta_{\rm c} - q}$$

In general one can write from Eq. 2.36

$$\ddot{M}_2 = -2\frac{\dot{M}_0}{M_2}\frac{\partial f}{\partial \Delta R_2}(q_{\rm stable} - q)\left(\dot{M}_2 - (\dot{M}_2)_{\rm eq}\right). \tag{2.39}$$

When $q < q_{\rm stable}$, the pre-factor on the RHS is negative and thus the mass transfer rate tends toward the equilibrium value implying that the mass transfer is stable. On the other hand, when $q > q_{\rm stable}$, we can see that the system cannot reach the equilibrium value and this implies that the mass transfer is unstable. It is possible during the course of the evolution that a system that initially has $q > q_{\rm stable}$ can evolve into a system with $q < q_{\rm stable}$ – thus an initially unstable system can survive as a stable system (see Chapter 4 & Section 5.2).

2.4 Timescales

Each of the astrophysical effects we have enumerated in Section 2.1 are associated with a characteristic timescale. A relatively short timescale corresponds to that particular effect being highly efficient, whereas a relatively long timescale usually implies inefficiency and relative unimportance. The effect with the shortest timescale at a given point in the evolution is more likely to be the dominant effect in determining the evolutionary fate of the binary.

- **Mass transfer timescale**: The mass transfer timescale is defined by $\tau_{M_2} = M_2/\dot{M}_2$, and it is a function of the driving rate and the depth of contact Δ. The mass transfer timescale is extremely short during unstable mass transfer, and can result in the tidal disruption of the donor due to *mass transfer instability*.

- **GWR timescale**: In the case of compact binaries, the GWR timescale $\tau_{\rm GWR}$ corresponds to the driving timescale of the binary. It represents the rate at which angular momentum is lost from the system. If this timescale is shorter than the other timescales in the binary, the inevitable result is a merger with a characteristic chirp signal (Section 5.4). During stable mass transfer, $\tau_{\rm GWR} \sim \tau_{M_2}$, where as during unstable mass transfer, $\tau_{\rm GWR} \gg \tau_{M_2}$.

- **Tidal timescale**: The tidal timescale $\tau_{\rm s_i}$ represents the level of spin-orbit coupling between the spins of the component stars and the orbit. This is the parameter that is most uncertain in our study, and we treat it as a free parameter. Usually one assumes that the donor, which is tidally locked with the orbit, has an extremely short tidal timescale (as compared to say $\tau_{\rm GWR}$ or τ_{M_2}) where as the accretor has an extremely long tidal timescale, and is effectively decoupled from the orbit. When an accretion disk is present around the accretor, the outer radius of the disk almost fills up the Roche lobe radius of the accretor. As a result, the tidal timescale of the disk is also very short.

- **Mass loss timescale**: We can define a timescale over which mass is lost from the binary system. This can either be a systemic mass loss or a consequential mass loss (Section 2.1.4). If the mass loss timescale, τ_M, is shorter than the GWR timescale, then the system will evolve on the mass loss timescale. In case of consequential mass loss, for example during super-Eddington accretion (Section 4.2), it is possible that τ_M is extremely short as compared to the other timescales in the system. This can result in the formation of a common envelop around the binary, which alters the behavior of the system significantly (Webbink & Iben, 1987).

- **Dynamic timescale**: The dynamical timescale is defined by

$$t_{\rm dyn} = \Big(\frac{3\pi}{16G\bar{\rho}}\Big)^{1/2} \tag{2.40}$$

  where $\bar{\rho}$ is the average density of the astrophysical object under consideration.

2.5 The Tidal Instability and the Contact Condition

For a fully synchronous configuration, it is easy to show using Eq. 2.2 that the total angular momentum and the total energy have a minimum at the same separation

$a_{\rm min} = [3(I_1 + I_2)/\mu]^{1/2}$, where the $I_i = k_i M_i R_i^2$ are the moments of inertia of the components, and μ is the reduced mass. Even if the orbital frequency and the spin frequency are not synchronized but remain proportional to one another ($\omega_i = f_i \Omega$), there is a minimum of $J_{\rm tot}$ at some $a_{\rm min}$. Also the total energy of the system will have a minimum but in general it will not occur at $a_{\rm min}$. It can be shown that for Riemann-S and Roche-Riemann sequences $\mathrm{d}E = \Omega \mathrm{d}J + \Lambda \mathrm{d}\mathcal{C}$, where Λ is the angular velocity of internal motions and $\mathcal{C}$ is the equatorial circulation (Lai et al., 1993b). Thus, as a binary evolves driven by gravitational wave radiation, circulation is conserved and the minima of E and J will coincide. However tidal dissipation does not preserve $\mathcal{C}$ and thus in general the minima will *not* coincide in the presence of tidal spin-orbit coupling.

For our purposes, it will be sufficient to work with the approximate form of equation (2.2) given above. A more complete and thorough discussion of the secular and dynamical stability of polytropic binaries has been presented in two well-known series of papers by Lai, Rasio & Shapiro (LRS1-LRS5) and further developed with SPH simulations in papers by Rasio & Shapiro (RS1-RS3), who also addressed the role of mass-transfer.

For binary configurations with the orbital separation $a < a_{\rm min}$, tidal synchronization leads to an unstable situation due to the positive feedback between the spins and the orbit. For example, when $a < a_{\rm min}$, any loss of angular momentum from the system (say, by GWR emission), *must* result in the breakdown of synchronism, for if the system were to remain synchronous, according to Fig. 2.3 we see that the total angular momentum actually should increase (which is impossible since we are draining angular momentum from the system). Now, loss of angular momentum results in decreasing the separation a, and an increase of the orbital frequency Ω, whilst the spin frequencies of the components remain at best constant (if all of the angular momentum lost comes from the orbit), or decrease. Tides try to restore synchronism by supplying some of the excess orbital angular momentum to the spins, which in turn leads to further decrease in the orbital separation, and a further increase in Ω. Thus the positive feedback between the spin and the orbit when $a < a_{\rm min}$ leads to an unstable situation, which is referred to as the 'tidal instability'. If, however, a system gets into contact *before* reaching $a_{\rm min}$, then the effects of mass transfer and the resulting angular momentum redistribution can lead to an increase in the orbital separation, away from the tidal instability. Whether the system gets into contact before or after $a_{\rm min}$ depends on the mass-radius relationship and the compactness of the component stars under consideration.

Let us consider for simplicity, polytropic stars which obey a mass radius relationship:

$$R_i = \left(\frac{K_i}{N_n G}\right)^{\frac{n}{3-n}} M_i^{\frac{n-1}{n-3}} \tag{2.41}$$

where, K_i is the polytropic constant, n is the polytropic index and N_n is a numerical factor which is a function of n (Chandrasekhar, 1939). Consider the case when $q =$

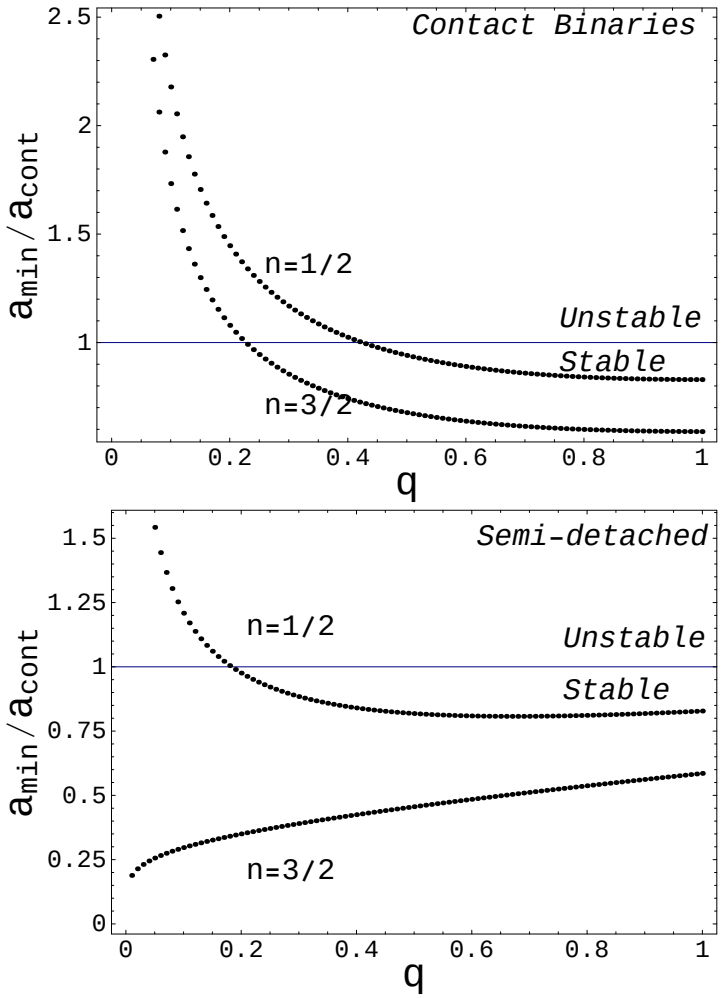

FIGURE 2.3. Minimum separation and the separation at contact for n=1/2 and n=3/2 for semi-detached (polytropic constant $K_1 = K_2$) and contact binaries ($K_1 \neq K_2$). *Top Panel:* Plot of $a_{\rm min}/a_{\rm cont}$ as a function of q for a $n = 1/2$ polytrope and $n = 3/2$ polytrope for **Contact binaries**. In the case of $n = 3/2$ ($k_i \sim 0.2$) polytropes, for mass ratios $q \leq 0.2$, the binary reaches the tidal instability before it becomes semi-detached. On the other hand, the $n = 1/2$ ($k_i \sim 0.4$) polytropes are unstable for $q \leq 0.4$. Notice that minimum value of the mass ratio $q_{\rm min} \sim k_i$ for each case. *Bottom Panel:* Plot of $a_{\rm min}/a_{\rm cont}$ as a function of q for a $n = 1/2$ polytrope and $n = 3/2$ polytrope for **Semi-detached binaries**. In the case of $n = 1/2$ polytropes, for mass ratios $q \leq 0.2$, the binary reaches the tidal instability before it becomes semi-detached. On the other hand, the $n = 3/2$ polytropes are stable for all values of q.

1 for a $n = 1/2$ polytrope and $k_i = 1/5$. This corresponds to a contact binary with components satisfying a 'stiff' equation of state, which corresponds to say, a binary consisting of neutron stars. Thus in this case we find, $a_{\rm min}/2R \sim (6/5)^{1/2} > 1$, i.e., the binary reaches the instability limit before it can get into contact. This implies that for stiff equations of state like $n = 1/2$, the tidal instability can quickly set in, which leads to merger over dynamical timescales. On the other hand, for $k_i = 1/5$,

corresponding to softer equations of state (for example n=3/2), and in this case $a_{\rm min}/2R \sim (3/5)^{1/2} < 1$, and thus the system gets into contact before it reaches the tidal limit.

In nature, one finds contact binaries with mass ratios different from unity. From the mass-radius relation we are considering here, in order for the masses of the components of a contact binary to have different masses and yet for both of them to fill up their Roche lobes, they must have different K_i's. Specifically, the more massive component (which has a smaller radius if the K's are the same but a larger Roche lobe), has to have a larger polytropic constant in order to puff-up the star upto its Roche surface. Thus, for such contact binaries, the moment of inertia of the more massive component is much greater than the less massive component, $I_1 >> I_2$. In such cases, we have

$$a_{\rm min} = k_i \Big[\frac{3(1+q)}{q}\Big]^{1/2} R_1 \tag{2.42}$$

The contact condition for such systems can be obtained by requiring $R_i = R_{L_i}$, i.e., the radii of the stars equal their respective Roche lobe radii. For $n = 3/2$ ($k_i = 0.2$) polytropes, we thus have a value of q below which the the system always reaches this minimum before it gets into contact. Rasio (1995) realized that an (fortuitous) approximate relationship exists between this minimum value of the mass ratio $q_{\rm min}$ and the dimensionless radius of gyration k_i given by $k_i \approx q_{\rm min}$ (Fig. 2.3).

In the above discussion we are considering contact binaries, which allows us to make certain simplifications. In general, for semi-detached binaries, whether $a_{\rm cont}$ is greater than or less than $a_{\rm min}$, will depend on both the equation of state and the mass ratio (See Fig. 2.3, bottom panel). If the donor has a relatively soft equation of state and if $q \neq 1$, the binary tends to become semi-detached and mass-transfer occurs before it falls prey to the tidal instability mentioned above. Mass transfer changes the initial configuration as the system evolves and may either drive the system to smaller separations and thus closer to the onset of the tidal instability or to larger separations and toward stability.

In Fig. 2.4, we plot the total angular momentum for a synchronous $n = 3/2$ polytrope as a function of orbital separation using Eq. 2.2 (dashed curve). This curve can be thought of as a series of equilibrium models with the same total mass and mass ratio, but achieving contact at smaller and smaller separations. Alternatively, one can think of the red curve as the evolution of a detached system, slowly driven to smaller orbital separations by the loss of orbital angular momentum. The white dwarf, represented here as a $n = 3/2$ polytrope, achieves contact much before the minimum separation corresponding to the tidal instability $a_{\rm min}$ (solid curve in Fig. 2.4), and evolves to a higher separation. On the other hand, a $n = 1/2$ polytrope, which is a much stiffer equation of state corresponding to say a neutron star, achieves contact much closer to $a_{\rm min}$, and is much more prone to the tidal instability.

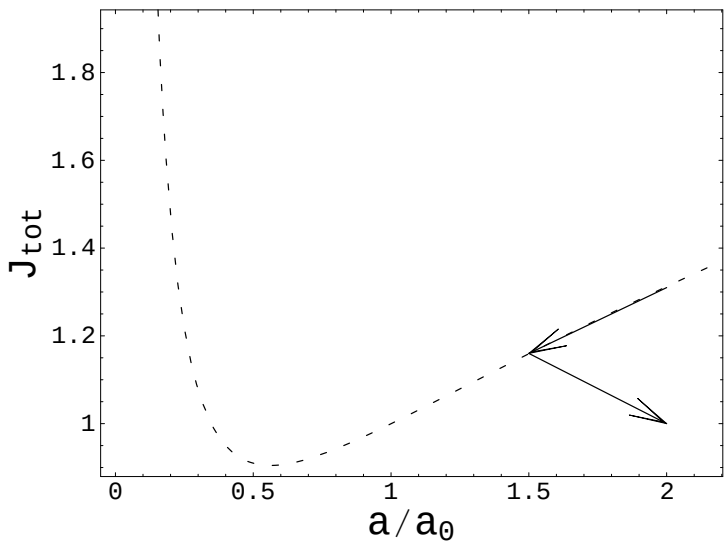

FIGURE 2.4. Plot of the total angular momentum for the synchronous case against the orbital separation. The dashed curve represents a series of models when contact is reached, for a fixed total mass. The solid curve represents the evolution of a DWD binary with $q = 0.2$, which gets into contact much before $a_{\rm min}$ and evolves to higher separation as indicated by the arrows, thus avoiding the tidal instability.

Note that in the above analysis, we have assumed that the stars are not tidally distorted, and that the Roche limit serves as the point at which the donor gets into contact, which are both rather crude approximations, especially whilst considering neutron stars ($n = 1/2$). We thus expect our results to be a fair representation at least in a qualitative sense, though the exact values of $q_{\rm min}$, $a_{\rm min}$ and so on may be different.

3. Analytic Solutions

Before embarking upon studying the complete numerical solutions for the evolution equations we derived in Chapter 2 for different astrophysical scenarios, we obtain analytic solutions for the time evolution of the mass transfer rate. We can do this only on the assumption that most of the parameters characterizing the binary remain constant or evolve slowly as compared to the evolution of the mass transfer rate. Webbink and Iben (1987) were among the first to attempt such analysis and following them, we generalize their results to an arbitrary polytropic index and to isothermal atmospheres. Analytic solutions are useful in providing physical insights into the expected behavior of the binary system in the limit where the assumptions imposed to obtain the analytic solutions are valid approximately.

3.1 Polytropic Binaries

Polytropic stars are used in many 3-D hydrodynamic simulations to study the dynamic behavior of binaries D'Souza et al. (2006) because of their simple structure. We shall thus obtain analytic as well as numerical solutions for a general polytropic index n to compare our results with those obtained from a full numerical evolution. The mass transfer rate for a polytropic donor is given by Jędrzejec (1969) assuming laminar flow, and quoted by Paczyński & Sienkiewicz (1972) is given by

$$-\dot{M}_2 = \dot{M}_0 \Big(\frac{R_2 - R_{\rm L}}{R_2} \Big)^{n+3/2} \tag{3.1}$$

Raising both sides of the above equation to the power $2/(2n+3)$ and differentiating, we obtain

$$\frac{\rm d}{{\rm d}t}(-\dot{M}_2)^{2/2n+3} = (\dot{M}_0)^{2/2n+3}[(\nu_2 - \nu_{\rm L}) + \frac{\dot{M}_2}{M_2}(\zeta_2 - \zeta_{\rm L})], \tag{3.2}$$

where we have set the factor $R_{\rm L}/R_2$ to unity, given that in most situations $\Delta R_2 \ll R_2$. The analytic solutions discussed here assume that the driving rates ν_2 and $\nu_{\rm L}$ remain constant while the depth of contact changes. This is only approximately true; and a self-consistent solution will require numerical integrations. It is instructive to first look at the implications of equation (3.2) when no driving is present. This is a situation we encounter in some large-scale hydrodynamic simulations of mass transfer in polytropic binaries (D'Souza et al., 2006). Defining a positive dimensionless mass transfer $y = (-\dot{M}_2/\dot{M}_0)^{2/(2n+3)}$, and a characteristic time scale $\tau = M_2/\dot{M}_0$, eq. (3.2) becomes

$$\frac{{\rm d}y}{{\rm d}t} = -\frac{\zeta_2 - \zeta_{\rm L}}{\tau} y^{n+3/2}. \tag{3.3}$$

The solution can be easily inverted to yield

$$y(t) = y(0)\left[1 + y(0)^{n+1/2}(n+1/2)(\zeta_2 - \zeta_{\rm L})t/\tau\right]^{-\frac{2}{2n+1}}\ , \tag{3.4}$$

where $y(0)$ is the initial mass transfer rate, normalized as above. We note that in the stable case, $\zeta_2 > \zeta_{\rm L}$ ($q < q_{\rm stable}$), the mass transfer decays asymptotically to zero over a characteristic time $\tau_{\rm chr} = \tau/[(n+1/2)y(0)^{n+1/2}(\zeta_2 - \zeta_{\rm L})]$, whereas in the unstable case, $\zeta_2 < \zeta_{\rm L}$ ($q > q_{\rm stable}$), it will blow up in finite time equal to $\tau_{\rm chr}$. Thus, the essence of the stability of mass transfer in a binary is already contained in the simple case of no driving. The presence of driving exacerbates the natural instability or, in the stable case, it settles asymptotically to a non-zero stable mass transfer, which we observe in AM CVns, CVs and LMXBs.

Returning now to Eq. (3.2), with the same definitions as above for y and τ, we obtain for the general case in which driving is present,

$$\frac{{\rm d}y}{{\rm d}t} = -\frac{\zeta_2 - \zeta_{\rm L}}{\tau}(y^{n+3/2} - y_{\rm eq}^{n+3/2})\,, \tag{3.5}$$

where $y_{\rm eq}^{n+3/2} \equiv -(\dot{M}_2)_{\rm eq}/\dot{M}_0 = (\nu_2 - \nu_{\rm L})\tau/(\zeta_2 - \zeta_{\rm L})$ is the equilibrium value normalized to $\dot{M}_0$. Note that in the stable case, this value is positive; while it is negative in the unstable case. Before we attempt to solve the above differential equation, it is clear from its form and the signs just discussed, that it describes a stable solution in which $y \to y_{\rm eq}$ when $q < q_{\rm stable}$. If, however, $q > q_{\rm stable}$, the r.h.s is positive even if the mass transfer vanishes initially, and it just gets bigger as the mass transfer grows. Since y diverges for the no-driving case in a finite time, the driven case diverges even sooner.

Considering Eq. 3.2 again, we define $y_* \equiv [\dot{M}_2/(\dot{M}_2)_{\rm eq}]^{2/(2n+3)}$, and $1/\tau_* \equiv (\nu_2 - \nu_{\rm L})(\dot{M}_2/|(\dot{M}_2)_{\rm eq}|)^{2/(2n+3)}$. The differential equation for the evolution of mass transfer now becomes

$$\frac{{\rm d}y_*}{{\rm d}t} = {\rm sgn}(y_*)\frac{1}{\tau_*}(1 - {\rm sgn}(y_*)|y_*|^{n+3/2}) \tag{3.6}$$

where ${\rm sgn}(y_*)$ is the sign of y_*. Thus, for the stable case $y_* > 0$, while $y_* < 0$ for the unstable case, and τ_* is defined positive. The general analytic solution comprising both the stable and the unstable case can be given in terms of the hypergeometric function, as follows

$$\frac{t}{\tau_*} = y_{*2}F_1(1, \frac{1}{n+3/2}; 1 + \frac{1}{n+3/2}, {\rm sgn}(y_*)|y_*|^{n+3/2}) \tag{3.7}$$

Though it is not possible to invert this general solution to obtain the mass transfer rate y as a function of time, particular solutions for specific values of n can be inverted to obtain simple solutions. For example, $n = 3/2$ yields the Webbink-Iben solution

$$\frac{t}{\tau} = -\frac{1}{2}\ln\Big[\frac{(1-y)^3}{(1-y^3)}\Big] + \sqrt{3}\,[\arctan\Big(\frac{2{\rm y}+1}{\sqrt{3}}\Big) - \frac{\pi}{6}] \tag{3.8}$$

where, $y = (-\dot{M}_2/\mu)^{1/3}$, $\tau = \frac{1}{3}\left\{\frac{\dot{M}_0}{M_2}(\zeta_2 - \zeta_L)(\nu_2 - \nu_L)\right\}^{-1/3}$.

Likewise, $n = 1/2$ yields

$$\begin{array}{lcll} y_* & = & -\tan(t/\tau_*) & y_* < 0 \quad \text{unstable} \\ y_* & = & \tanh(t/\tau_*) & y_* > 0 \quad \text{stable} \end{array} \tag{3.9}$$

3.2 Isothermal Atmospheres

In case of isothermal atmospheres, the mass transfer rate Ritter (1988) is given by:

$$\dot{M}_2 = -\dot{M}_0 \, e^{(R_2 - R_\mathrm{L})/H} \tag{3.10}$$

where, H is the scale height. This form of the mass transfer equation is much simpler to integrate than the one for the polytropes considered above. With the same approximations and notation as in the steps leading to Eq. (3.5), and defining $y = -\dot{M}_2/\dot{M}_0 = \exp((R_2 - R_\mathrm{L})/H)$, we obtain

$$\frac{1}{y}\frac{dy}{dt} = -\frac{\zeta_2 - \zeta_\mathrm{L}}{\tau}\frac{R_2}{H}(y - y_\mathrm{eq}) \, . \tag{3.11}$$

This is easily integrable and invertible to get the following:

$$y = \frac{y_\mathrm{eq}}{1 - (1 - y_\mathrm{eq}/y_0)e^{-t/\tau_\mathrm{iso}}} \tag{3.12}$$

where $\tau_\mathrm{iso} \equiv H/R_2(\nu_2 - \nu_\mathrm{L})$ is the timescale required for the driving to change the depth of contact by $\sim H$, and y_0 is the initial value, always positive for physically meaningful cases. In the stable case $y_\mathrm{eq} > 0$, and $y \to y_\mathrm{eq}$, while $y_\mathrm{eq} < 0$ for the unstable case and y diverges in a finite time $t_\mathrm{div} = \tau_\mathrm{iso} \ln(1 - y_\mathrm{eq}/y_0)$. If no driving is present, we may set $y_\mathrm{eq} = 0$ and integrate Eq. (3.11) for an isothermal donor. The result is again simple and instructive

$$y = \frac{y_0}{1 + (\zeta_2 - \zeta_\mathrm{L})y_0 \frac{R_2}{H}\frac{t}{\tau}} \, . \tag{3.13}$$

In the stable case, for any initial mass transfer, the system will detach and mass transfer will tend to zero. In the unstable case, any non-zero initial mass transfer will grow and diverge in a finite time.

3.3 The Webbink-Iben Binary

It is worthwhile to describe the binary parameters used by Webbink & Iben (WI, Webbink & Iben (1987)) in their pioneering analysis in some detail, since we are using it as a comparison to our numerical solutions in Chapter 4. In Table 3.1 we specify the parameters of the binary at its *initial state*. For the initial parameters for the WI binary, it turns out that the adiabatic coefficients $\zeta_2 \sim$ -0.64 and $\zeta_{L_2} \sim$

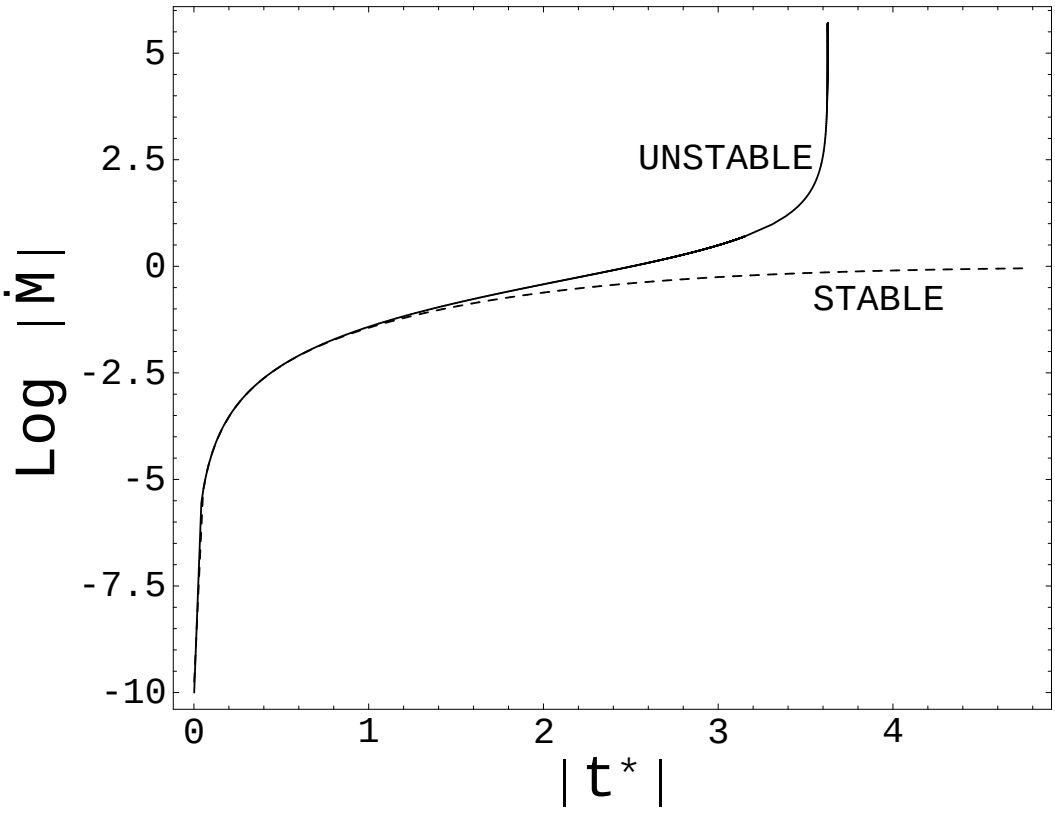

FIGURE 3.1. The Webbink-Iben solutions for the stable (dotted line) and unstable cases.

-0.48. Note that since $|\zeta_2| > |\zeta_{L_2}|$; the radius of the star increases at a rate faster than the Roche lobe radius, and the resulting mass transfer is unstable.

The analytic solutions, both the stable and the unstable, are shown in Fig. 3.1. Note that initially, the stable and unstable solutions almost exactly overlap. This is true as long as the system is either detached or the depth of contact is relatively small. As soon as the binary evolves to deeper contact, the unstable solution diverges rapidly and blows up in a finite time. This corresponds physically to catastrophic mass transfer in the binary – either super-Eddington accretion, tidal disruption of the donor or more likely, a merger over dynamic timescales after a brief phase of common envelope evolution (Webbink & Iben, 1987). Note

TABLE 3.1. Initial parameters of the Webbink-Iben binary

		Primary	Secondary
Mass	M ($M_\odot$)	1.1	0.62
Radius	R ($R_\odot$)	0.0072	0.0124
Roche Lobe Radius	R (R_L)	0.429	0.331
Orbital Separation	a ($R_\odot$)	0.0376	
Orbital Period	P (s)	55.8	

that this outcome is predicted by the unstable analytic solution which has been obtained by assuming that the basic primary parameters: the mass ratio q, driving rate ν_L and the masses of the components do not change during the evolution. This is obviously not true, especially in the unstable case, since by definition in the unstable case these parameters are evolving rather rapidly. As we shall see in the next chapter, when the system parameters are allowed to change, the binary can transit from an unstable to a stable system and follow the red curve in Fig. 3.1.

4. Numerical Solutions

In the previous two chapters, we have derived the evolution equations and the corresponding analytic solutions for different cases, under certain restrictive approximations. These analytic solutions are a useful reference to compare our numerical results to, since in the limit that the assumptions used to derive the analytic solution are met, the numerical solutions should approach the analytic ones. However, in general, the analytic solutions cannot explain the behavior of a given system accurately and especially when the system evolves rapidly, solving the evolution equations numerically leads to a different outcome than what one would expect analytically. In the following sections, we describe some of the numerical results for a generic binary Webbink & Iben (1987), followed by more examples of different classes of binaries that can be described by numerically integrating the evolution equations.

4.1 Limitations of the Analytic Solutions

The analytic solutions of Chapter 3 are obtained under the following assumptions:

1. The driving rate given by ν_L is constant throughout the evolution,
2. The separation a of the binary is effectively constant even though the mass transfer rate changes, which is not true for a 'real system' (see Eq. 2.16).
3. The tidal effects are effectively ignored,
4. Super-Eddington accretion (See Section 4.2) is not accounted for,
5. A system that is initially unstable ($q > q_{\rm stable}$), remains so throughout the evolution, since q is assumed to be the same throughout. As we shall see below, since q is itself evolving, it is possible for an initially unstable system to evolve to a stable configuration.

In order to overcome some of these shortcomings one has to numerically integrate the evolution equations in a self-consistent way. In particular, in what follows, we allow for the changes in the masses of the components assuming conservative mass transfer (and hence the mass ratio q), allow the binary separation to change as a result of any driving present, and compute the values of ζ_2 and $\zeta_{\rm L}$ as they evolve. The values of ζ_2 depend on the adopted mass-radius relationship for the donor. To calculate $\zeta_{\rm L}$, we need to specify how the mass and angular momentum are redistributed in the binary during mass transfer – which depends on the particular case at hand. For example, it depends on whether the stream impacts the accretor or if an accretion disk is present; if the mass transfer is subcritical and conservative,

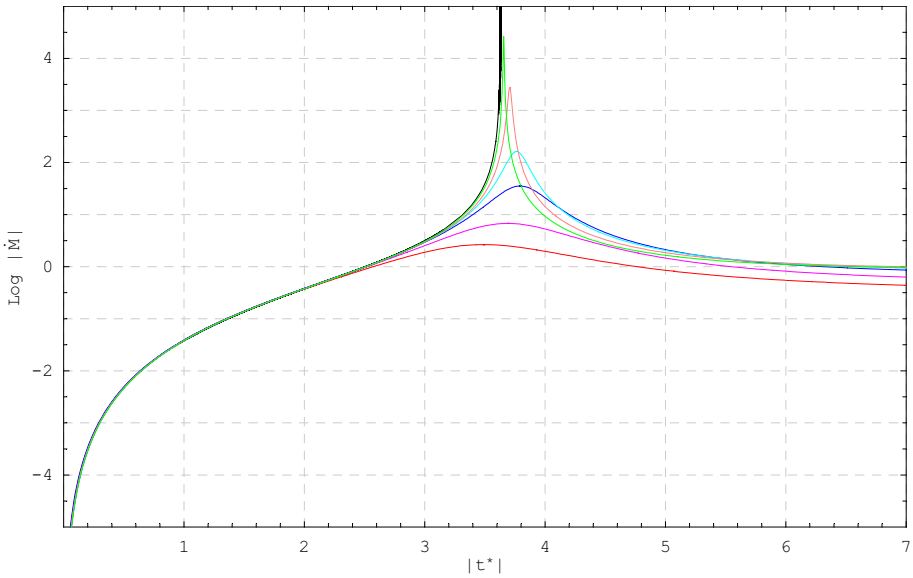

FIGURE 4.1. Numerical and Analytic Solutions for Polytropes. Comparison of numerical integrations with the analytic solution by Webbink and Iben. The mass transfer rate normalized to the *initial* equilibrium rate as a function of time in units of the *initial* τ: Analytic (Black curve) and numerical – green ($q = 0.663$), orange (0.613), cyan (0.563 same as WI), blue (0.543), magenta (0.523) and red (0.513).

or if mass and angular momentum are being ejected from the system following supercritical mass transfer.

We begin our investigation by considering one of the simplest cases – the WI binary – the analytic solution for which we derived in Chapter 3. We simulate exactly the same initial conditions as the ones assumed to derive the analytic solution – a constant driving rate and the same mass-radius relationship. We then relax the constraints and let the system evolve in a self-consistent manner for different values of the mass ratio q. The results are shown in Fig. 4.1 where we plot the mass transfer rate normalized to the equilibrium rate against time normalized to the initial τ. We observe that initially all the curves overlap, but as the depth of contact increases, the mass transfer rate increases. The rate of increase is a function of $q - q_{\rm stable}$ which defines how unstable the initial configuration is. Consequently, the curves begin to deviate with the most unstable curve having the sharpest spike. As the system evolves, the orbital separation, which is decreasing initially, begins to increase as per Eq. 2.16 which in turn decreases the driving rate. At some point during the evolution q becomes less than $q_{\rm stable}$ and the system evolves to stable mass transfer rates. From our analysis in Section 2.3, we expect the systems with $q > q_{\rm stable}$ to be unstable, and the higher the mass ratio, the more unstable the system is. This is indeed what we observe in the numerical solutions. We observe that though some of the systems are *initially* unstable, they evolve to stable mass transfer after an initial spike. As we have seen in Chapter 3, $q_{\rm stable} \sim 0.49$ for the WI binary. Consequently, the analytic solutions for any $q > 0.49$ follow the unstable curve and diverge in a finite time. On the other hand, the numerical

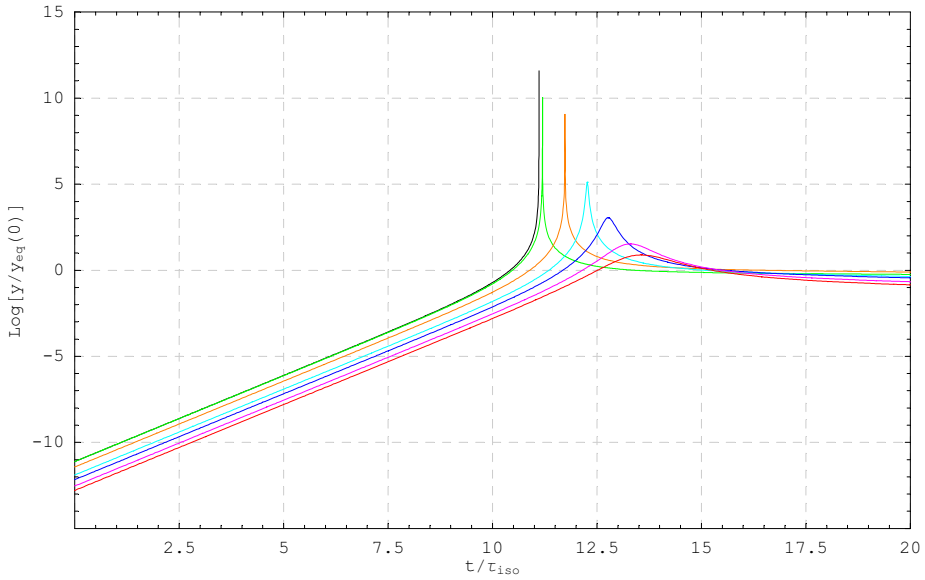

FIGURE 4.2. Comparison of numerical integrations with the analytic solutions for isothermal atmospheres. The natural logarithm of the mass transfer rate normalized to the *initial* equilibrium rate for the case with $q = 0.663$, is shown as a function of time in units of $\tau_{\rm iso}$: Analytic (Black curve) and numerical – green ($q = 0.663$), orange (0.613), cyan (0.563 same as WI), blue (0.543), magenta (0.523) and red (0.513).

solutions reach a peak in the mass transfer rate in a finite time, but turn around and a stable mass transfer is established. We must keep in mind though, that the OAE we use for our numerical integrations themselves break down whenever the system parameters change significantly over timescales of approximately an orbital period. In any case, our results suggest and demonstrate that at least some of the binaries that start off unstable do survive the mass transfer instability and evolve into systems like AM CVn – evolving to higher separations and diminishing mass transfer rates. This result, which is not predicted by the analytic solution, has important consequences for population synthesis, understanding AM CVn type systems and for understanding 3-D hydro-simulation results, as we shall see in Chapter 5.

In Fig. 4.2, we plot the analytic and numerical solutions for an isothermal donor for different values of the mass ratio. Unlike the polytropic donor case, which has a fixed reference point where the donor fills its Roche Lobe ($R_2 = R_{\rm L}$), the isothermal case does not have a fixed reference point to which we can normalize our results. We, rather arbitrarily start the integrations when the depth of contact is $R_2 - R_{\rm L} = -11.5H$, corresponding to an initial mass transfer rate of 10^{-5} of the reference rate. The behavior of the systems is qualitatively the same as the polytropic donors. Note that the y-axis in Fig. 4.2 is the natural logarithm of y which from Section 3.2, is just the depth of contact $R_2 - R_{\rm L}$ in units of the pressure scale height H, normalized to the reference depth corresponding to the equilibrium rate for $q = 0.663$.

Another aspect of mass transfer that can alter the evolution of the binary which the analytic solutions are unable to account for, is mass loss due to super-Eddington accretion. We discuss this next followed by some simple examples of binary evolutions based on our OAE.

4.2 Super-Eddington Accretion

Han & Webbink (1999) discuss the possibility of mass transfer at rates higher than the Eddington rate, which results in mass loss from the system. The Eddington Luminosity (Frank et al., 2002) is given by

$$L_{\rm Edd} = \frac{4\pi R_1^2 cg}{\kappa} \tag{4.1}$$

where, $\kappa = 0.2(1+X){\rm cm}^2{\rm g}^{-1}$ is the opacity of the accreted gas. X is the hydrogen mass fraction of the gas, which we assume is zero. The accretion luminosity is a function of the potential difference between the L_1 point and the surface of the accretor R_1 and given by

$$L_{\rm acc} = \dot{M}_2(\phi_{\rm L_1} - \phi_{\rm R_1}), \tag{4.2}$$

Thus the Eddington mass transfer rate is given by

$$\dot{M}_{\rm Edd} = \frac{4\pi R_1^2 c\bar{g}}{\kappa(\phi_{\rm L_1} - \phi_{\rm R_1})} \tag{4.3}$$

where $\bar{g}$ is the mean surface gravity on the accretor –

$$\bar{g} = \frac{GM_1}{R_1^2} - \frac{2}{3}R_1\frac{GM}{a^3} \tag{4.4}$$

If $-\dot{M}_2 > \dot{M}_{\rm Edd}$, radiation pressure is capable of driving mass away from the accretor even as it approaches the accretor via the L_1 point. As described by Han & Webbink (1999), we assume that any accretion luminosity in excess of the accretion luminosity helps in driving mass loss from the system, but the radiative losses do not contribute to the mass flow. Assuming that a fraction β of the mass is lost from the system such that $\dot{M}_2 = -\beta\dot{M}_1$ we have from energy conservation

$$\beta = \frac{L_{\rm Edd}}{\phi_{\rm R_1}\dot{M}_2} + \frac{\phi_{\rm L_1}}{\phi_{\rm R_1}} \tag{4.5}$$

The evolution equations we have derived before need to be modified to account for the mass loss from the system. We thus have

$$\dot{J}_1 = -\beta\dot{M}_2 j_1 + \dot{J}_{1,\rm tid} \ , \tag{4.6}$$

$$\dot{J}_2 = \dot{M}_2 j_2 + \dot{J}_{2,\rm tid} \ , \tag{4.7}$$

$$\dot{J}_{\rm orb} = \dot{J}_{\rm sys} - \left(-\dot{M}_2[\beta j_1 - j_2 + (1-\beta)j_{\rm w}] + \dot{J}_{1,\rm tid} + \dot{J}_{2,\rm tid}\right) \ , \tag{4.8}$$

$$\frac{\dot{a}}{2a} = \frac{\dot{J}_{\rm orb}}{J_{\rm orb}} - \frac{\dot{M}_2}{M_2}\left(1 - \beta q - \frac{1-\beta}{2(1+q)}\right) \ . \tag{4.9}$$

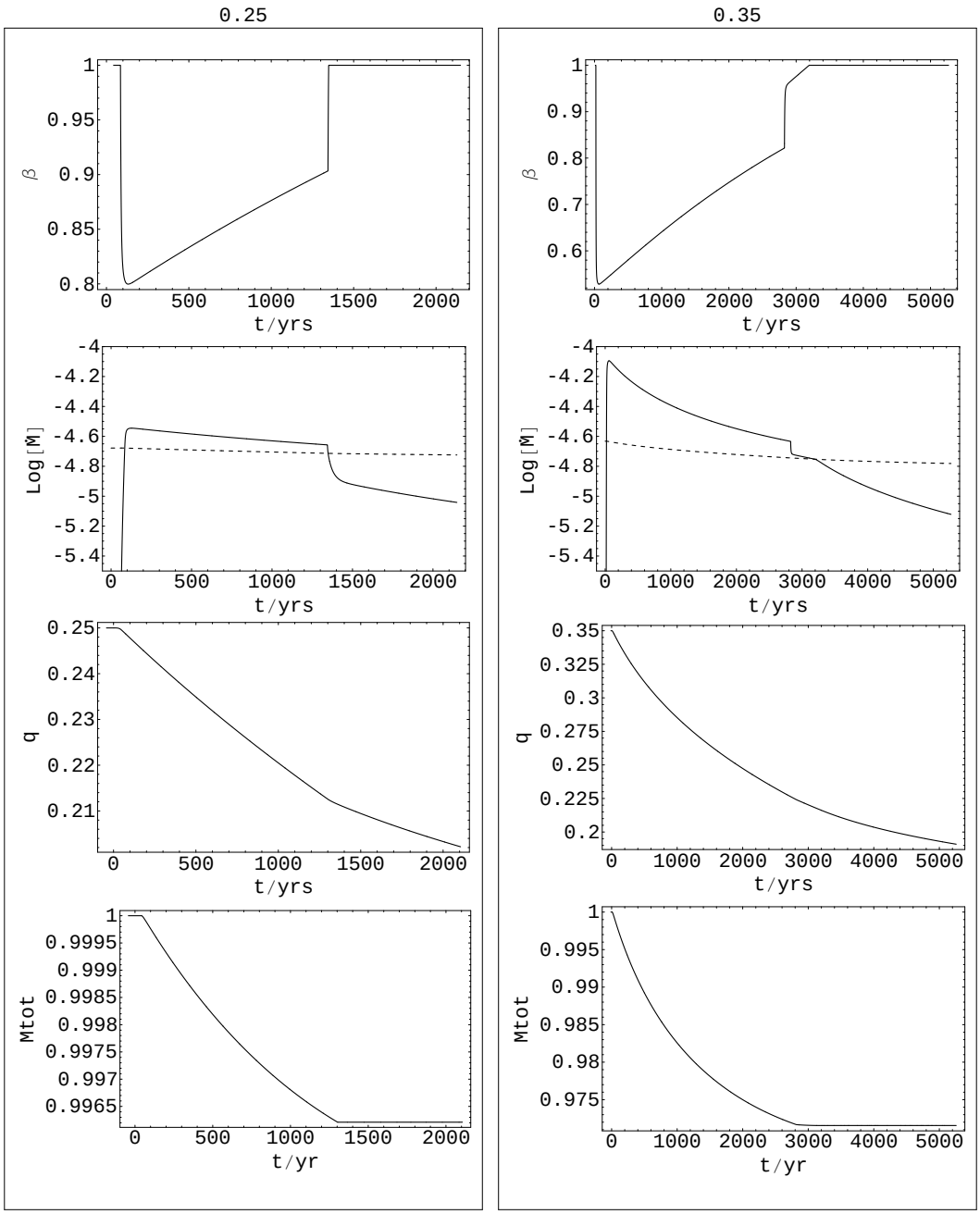

FIGURE 4.3. Super-Eddington Accretion. Various parameters for super-Eddington accretion with direct impact with $q = 0.25$, just above $q_{\rm stable}$ and $q = 0.35$, well above $q_{\rm stable}$. The panels show from the top down: the accreted fraction β; the logarithm of the mass transfer rate and the corresponding critical rate (dashed line) in $M_\odot$/yr; the mass ratio q; and the total mass normalized to the initial value. The abscissa shows times in years from the time of first contact. The lower q accretes at super-Eddington rates for less time as compared to the higher q; and it does so more gradually losing less mass (last panel). Even for the initially more unstable mass transfer (larger q), the fraction of mass lost is below 3%.

It is reasonable to assume that the specific angular momentum of the material blown away equals that of the stream in case of a DI system : $j_{\rm w} = j_1$. When the stream forms a disk around the accretor, the specific angular momentum carried by the wind is more difficult to calculate since it depends on the details of the flow. These considerations are beyond the scope of our study, and for simplicity we assume that $j_{\rm w} = j_1$ throughout. Thus Eq. 4.8 reduces to Eq. 2.15 and Eq. 4.9 reduces to Eq. 2.17 if we define

$$q_a \equiv 1 + (1-\beta)q - \frac{1-\beta}{2(1+q)} - M_2 \frac{\beta j_1 - j_2 + (1-\beta) j_{\rm w}}{J_{\rm orb}} \ , \qquad (4.10)$$

Note that when $\beta = 1$, the above expression reduces to eq. (2.18), as it should. Also, the explicit appearance of q above implies that q_a must be calculated self-consistently during the evolution. Notice that since the mass loss is proportional to the mass transfer rate, the critical value of q which determines the stability properties of the initial configuration of the binary, $q_{\rm stable}$, is different than what it would be in the absence of mass loss due to Super-Eddington mass transfer.

Fig. 4.3 shows two examples of evolutions with a super-critical mass-transfer phase. Because the OAE do not include tidal distortions of the components or dissipative effects (arising for example from friction during a common envelope phase) they always predict survival, no matter how high the mass transfer rate gets during an unstable phase.

4.3 Examples

In the next chapter, we shall employ the evolution equations to investigate different aspects of compact binary evolution in detail. Before we embark on this, we illustrate below simple applications of the OAE in order to demonstrate that when the proper limiting conditions or approximations are imposed (like ignoring tides or direct impact accretion or the advective terms), known results can be extracted from our generalized treatment.

4.3.1 Double White Dwarfs & AM CVn Type Systems

As discussed in Section 1.4, DWD binaries are compact binaries in which both components are either Helium or C/O white dwarfs. AM CVn systems are a particular type of DWDs; characterized by mass transfer and extremely short orbital periods. Because of the mass-radius relation for white dwarfs, the radius of a less massive white dwarf is greater than the radius of a white dwarf with higher mass. Indeed, a mass transferring donor is expected to increase in size as a consequence of mass transfer. One consequence of this is that the orbital separation of an AM CVn type systems increases as a result of mass transfer. We have described the observational properties and models to explain the observations in Section 1.4. Here we concentrate on the dynamical properties of the binary and how our orbit averaged equations (OAE) predict the evolution of these systems. The mass-radius relationship for old, cold white dwarf donors is given by Verbunt & Rappaport

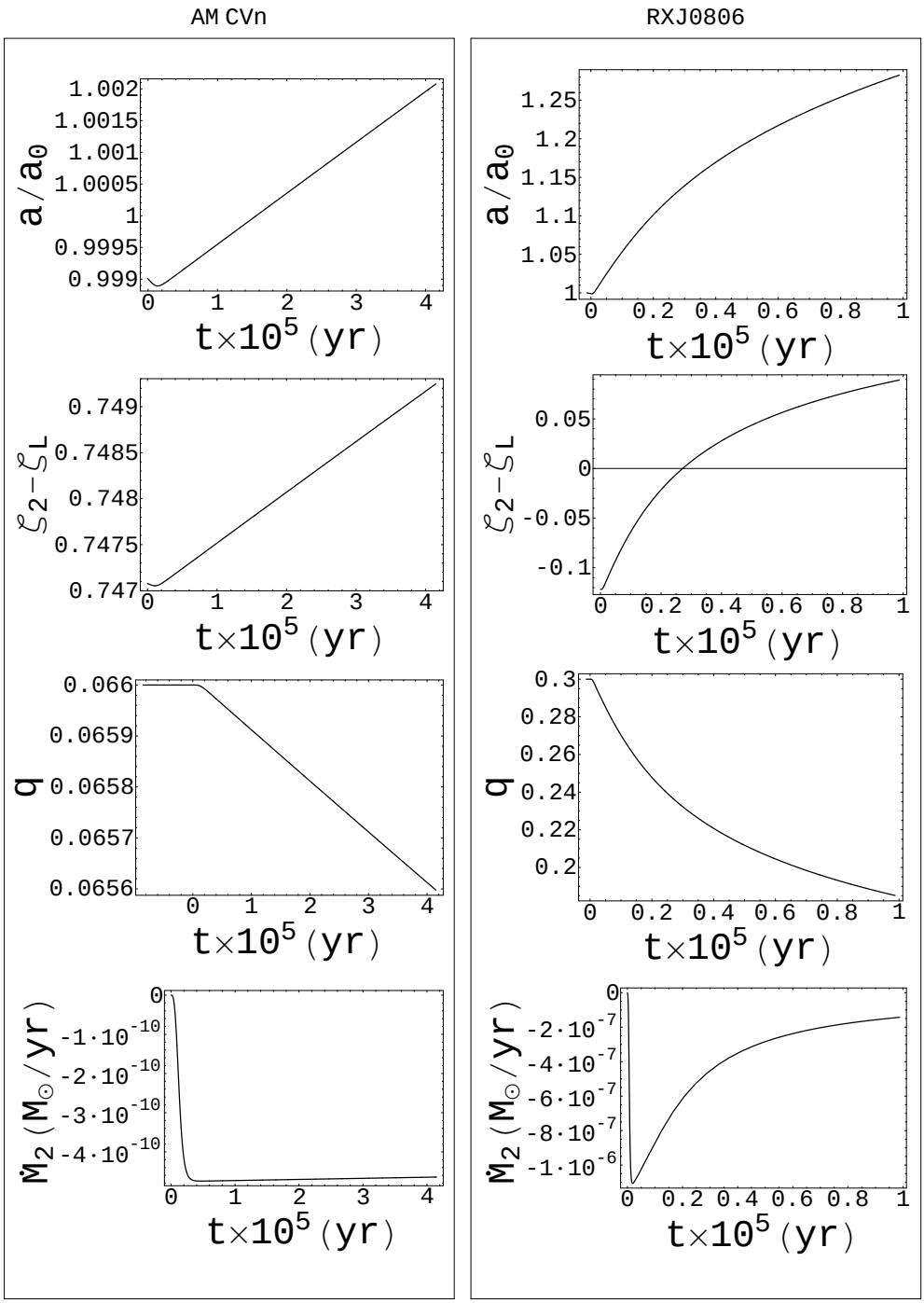

FIGURE 4.4. Evolution of typical AM CVn systems under simplified conditions: AM CVn (left panel) and RXJ0806 (right panel). Notice the relatively rapid rate of evolution for RXJ0806, which in its initial state is marginally unstable ($\zeta_2 - \zeta_L < 0$), but evolves to a state of stability ($\zeta_2 - \zeta_L > 0$) eventually. The overall mass transfer rate for RXJ0806 rises to at least 3 orders of magnitude over AM CVn. Note that the initial periods for the two systems are $\sim$ 350 s (RXJ0806) and $\sim$ 1120 s (AM CVn) resulting in a much higher driving rate in the former system.

(1988)

$$R_i = 0.01125\Big[\Big(\frac{M_i}{M_{\rm ch}}\Big)^{-2/3} - \Big(\frac{M_i}{M_{\rm ch}}\Big)^{2/3}\Big]^{1/2}\Big[1 + 3.5\Big(\frac{M_i}{M_p}\Big)^{-2/3} + \Big(\frac{M_i}{M_p}\Big)^{-1}\Big]^{-2/3} R_\odot \tag{4.11}$$

where $M_{\rm ch} = 1.44 M_\odot$ and $M_{\rm p} = 0.00057 M_\odot$. This relation has the advantage that it can be used over the entire range of relevant white dwarf masses: $0 < M_i < 1.44 M_\odot$. In the range where $M_i >> M_{\rm p}$ and $M_i < M_{\rm ch}$, $R_i \propto M_i^{-1/3}$ as is expected for white dwarfs. We plot the mass-radius relation for a white dwarf in Fig. 4.5. Using Eq. 2.6 and $R_i \propto M_i^{-1/3}$, the orbital period at the point of initial contact can be calculated be demanding $R_2 = R_{\rm L_2}$ which yields

$$\begin{aligned} P &\approx 2\pi \left[\frac{0.014}{0.462}\Big(\frac{1}{M_{\rm ch}}\Big)^{-1/3}\right]^{3/2}\Big(\frac{R_\odot^3}{G}\Big)^{1/2}\frac{1}{M_2} \\ &= 63.39\left(\frac{M_\odot}{M_2}\right) \text{ seconds} \end{aligned} \tag{4.12}$$

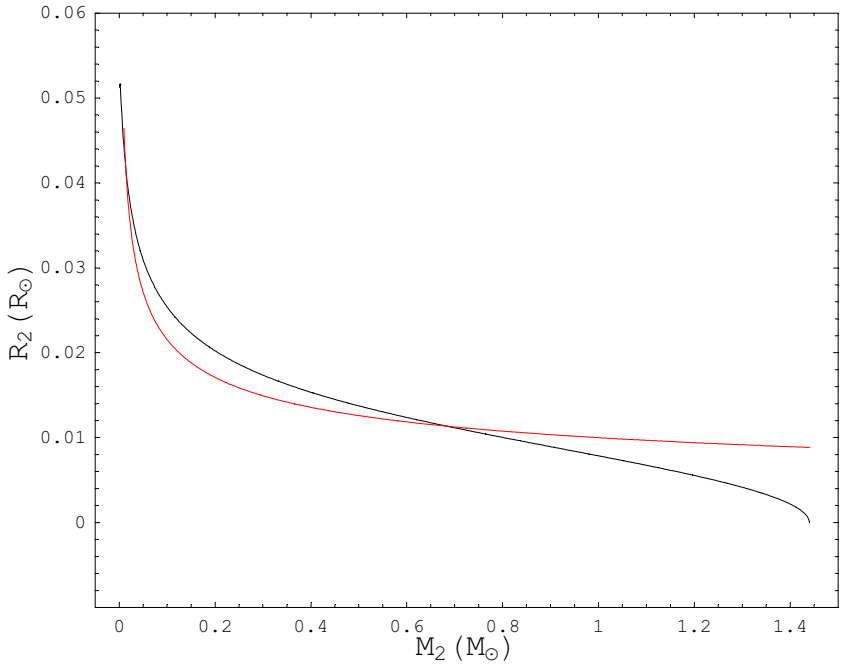

FIGURE 4.5. The Nauenberg Mass-Radius Relationship (black curve). The red curve represents the standard polytropic relationship $R_2 \propto M_2^{-1/3}$.

This implies that for a donor of mass $0.1 M_\odot$, the period at which contact occurs is approximately 634 seconds, which is of the order of the shortest periods in Table 1.1. In general, the period of contact also depends on the total mass and the mass ratio q – we have used simplified equations for R_2 and R_L to derive Eq. 4.12. We are now in a position to explore the evolution of a typical AM CVn system. We choose a couple of systems with typical values of the known AM CVn systems: RXJ0806

($M_1 = 0.4M_\odot$, $M_2 = 0.12M_\odot$) and AM CVn itself ($M_1 = 0.5M_\odot$, $M_2 = 0.033M_\odot$) for illustrative purposes. Note that RXJ0806 is 'peculiar' in that the orbital period of this object appears to be decreasing. We shall explore some possibilities as to why this might be the case in the next chapter. Here, for the sake of simplicity, we ignore complicating physical mechanisms like tides, and instead assume that the donor is completely synchronized with the orbit, and the accretor is completely decoupled. This is close to the 'standard' treatment of binary evolution, and serves as one extreme limit in our calculations – the limit in which the accretor essentially acts as an angular momentum sink and returns none of the angular momentum it gains from the orbit via the accretion stream or the inner edge of the disk.

In Fig. 4.4, we have plotted several of the parameters like the separation a, mass ratio q and the mass transfer rate $\dot{M}_2$ in units of solar masses per year. We have also plotted the parameter $\zeta_2 - \zeta_L$ (Section 2.3) which indicates whether the system undergoes stable or unstable mass transfer. Initially, as both systems evolve towards contact, the separation decreases and keeps decreasing for a short duration ($\sim$ 1000 yr) even after contact is established. After this, as is expected for AM CVn type systems, the separation increases monotonically. We notice the relatively slow rate of evolution of AM CVn as compared to RXJ0806. The mass of the donor for AM CVn in much smaller as compared to RXJ0806 and so the former gets into contact at a much higher separation than does the latter. As a result the driving rate for AM CVn is much lower than RXJ0806. Since we have excluded the effects of tides for simplicity, the GWR timescale is the only relevant timescale, especially for AM CVn. In the second panel we have plotted $\zeta_2 - \zeta_L$, which is positive for AM CVn indicating stability, whilst for RXJ0806, it starts negative (indicating unstable mass transfer) and becomes positive after about 20000 yrs of evolution. The higher mass transfer rate, and the resulting high rate of change of the mass ratio q, for RXJ0806 is a direct consequence of the fact that the driving rate is much higher in this system and that it begins mass transfer in the unstable state. Thus, RXJ0806 (q $\sim$ 0.3), considered to be an AM CVn 'progenitor' system evolves at a much higher rate than AM CVn (q $\sim$ 0.066).

In the next chapter we shall study DWD systems with a wide variety of masses and mass ratio's, undergoing mass transfer along with tidal effects. The above discussion illustrates that, in general, the more massive the donor, the higher the driving rate and the subsequent mass transfer rate and the overall evolution rate of the system. The presence of tides introduces another timescale (tidal) into the system evolution equations, which leads to interesting phenomena like tidally induced oscillation cycles.

4.3.2 Cataclysmic Variables

Cataclysmic Variables (CVs) are a class of mass transferring binary stars in which the main sequence donor fills its Roche lobe and transfers mass to a white dwarf accretor. The orbit averaged equations derived above can be used to study the evolution of such objects. The mass-radius relationship for main sequence stars

can be written as

$$\frac{R_2}{R_\odot} = \frac{M_2}{M_\odot} \tag{4.13}$$

i.e., $R_2 \propto M_2$: the more massive star has the bigger radius and fills up its Roche lobe first. The Roche lobe radius is given by Eq. 2.7 as before. Following the analysis in Section 2.3, in the case of CVs we have

$$\Big(\frac{\dot{M}_2}{M_2}\Big)_{\rm eq} = \frac{\dot{J}_{\rm sys}/J_{\rm orb}}{4/3 - \zeta_{\rm c} - q}$$

One can readily show that for CVs, $M_2/M_\odot \sim 0.11\ P_{\rm hr}$. $P_{\rm hr}$ denotes the period at contact in hours. Since the mass-radius relationship is linear for main-sequence stars, we expect that the donor will shrink as a result of mass transfer. As a result, the binary separation a also decreases as the system loses angular momentum. Assuming that the loss of angular momentum is due to GWR, given by Eq. 2.5, one can also show (King, 1988)

$$\dot{M}_2 \simeq 10^{-10}\Big(\frac{P_{\rm h}}{2}\Big)^{-3/2} M_\odot\ {\rm yr}^{-1} \tag{4.14}$$

For orbital periods above 3 hrs., the mass transfer rate given by Eq. 4.14 is much lower than what the observations suggest, but below about 2 hrs., the mass transfer rate is consistent with Eq. 4.14. Thus for $P > 3$ hrs., GWR is not the dominant mechanism which drives the mass transfer. It is suggested that this mechanism is magnetic braking (section 2.1.4), in which case (King, 1988)

$$\dot{M}_2 \simeq 6\ \times\ 10^{-10}\Big(\frac{P_{\rm h}}{3}\Big)^{5/3} M_\odot\ {\rm yr}^{-1} \tag{4.15}$$

In either case, there exists a relationship between the driving mechanism, the corresponding mass transfer rate and the period of the binary. Unfortunately, observations imply a much wider spread in the inferred mass transfer rates than the above equations suggest. Several explanations have been proposed (see Patterson (1984) for an entertaining overview of theoretical and observational aspects of CVs), and we shall consider one such possibility in section 7.1 in Part II of this work.

4.3.3 Contact Binaries

Contact binary systems involve components that are both filling up their Roche lobes simultaneously. The simplest case that one can expect this to occur is when the mass ratio $q = 1$, i.e., both components have equal mass and hence the same radii and Roche volumes. However, in nature, of the systems for which the mass ratio can be determined with any reasonable accuracy, contact binaries with mass ratios different from unity have been observed commonly. WUMa type contact binaries are some of the most common of contact binaries. These objects contain stars with convective envelops – usually O to K spectral type. The main theoretical

difficulty in understanding these systems is the near impossibility to construct structurally stable configurations with components in physical contact, sharing a common convective envelope (Webbink, 2003). We do not attempt here to address this problem, but instead use our binary evolution equations to obtain insight into the dynamical properties of contact binaries. This analysis is useful in interpreting results from more involved 3-D hydrodynamic simulations of contact binaries. From Section 2.5 we know that for a $n = 3/2$ polytrope, a contact binary with $q < 0.2$ is tidally unstable, whilst for a $n = 1/2$ polytrope, contact binaries with $q < 0.4$ are tidally unstable. We also realize that when the mass ratio is different from unity, the components can remain in contact with their respective Roche lobes only if they have different entropies (or different polytropic constants K_i).

We first write an *effective* mass transfer rate as:

$$\dot{M}_{2_{\rm eff}} = \dot{M}_2 - \dot{M}_1 \equiv -\dot{M}_{1_{\rm eff}} \tag{4.16}$$

The labels on the components "2" and "1" are arbitrary as long as the mass ratio, $q = M_2/M_1$, is exactly 1. However as soon as q deviates from one (for whatever reason) we shall adopt the convention that M_2 is the donor and M_1 is the accretor (irrespective of which one of the two components is more massive).

The instantaneous mass transfer rates in Eq. 4.16 are given as

$$\dot{M}_i = -\dot{M}_0 \Big(\frac{R_i - R_{L_i}}{R_i} \Big)^3 \tag{4.17}$$

with 'i' standing for each of the components respectively. Here R_{L_i} and R_i stand for the Roche lobe radii and the stellar radii of the components. As before (Section 2.2), ζ_i and ζ_{L_i} define the rate of change of the radii of the two components as a result of mass transfer. The rate at which the binary separation a changes is given by

$$\frac{\dot{a}}{a} = \frac{2\dot{J}}{J} - \frac{2\dot{M}_{2_{\rm eff}}}{M_2}(1 - \zeta_c - q), \tag{4.18}$$

where ζ_c represents the consequential angular momentum losses (Eq. 2.32) and $2\dot{J}/J$ includes both, the GWR and tidal terms. Also, the Roche lobe radii of the stars (given by 2.6) evolve as

$$\frac{\dot{R}_{L_1}}{R_{L_1}} = \frac{1}{3}\frac{\dot{M}_{1_{\rm eff}}}{M_1} + \frac{\dot{a}}{a} = \frac{2\dot{J}}{J} - \frac{\dot{M}_{2_{\rm eff}}}{M_2}(1 - \zeta_c - \frac{5}{6}\, q) \tag{4.19}$$

$$\frac{\dot{R}_{L_2}}{R_{L_2}} = \frac{1}{3}\frac{\dot{M}_{2_{\rm eff}}}{M_2} + \frac{\dot{a}}{a} = \frac{2\dot{J}}{J} - \frac{\dot{M}_{2_{\rm eff}}}{M_2}(\frac{5}{6} - \zeta_c - q) \tag{4.20}$$

In the above, note that the equations are symmetric, i.e., if we interchange label 1 and 2, we recover the original equations. This should indeed be the case, because as we have mentioned before, the labels '1' and '2' are assigned arbitrarily.

Once the mass-radius relationship is defined, we can numerically integrate the above equations and obtain the behavior of contact systems as a function of time.

We first consider DWD contact binaries and then consider main sequence contact binaries, for cases when the mass ratio is equal to or very close to unity. Due to the inherent symmetry of such configurations, we can then assume that the mass transferred from one component to the other has the same specific angular momentum as from the other component, and that whatever angular momentum is carried by the mass is returned to the orbit via tides. Thus, we simply set ζ_c and the tidal terms to zero. In principle, we can also follow systems with q different from 1 by explicitly estimating the specific angular momentum of each stream, applying the different tidal timescales and so on. However, these systems will have different polytropic constants, and we cannot incorporate the effect of mixing material with different entropies in the present formulation. We will not pursue these type of systems here, but it is certainly possible to generalize our formulation to unequal mass contact binary systems.

DWD Contact Binary System

In this case, we can use either the Nauenberg mass radius relation (Eq. 4.11) or a simpler form of a $n = 3/2$ polytrope.

$$K_i = 0.42422 G M_i^{1/3} R_i \tag{4.21}$$

i.e., essentially, $R_i \propto M_i^{-1/3}$. In the numerical integration we use the Nauenberg form, but for our analysis we use the polytropic form on account of its simplicity. Thus,

$$\frac{\dot{R}_i}{R_i} = -\frac{1}{3}\frac{\dot{M}_{i_{\rm eff}}}{M_i}$$

and so the mass transfer rate (or the depth of contact) itself evolves as,

$$\frac{d}{dt}\Big(\frac{\dot{M}_{1_{\rm eff}}}{\dot{M}_0}\Big)^{1/3} \propto \frac{\dot{R}_1}{R_1} - \frac{\dot{R}_{L_1}}{R_{L_1}} = -\frac{2\dot{J}}{J} + \frac{2\dot{M}_{2_{\rm eff}}}{M_2}(1 - \frac{2}{3}\,q) \tag{4.22}$$

$$\frac{d}{dt}\Big(\frac{\dot{M}_{2_{\rm eff}}}{\dot{M}_0}\Big)^{1/3} \propto \frac{\dot{R}_2}{R_2} - \frac{\dot{R}_{L_2}}{R_{L_2}} = -\frac{2\dot{J}}{J} + \frac{2\dot{M}_{2_{\rm eff}}}{M_2}(\frac{2}{3} - q) \tag{4.23}$$

When $q = 1$ exactly, then from Eq. 4.16 we see that $\dot{M}_{2_{\rm eff}} = 0$ and so from Eq. 4.18 we see that the binary shrinks at twice the rate of GWR. Also, the mass transfer rate increases at the driving rate as well. The binary thus merges, maintaining a mass ratio of unity. On the other hand, if q is slightly less than unity, say $q = 0.999$, the 'accretor' loses contact with its Roche lobe and the 'donor' mass transfer rate increases as the system evolves. Since $q > q_{\rm stable}$, the mass transfer is extremely unstable, but returns to stability once $q < q_{\rm stable}$.

In Fig. 4.6, we plot two $q = 1$ contact binary systems and a 'near contact binary' ($\mathrm{q} \sim 1 = 0.999$) and these plots confirm our analysis above. The q=1 binary evolves toward smaller separations due to the loss of angular momentum by GWR and eventually merges in a finite time. The q=0.999 binary evolves rapidly to a stable

configuration ($q < q_{\rm stable}$) after an extremely unstable mass transfer phase. Note that, since our OAE do not account for tidal disruption and here we have ignored the effects of super-Eddington accretion, the q=0.999 binary survives as a stable binary. Strictly speaking, this outcome is unrealistic, since for such an extreme mass ratio tidal disruption of the accretor is almost guaranteed.

Main Sequence Contact Binary System

In this case, we assume simply that $M_i \propto R_i$ and so

$$\frac{\dot{M}_{i_{\rm eff}}}{M_i} = \frac{\dot{R}_i}{R_i} \tag{4.24}$$

In this case, the radius of the star increases with an increase in mass. Thus we get

$$\frac{d}{dt}\Big(\frac{\dot{M}_{1_{\rm eff}}}{\dot{M}_0}\Big)^{1/3} \propto \frac{\dot{R}_1}{R_1} - \frac{\dot{R}_{L_1}}{R_{L_1}} = -\frac{2\dot{J}}{J} + \frac{2\dot{M}_{2_{\rm eff}}}{M_2}(1 - \frac{4}{3}\,q) \tag{4.25}$$

$$\frac{d}{dt}\Big(\frac{\dot{M}_{2_{\rm eff}}}{\dot{M}_0}\Big)^{1/3} \propto \frac{\dot{R}_2}{R_2} - \frac{\dot{R}_{L_2}}{R_{L_2}} = -\frac{2\dot{J}}{J} + \frac{2\dot{M}_{2_{\rm eff}}}{M_2}(\frac{4}{3} - q) \tag{4.26}$$

When $q = 1$ exactly, the *effective* mass transfer rate $\dot{M}_{2_{\rm eff}} = 0$, and so the system evolves at the driving rate, which in this case is given by magnetic breaking (Eq. 2.11). The binary eventually merges with ever increasing $\dot{M}_i$'s as the depth of contact increases with decreasing separation. When $q \gtrsim 1$, the donor M_2 transfers mass to the accretor M_1 until $q = 1$ exactly, after which it evolves as above. Since $q < q_{\rm stable}$ (for $q \gtrsim 1$) this happens at the steady, equilibrium mass transfer rate [1].

In fig. 4.7, we have plotted the evolution of 2 systems, one with q = 1 and the other with q = 1.1. As with the DWD contact system, the q=1 binary slowly plunges into catastrophic merger as a result on an inspiral due to the loss of orbital angular momentum via GWR. The behavior of the q = 1.1 system is different from the DWD case of q = 0.999. In case of main sequence stars, the more massive star fills up its Roche lobe first, and thus transfers mass to the lower mass star. As a result, the mass ratio always tends towards unity. But as and when the mass ratio q =1, the binary follows the evolutionary trajectory towards merger as described in the case above. Thus, by design, double main sequence stars evolve towards being contact systems unless one of the stars evolves much faster than the other, and leaves the main sequence before the mass transfer can drive the system towards a mass ratio of 1. On the other hand, DWD contact binaries tend toward unstable mass transfer for mass ratios of the order of 1.

[1] The value of $q_{\rm stable}$ for main sequence donors is $\sim 4/3$.

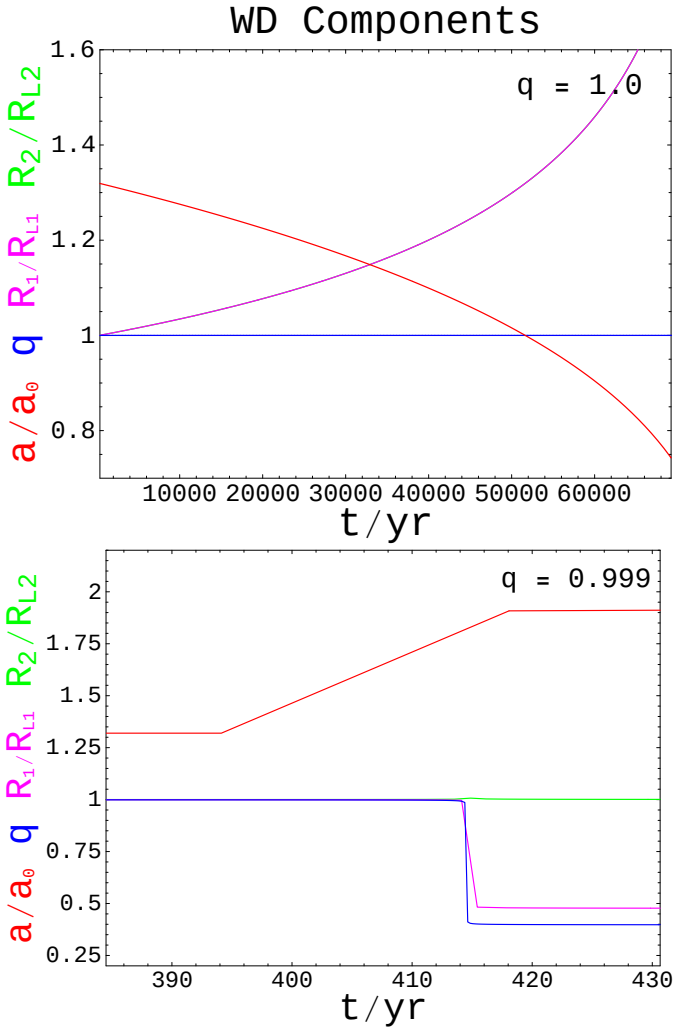

FIGURE 4.6. The evolution of DWD contact binary. System parameters for a DWD contact binary system as a function of time for $q = 1.0$ and total mass $M = 0.4M_{\odot}$, and for $q = 0.999$ and $M = 0.4002M_{\odot}$: the mass ratio q (blue), the separation a, the Roche lobe radii: R_{L_1} (magenta) and R_{L_2} (green). In the $q = 1$ case, the Roche lobe radii overlap exactly.

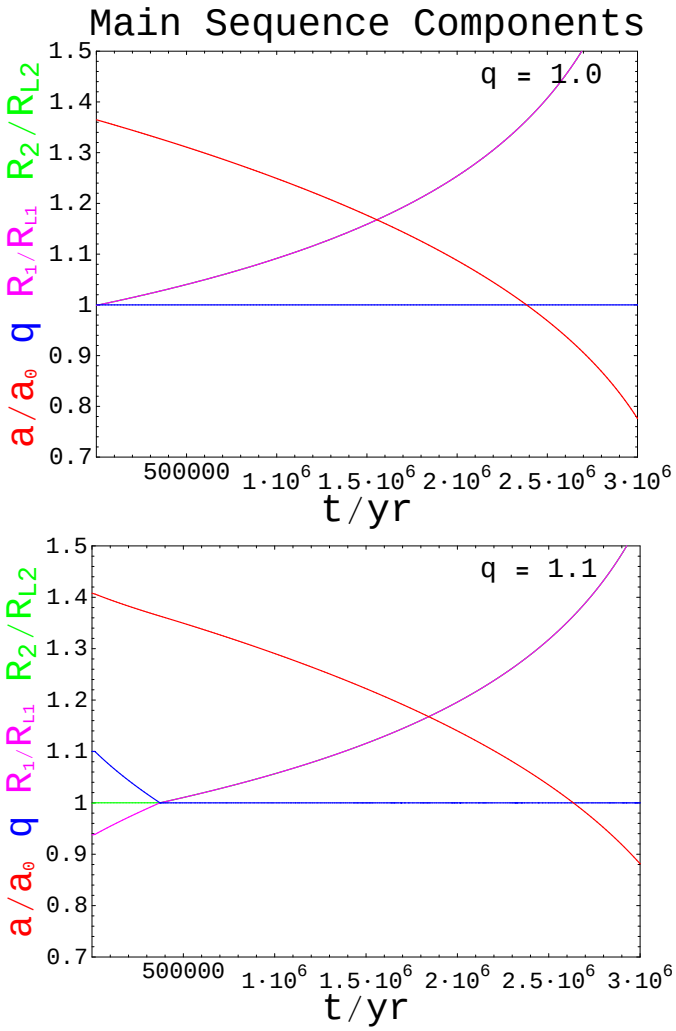

FIGURE 4.7. The evolution of main sequence contact binary. System parameters as a function of time for $q = 1.0$ and total mass $M = 1.0M_{\odot}$, and for $q = 1.1$ & $M = 0.955M_{\odot}$ for a binary with main sequence components: the mass ratio q (blue), the separation a, the Roche lobe radii: R_{L_1} (magenta) and R_{L_2} (green). Once $q = 1$, the Roche lobe radii overlap exactly.

5. Applications

Having established the basic binary evolution equations in Chapter 2 and seen some simple applications of them in Chapters 3 and 4, we are now ready to investigate in detail the behavior of the binary when all physical mechanisms described in Section 2.1 are in play at the same time. We concentrate on DWD systems in particular, but since our evolution equations are quite general, some of the effects we are studying in the following sections are applicable even for other types of binaries. We begin first by investigating an important consequence of the tidal coupling of the spin and orbit – that of possible tidally induced oscillations. Following this, we evolve a grid of binaries with different initial masses and describe the expected behavior of the systems in the $M_2 - M_1$ parameter space. Following this, we compare our OAE based results to full 3-D hydro-simulation results. This study is useful in interpreting the complicated and often intractable behavior of the hydro-simulations. Finally, we investigate the impact of some effects like DI accretion, unstable mass transfer and tidally induced oscillations on the GWR signature of typical AM CVn systems with respect to GWR detectors like LISA.

Before we proceed we note that the kinds of system we are considering in the following are old systems which follow the cold white dwarf mass-radius relationship (Eq. 4.11). As DWDs emerge from common envelope evolution, it is reasonable to assume that some of the systems are young. For these young systems, it is possible that the donor is surrounded by a massive hydrogen envelope which can survive for long periods supported by nuclear burning (D'Antona et al., 2006). In such a situation, the radial variation rate ν_2 is non-zero, and in fact can reduce the *net driving rate* $\nu_L - \nu_2$, leading to a lower value for the equilibrium mass transfer (see Eq. 2.37). Also, it is likely that $\zeta_2 > 1$ as long the non-degenerate envelope is present. This clearly affects the stability and evolution at the onset of mass transfer and can lead to shrinking orbits even if the mass transfer is stable with $\ddot{M}_2 \approx 0$.

Unless the system is very young, the depth of contact required to sustain the equilibrium rate exceeds the scale height of the envelope. Consequently, in our subsequent analysis, we set $\nu_2 = 0$ and use the zero-temperature mass-radius relationship. We note that for the study of the onset of mass transfer in young, finite entropy systems like the ones addressed by D'Antona et al. (2006), a more realistic model for the donor is required.

5.1 Tidally Induced Cycles

In the usual treatment of binary evolution, it is implicitly assumed that the donor star is synchronized with the orbit. As far as the accretor is concerned, in the case of disk accretion, the amount of angular momentum advected at the inner edge of the disk is usually quite small, and so the accretor spin-up is relatively minor and

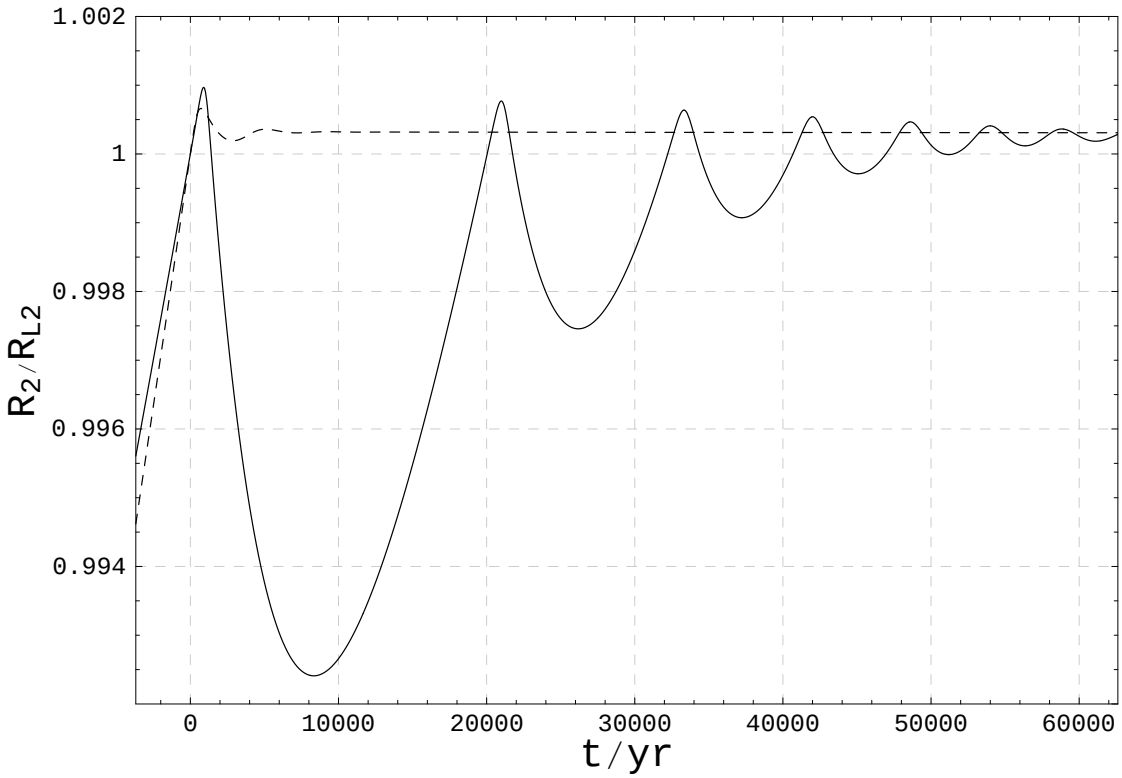

FIGURE 5.1. The Evolution of the Roche Lobe Radius and Radius of Donor. The ratio of the radius of the donor and the Roche lobe radius for q = 0.2 (dotted curve) and q = 0.28 (solid curve) for $\tau_{s_1} = 5000$ yrs. Whenever $R_2 < R_{L_2}$, the system detaches and the mass transfer rate goes to zero.

can be neglected in most cases. But in case of DWD binaries, even through disk accretion the accretor can be spun up significantly. This spin-up is much enhanced in the case of DI accretion as we shall see presently. We have seen in the previous chapter that the tendency of an AM CVn system is to evolve to higher separations (lower orbital frequencies) once mass transfer is well underway. Thus it is possible that the orbit and the accretor are significantly 'out of sync' and consequently, the tidal terms in Eq. 2.17 are no longer negligible. On the other hand, the rate of change of the donor radius depends only on the mass of the donor (Eq. 2.23). Thus using Eq. 2.19 & Eq. 2.23, we have

$$\begin{aligned} \frac{\dot{R}_{\rm L}}{R_{\rm L}} - \frac{\dot{R}_2}{R_2} &= \frac{2\dot{J}_{\rm sys}}{J_{\rm orb}} - 2\frac{\dot{J}_{1,\rm tid} + \dot{J}_{2,\rm tid}}{J_{\rm orb}} - \frac{2\dot{M}_2}{M_2}[q_a - \frac{\zeta_{r_{\rm L}} + \zeta_2}{2} - q] \\ &= \frac{2\dot{J}_{\rm sys}}{J_{\rm orb}} - 2\frac{\dot{J}_{1,\rm tid} + \dot{J}_{2,\rm tid}}{J_{\rm orb}} - \frac{2\dot{M}_2}{M_2}[\frac{\zeta_2 - \zeta_{\rm L}}{2}] \end{aligned} \tag{5.1}$$

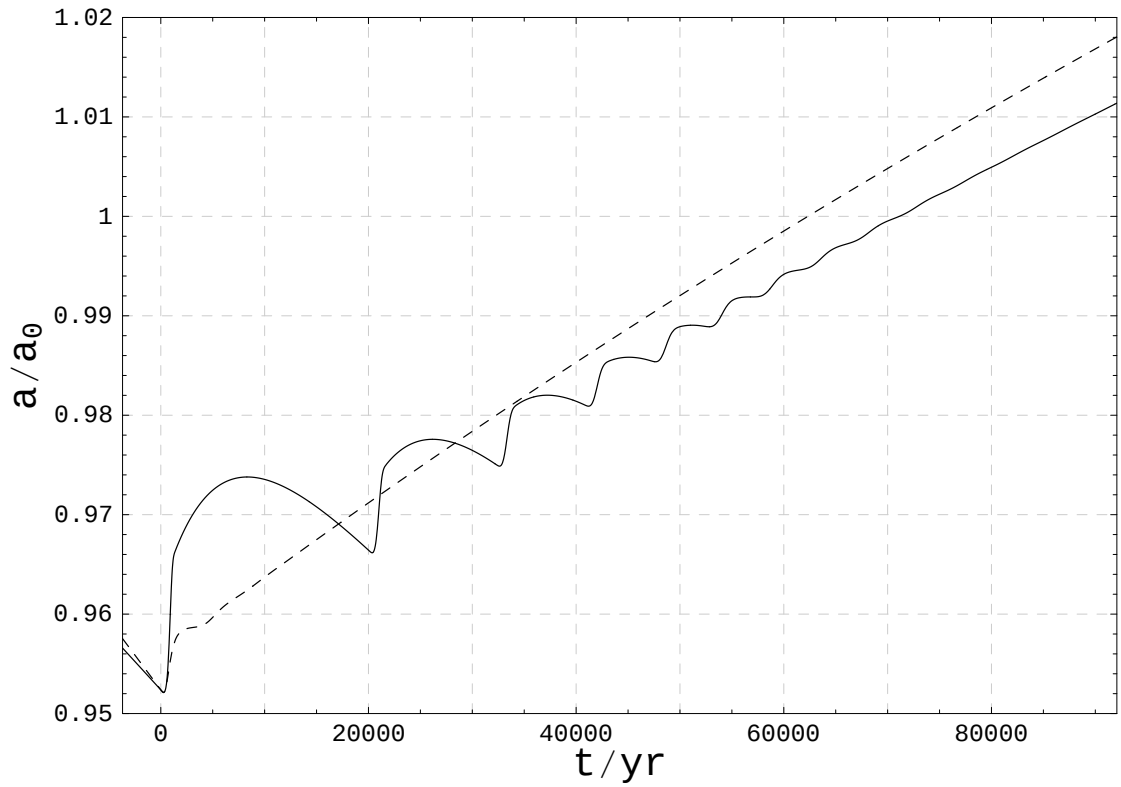

FIGURE 5.2. The orbital separation, normalized to the initial separation, as a function of time for q = 0.2 (dotted curve) and q = 0.28 (solid curve) for $\tau_{s_1} = 5000$ yrs.

The right side of Eq. 5.1 tells us the evolutionary trend for a given binary system.

$$\begin{aligned} \frac{\dot{R}_{\rm L}}{R_{\rm L}} - \frac{\dot{R}_2}{R_2} &= 0 \quad \Rightarrow \text{Stable Mass transfer} \\ &< 0 \quad \Rightarrow \text{Unstable Mass transfer} \\ &> 0 \quad \Rightarrow \text{Detachment} \end{aligned}$$

Usually the tidal terms are negligibly small, and consequently the only timescale in the equation is that of the driving – in our case the gravitational radiation rate. The mass transfer rate will tend to adjust itself to this rate and equilibrium mass transfer holds as long as $q < q_{\rm stable}$. When $q > q_{\rm stable}$, the radius of the donor increases at a faster rate than its Roche lobe radius and unstable mass transfer results. Now, when the tidal terms cannot be ignored, the behavior of the system is not easily predictable because we have a new timescale involved which may be very different from the GWR timescale. Moreover, the tidal timescale itself evolves as per Eq. 2.10. Considering Eq. 5.1 again, it is possible that the sum of the driving terms (GWR + tidal terms) can indeed be positive *if* the tidal timescale is of the same order as the mass transfer timescale *and* sufficient asynchronism has been built up in the accretor. Consequently, the Roche lobe radius increases at a faster rate than the donor radius and this results in detachment. To illustrate the above situation, we consider two hypothetical DWD systems, one with a mass

ratio q = 0.2 and the other with q = 0.28. The reason for this choice is that the former has a mass ratio of $q < q_{\rm stable}$ and hence is expected to undergo stable mass transfer whilst the latter is expected to have unstable mass transfer at first contact. In Fig. 5.1 we plot the ratio of the donor radius and the Roche lobe radius, $R_2/R_{\rm L_2}$ as a function of time for both cases. The corresponding evolution of the orbital separation is shown in Fig. 5.2. Also in Fig. 5.3 we plot the spin frequencies of the accretor and donor, normalized to the orbital frequency as a function of time. Notice first that for the unstable case, the accretor is violently spun up on relatively short timescales (a few hundred years) for the unstable case, whilst the spin up is not very significant for the q = 0.2 case. This is a consequence of the mass transfer rate, which as mentioned above is high for the unstable case. Notice also that in *both* cases, the donor spin frequency is not significantly different from the orbital frequency, and for the moment we neglect the asynchronism between the donor and the orbit. From our discussion in Section 2.1.3, we realize that the tidal synchronization timescale for WDs is not well known, and so we treat it as a free parameter and try different values to study the consequences. In this case, we choose $\tau_{\rm s_0}$ in Eq. 2.10 to be such that that *initial* timescales are $\tau_{\rm s_1} = 5000$ yrs and $\tau_{\rm s_2} = 10$ yrs, but let these evolve as per Eq. 2.10.

Once the accretor has spun up sufficiently, the tidal torque between the accretor and the orbit leads to the return of angular momentum to the orbit. As a consequence, the separation and the Roche lobe increase at an enhanced rate, even as the mass transfer rate begins to drop due to the decreasing driving rate (GWR is proportional to a^{-4}). As we have discussed above this leads to detachment, and the ratio $R_2/R_{\rm L_2} < 1$ (Fig. 5.1). The accretor spin down continues till such time that the net driving rate becomes negative again, i.e. the GWR rate dominates. The orbit then begins shrinking and the donor approaches contact again with the components approximately synchronized with the orbit. If the new mass ratio $q > q_{\rm stable}$, the above mentioned phenomenon can recur – unstable mass transfer, accretor spin up, tidal torques returning excess accretor spin to the orbit and ultimately detachment. In fact, as can be seen from Fig. 5.1, this cycle can recur several times until finally the binary reaches a state where $q < q_{\rm stable}$ and accretor spin up becomes inefficient on mass transfer. The magnitude of the tidal term in Eq. 5.1, depends on the amount of asynchronism and the tidal timescale. The asynchronism as we have seen above depends on how unstable the binary mass transfer is, i.e. it depends on $q - q_{\rm stable}$. The more unstable the mass transfer, the higher the accretor spin up and for a given tidal timescale, the more violent the oscillations. In Fig. 5.4 we investigate the effect of different synchronization timescales on the evolution of the binary. In general we observe that the higher $\tau_{\rm s_1}$ is, the more violent the oscillations and so also the number of oscillations. This is due to the fact that a longer tidal timescale allows for a higher spin up of the accretor. As the timescale gets shorter, the intensity of the oscillations decreases, and for the shortest tidal timescales, the system is synonymous to a disk system, where tides are extremely efficient in returning most of the spin angular momentum back to the orbit. This efficient coupling does not allow for any substantial spin up of the accretor, and so

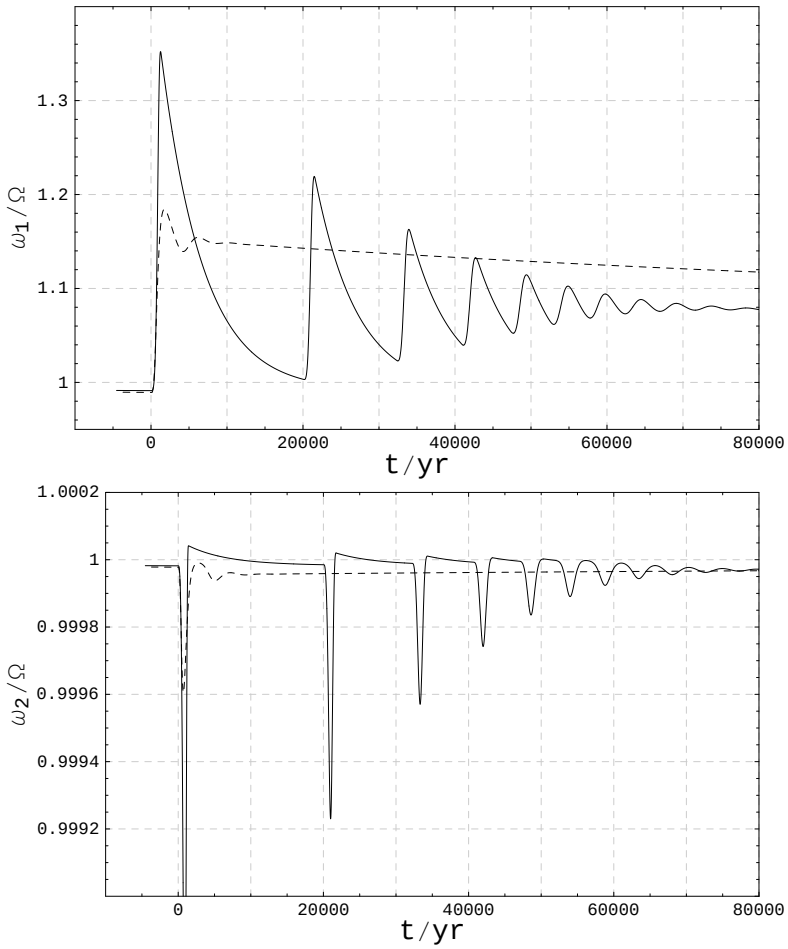

FIGURE 5.3. The evolution of the spin frequencies. The spin frequencies of the accretor (top panel) and donor (bottom) for q = 0.28 (solid curve) and q = 0.2 (dotted curve) for $\tau_{s_1} = 5000$ yrs. The amount of spin up of the accretor decreases as the system evolves towards stability. The donor remains approximately synchronous throughout for both cases.

we do not observe oscillations in this limit. Thus, in the extreme cases – for short tidal timescales the system behaves like a disk system and for long timescales the spin and orbit are effectively decoupled. It is also interesting that asymptotically, all systems seem to converge to the same rate of evolution – the tidal effects do not influence the long term evolution of the systems. This is expected, since the overall angular momentum content of all these systems is the same and once the tidal effects have petered out, the system should evolve on GWR timescales.

Tidally induced detachment has implications for ultra-compact DWD systems; in particular RX J0806 and V407. In these systems it is observed that the orbital period is decreasing at a rate consistent with GWR, but mass transfer is obviously underway in these systems. This is at odds with the theoretical expectation that the orbital period should increase. We see that it is possible for the binary to detach, especially in the case of unstable, direct impact systems. If indeed this

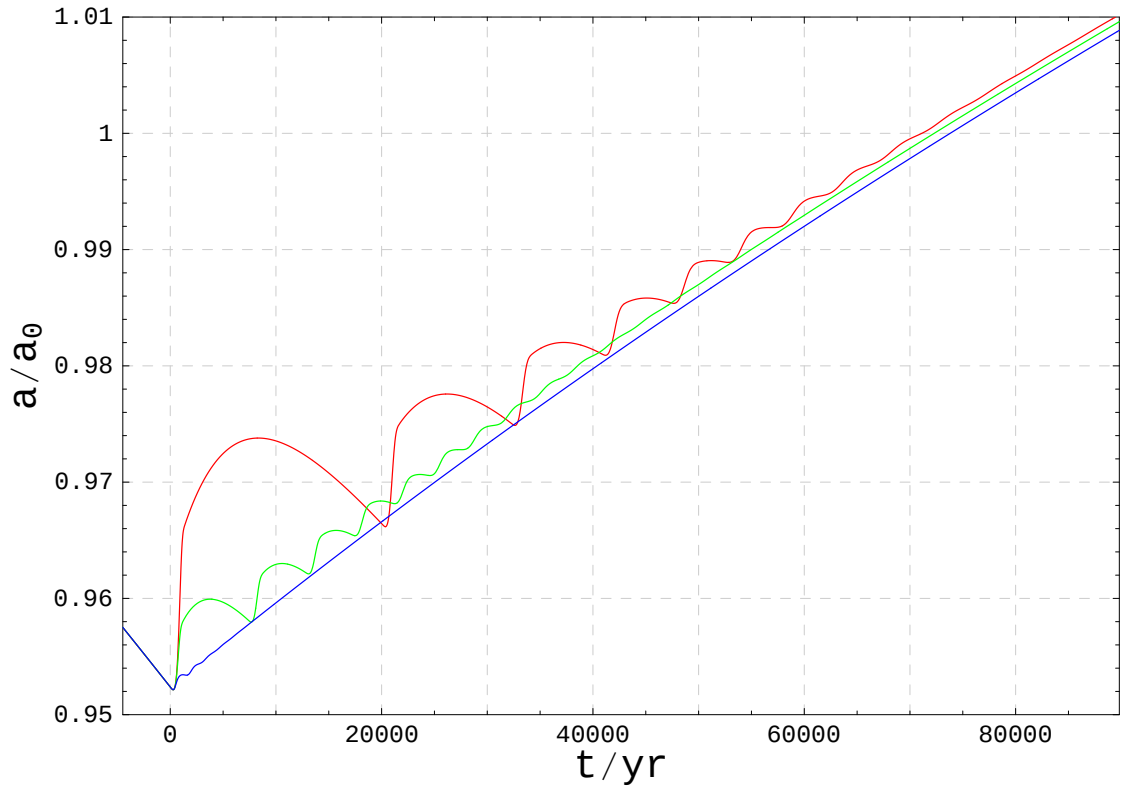

FIGURE 5.4. The orbital separation a with the tidal effects included. The orbital separation, normalized to the initial separation for a binary with q = 0.28 with the initial tidal synchronization timescale different for each run – $\tau_{s_1} = 5000$ yrs (Red curve), 2500 yrs (green) and 500 yrs (blue). The donors initial tidal timescale is taken to be 10 yrs in all cases.

occurs in 'real systems', then this increases the probability of us catching one of these systems in a phase where it is in contact and yet the orbit is shrinking. In fact, since the systems also spend quite a significant fraction of time out-of-contact, there should be many more systems with short periods than can be observed. Of the observable ones, we expect that some of them will have $\dot{P} > 0$ and some to have $\dot{P} < 0$. The system parameters like the mass of the donor, accretor and the various angular momentum loss mechanisms are not accurately known for the observed AM CVn systems. However, for the observed decrease in orbital period to be attributed to tidally induced detachment, the binary parameters should be such that $q \gtrsim q_{\rm stable}$ (See Fig. 5.9) and the stream must impact directly onto the accretor's surface and not form a disk.

In Table 5.1 we have recorded the relevant timescales as a function of the mass ratio q and the tidal timescale τ_{s_1} of the accretor. $T_{\rm osc} = T_1 + T_2 + T_3$ is the timescale for which the oscillations last after initial contact. T_1 represents the time when the binary is in contact but the separation is decreasing, T_2 is the time when the system is in contact and the separation is increasing, whilst T_3 represents the time for which the system is out-of-contact. $N_{\rm osc}$ represents the number of oscillations a

TABLE 5.1. Time spent (in years) in different regimes during the oscillation phase as a function of the mass ratio q and tidal timescale τ_{s_1}.

q	τ_{s_1}	T_{osc}	T_1	T_2	T_3	N_{osc}
0.28	1000	3200	1260	1000	936	1
0.28	2500	23000	4450	4125	14425	4
0.28	5000	64000	4025	11655	48320	5
0.26	1000	0	985	$\forall t > T_1$	0	0
0.26	2500	5400	1750	810	1840	1
0.26	5000	15200	1600	4100	9510	2
0.24	1000	0	710	$\forall t > T_1$	0	0
0.24	2500	3600	1130	1820	650	1
0.24	5000	5500	1110	2300	2100	1

system encounters during its evolution. We see that for a given mass ratio, a system tends to spend an increasing amount of time out of contact with increasing tidal timescales. Moreover, the more unstable the mass ratio, the larger the number of oscillations and the timescale for which the oscillations last.

A binary can spend a considerable amount of time in which tides are effective, especially in the case of unstable mass transfer. In fact, since the systems also spend quite a significant fraction of time out-of-contact, there should be many more systems with short periods than can be observed. However, even in the most favorable case, a given system spends less than 30% of its time in a regime where the system is in contact and the orbit is shrinking. Thus it is unlikely that tidally induced oscillations are responsible for the observations of $\dot{P} < 0$ for RX J0806 and V407. Nevertheless, the probability that we catch a system in contact with $\dot{P} < 0$ is enhanced significantly as compared to the case when there are no oscillations Willems & Kalogera (2005). For example, for the $q = 0.26$ case the system does not undergo any oscillations and $T_1 \sim 1000$ yrs for $\tau_{s_1} = 1000$ yrs.

5.2 Exploring Evolutionary Outcomes

In this section we study the long term evolution of a grid of systems in the $M_2 - M_1$ parameter space. We select the initial masses of the binary components and evolve them for 10^9 yrs. The aim of this study is to demarcate the regimes where the mass transfer is either stable or unstable, super-critical or sub-critical, undergoes DI accretion or disk accretion etc. Also in some of the high mass systems, the accretor can gain enough material to exceed the Chandrasekhar limit and these could be potential Type-Ia Supernova progenitors. This kind of study has been previously undertaken by Marsh et al. (2004) but we have the following additional aspects:

- We include the donor spin effects and the possibility of donor asynchronism. Also, as we shall see the advective term associated with the specific angular

momentum of the material on the donor has a significant impact on the stability properties of DWD systems.

- We study the effects of intermediate tidal synchronization timescales for the accretor, which leads to the interesting phenomenon of tidally induced detachment as described in Section 5.1.

The only 'free parameter' we have in these evolutions is the tidal synchronization timescales for the accretor and the donor. We specify arbitrary *initial* values for these and let the timescales evolve (according to Eq. 2.10) along with other system variables in a self-consistent manner.

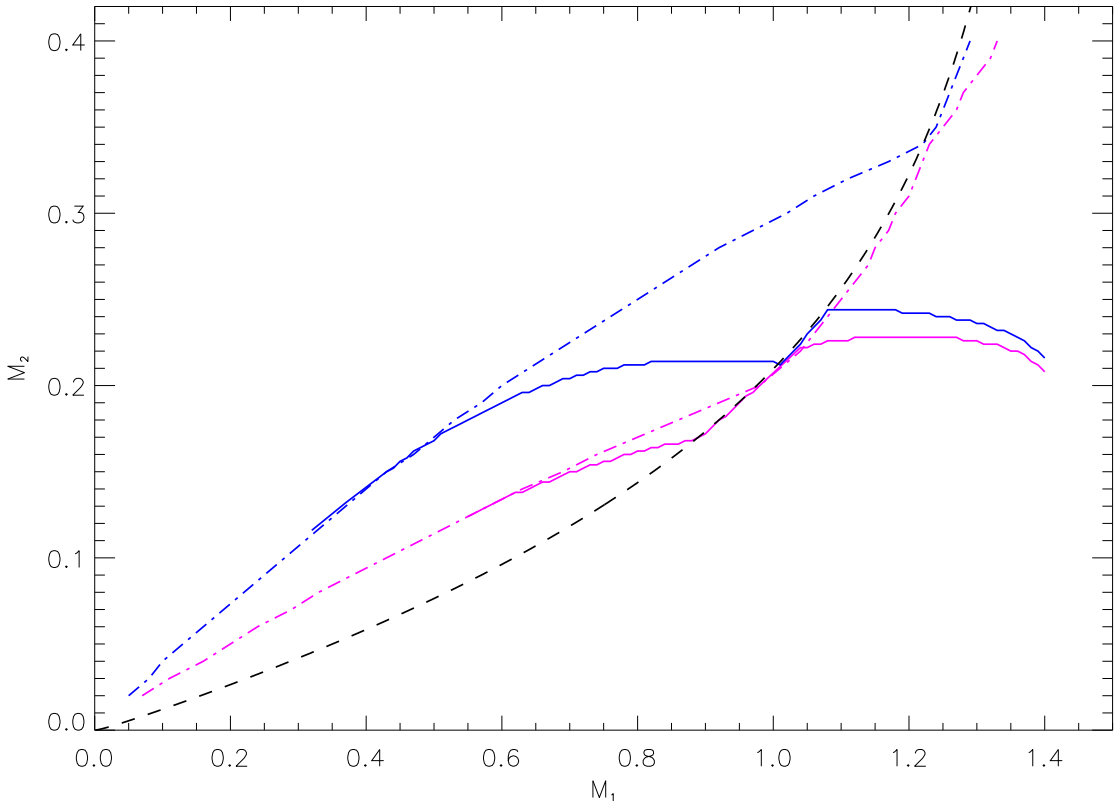

FIGURE 5.5. The stability curves: Mass-transfer stability limits (dash-dot lines) and super (above) and sub-Eddington (below) accretion boundaries (solid lines) with (blue) and without (magenta) the donor terms included. The thin dashed black line divides direct impact systems from disk accretion systems (Marsh & Steeghs, 2002). Because the transition from direct impact to disk accretion makes mass transfer more stable, both the stability limits and Eddington accretion rate boundaries follow closely the locus of that transition toward higher donor masses (see text for details).

Before presenting the results of the grid, it is useful to study the expected behavior of the systems, focussing on the stability limits and whether the mass transfer is

super-critical or not. In Fig. 5.5, we plot the locus of points corresponding to stable and unstable mass transfer with the donor spin accounted for (blue dotted line) and without the donor spin term (magenta dotted line). These points are obtained numerically by setting $q - q_{\rm stable} = 0$ in Eq. 2.37 at the initial point of contact. By design, the tidal terms are set to zero, since we assume that at the point of contact the binary is synchronous. Also plotted are the points corresponding to the transition between super-critical and sub-critical accretion with the donor spin affects included (blue solid line) and without the donor spin affects accounted for (magenta solid line). These points are obtained by setting $\dot{M}_{2,\rm eq} = \dot{M}_{\rm Edd}$ from Eqs. 2.37 and 4.3. Firstly, we notice that for low accretor masses, all the stable systems are sub-Eddington in both cases. Around an accretor mass of $0.3M_\odot$ ($0.55M_\odot$ if donor terms are neglected) till about $0.5M_\odot$ ($0.65M_\odot$ if donor terms are neglected), the stability curves and the curves for super/sub critical accretion overlap. From then on, even some of the stable systems are super-critical and the super/sub critical curve begins to flatten off around a donor mass of $0.215M_\odot$ ($0.165M_\odot$ if donor terms are neglected). This is because for such high donor masses, $\dot{M}_{2,\rm eq} > \dot{M}_{\rm Edd}$. It should be noted that these systems are all DI systems mainly because of the relatively low accretor masses which imply larger accretor radii. As we move toward higher accretor masses (and thus lower accretor radii), the systems transit from DI systems to accretion disk systems. This has the effect of increasing $q_{\rm stable}$, which is a stabilizing effect since the specific angular momentum lost at the inner edge of the disk is given by $\sqrt{GM_1R_1}$ as against $\sqrt{GM_1R_h}$ ($R_1 < R_h$). As a result, the equilibrium mass transfer rate for the disk systems drops and this is enough to let $\dot{M}_{2,\rm eq} < \dot{M}_{\rm Edd}$ around about $M_1 \sim 1.0M_\odot$ ($M_1 \sim 0.9M_\odot$ if donor terms are neglected). From there on, the stability curves and the super/sub critical curves overlap the DI-disk transition curve but only for a short region in the parameter space. Eventually, $\dot{M}_{2,\rm eq} > \dot{M}_{\rm Edd}$ again, even for disk systems with a donor mass of $M_2 \geq 0.24M_\odot$ ($M_2 \geq 0.225M_\odot$ if donor terms are neglected).

We also note that the stability curves with the donor spin included are much higher than the stability curves with the donor spin ignored. Thus many more systems are potentially stable when the donor spin contributes to angular momentum redistribution during the evolutions.

To demonstrate more clearly the effect the DI to disk transition has on super or sub-Eddington accretion, we plot on Fig. 5.6 the equilibrium mass transfer rate (Eq. 2.37) and the Eddington mass transfer rate (Eq. 4.3) for a fixed donor mass M_2 as a function of the accretor mass M_1, *at the point of contact*. Again, the tidal terms are effectively zero, since the components are assumed synchronized at the point of contact. We plot the mass transfer rate for different values of the donor mass: 0.21 $M_\odot$, 0.23 $M_\odot$ and 0.25 $M_\odot$. Notice that for the first case, the mass transfer rate is super-Eddington until $M_1 \sim 0.75$ $M_\odot$, after which it is sub-Eddington. For $M_2 = 0.23$ $M_\odot$, the mass transfer rate is appreciably super-Eddington, but as the accretor mass increases, at some point (around $M_1 \sim 1.05$ $M_\odot$), the systems transit

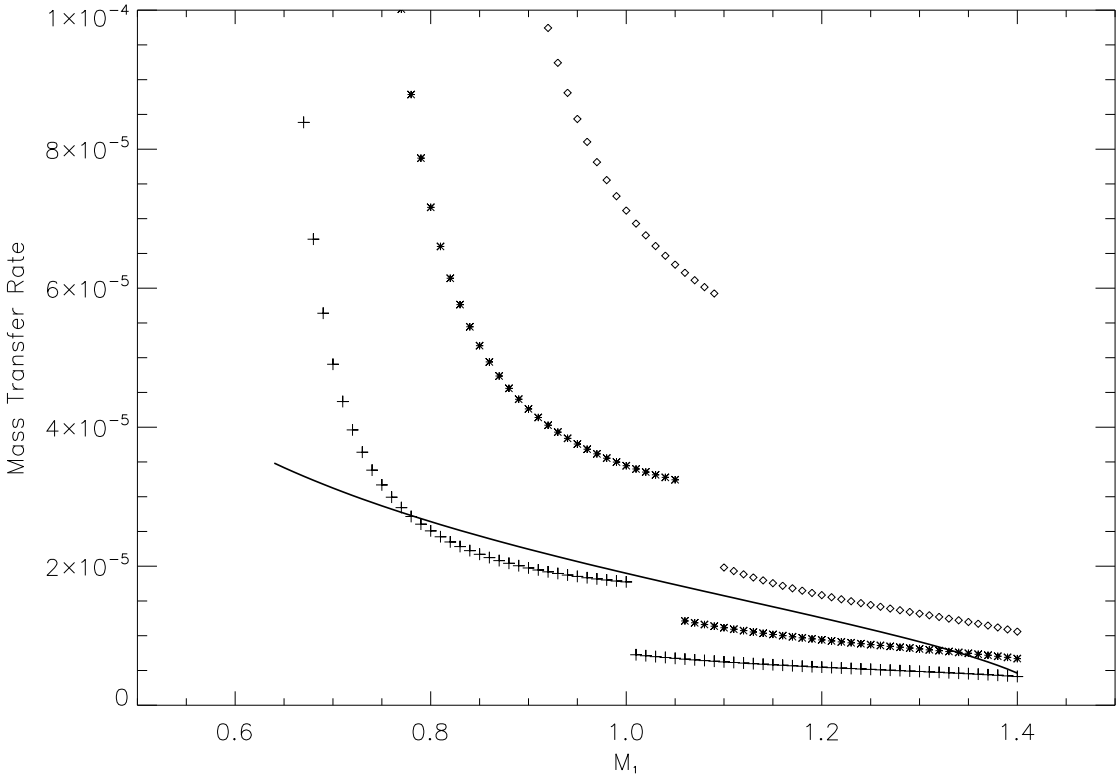

FIGURE 5.6. Mass transfer rates compared to the Eddington rates. Comparison of the *initial* equilibrium mass transfer rate (in $M_\odot$/yr) with the initial Eddington rate for different donor masses $M_2 = 0.21\ M_\odot$ (+), $0.23\ M_\odot$ (∗) and $0.25\ M_\odot$ (◊). The solid line denotes the Eddington rate for the $M_2 = 0.21$ case, the Eddington rate for the other donor masses almost exactly overlaps this curve.

from DI accretion to disk accretion and the equilibrium mass transfer rate abruptly decreases in accordance with the enhanced stability corresponding to disk accretion (Sections 2.2 & 5.2). Thus, for $M_2 = 0.23\ M_\odot$ systems with $M_1 > 1.05\ M_\odot$ are expected to accrete sub-critically. On the other hand, for systems with a donor mass $M_2 = 0.25\ M_\odot$, we notice that the mass transfer rate is much higher than for the other two cases we have considered here. In fact, even when the systems transit from being DI systems to disk accretion systems around a accretor mass of $1.1\ M_\odot$, the mass transfer rate is still super-critical! Comparing this with Fig. 5.5, we notice that indeed, systems with donor masses in excess of $\sim 0.25\ M_\odot$ accrete at super-critical rates.

We are now in a position to interpret the results of the full evolutions across the grid. We emphasize that the above analysis is carried out at the *initial* configuration of the systems and that the tidal effects are effectively ignored since the binary is assumed synchronous at the point of initial contact. Thus we expect that only in the case where the tidal timescale of the accretor is extremely long, and hence the tidal spin-orbit coupling is highly inefficient, that the evolutions should match our naive expectations depicted in Fig. 5.5. When the accretor's tidal timescale is

such that the tidal coupling is efficient, one would expect the systems to behave differently.

In order to compare our results to that of Marsh et al. (2004), we first evolve the systems in the grid by setting the same initial conditions as theirs, i.e. we ignore the advective and tidal terms associated with the donor. We set the tidal timescales to 10^{15} yrs (top panel) and 10 yrs (bottom panel) and evolve the systems for 10^9 yrs. As expected, we see that for the longer timescale, the tidal effects are negligible and the evolutions faithfully follow the limits shown in Fig. 5.5. Note especially, the slight incursion that occurs around $M_1 \sim 0.85 M_\odot$ where the super-critical systems encroach into the stable domain. This is also observed in Marsh et al. (2004), and as we can infer from Fig. 5.5, this is a result of the transition of the DI systems to disk systems. Specifically, as mentioned above, the systems with donor mass $M_2 > 0.165 M_\odot$ tend to be super-critical for DI systems. But once the accretor mass exceeds $0.9 M_\odot$, the systems transit to disk systems and consequently the mass transfer rates are lower due to the relatively enhanced stability of the disk systems. From there on the stability and critical curves follow the curve corresponding to the DI-disk transition until a donor mass of $0.24 M_\odot$ from where on all systems are super-critical. We have also shown the systems for which the accretor mass exceeds the Chandrasekhar limit during the evolution for 10^9 yrs. The bottom panel shows the systems with a tidal synchronization time of 10 yrs. Since the tides are extremely efficient in this case, this is analogous to what one would expect in the standard accretion disk case with practically no angular momentum lost to the accretor spin ($j_1 \sim 0$). The efficient return of the orbital angular momentum from the spin results in the effective driving rate to be much lower than that due to pure GWR. Consequently, the mass transfer rate is much lower and as can be seen in Fig. 5.7, is sub-critical even for otherwise 'unstable' systems. However for donor masses $M_2 > 0.28 M_\odot$ again, the mass transfer rates exceed the Eddington rate irrespective of the efficient coupling or DI-disk transitions.

In Fig. 5.8 we present the results with the effects of the donor spins included in the evolution. We see immediately that for the case with $\tau_{s_1} = 10^{15}$ yrs, the systems follow the stability curve corresponding to the one including the donor spins in Fig. 5.5 (the blue curves). Thus, the domain in which we have stable mass transfer and sub-Eddington accretion is greatly enhanced when we include the donor spin effects. As expected from our discussion above, the transition from super to sub-critical accretion overlaps the stability boundary until $M_2 \approx 0.21\ M_\odot$ after which it follows the stability curve defined by the DI to disk transition. Above a donor mass of $0.25\ M_\odot$ though, all systems accrete super-critically.

Similar to the case considered above, when the tidal synchronization timescale is short, the efficient return of angular momentum to the orbit results in a net reduction in the driving. Consequently, the region of sub-critical accretion is greatly enhanced. However, above a donor mass of $\sim 0.28 M_\odot$, the accretion rate is always above the Eddington limit. Note that at very high accretor masses ($\sim 1.3 M_\odot$), the curve that defines the boundary between sub and super critical accretion dips towards lower donor masses. This is because the Eddington rate for such high ac-

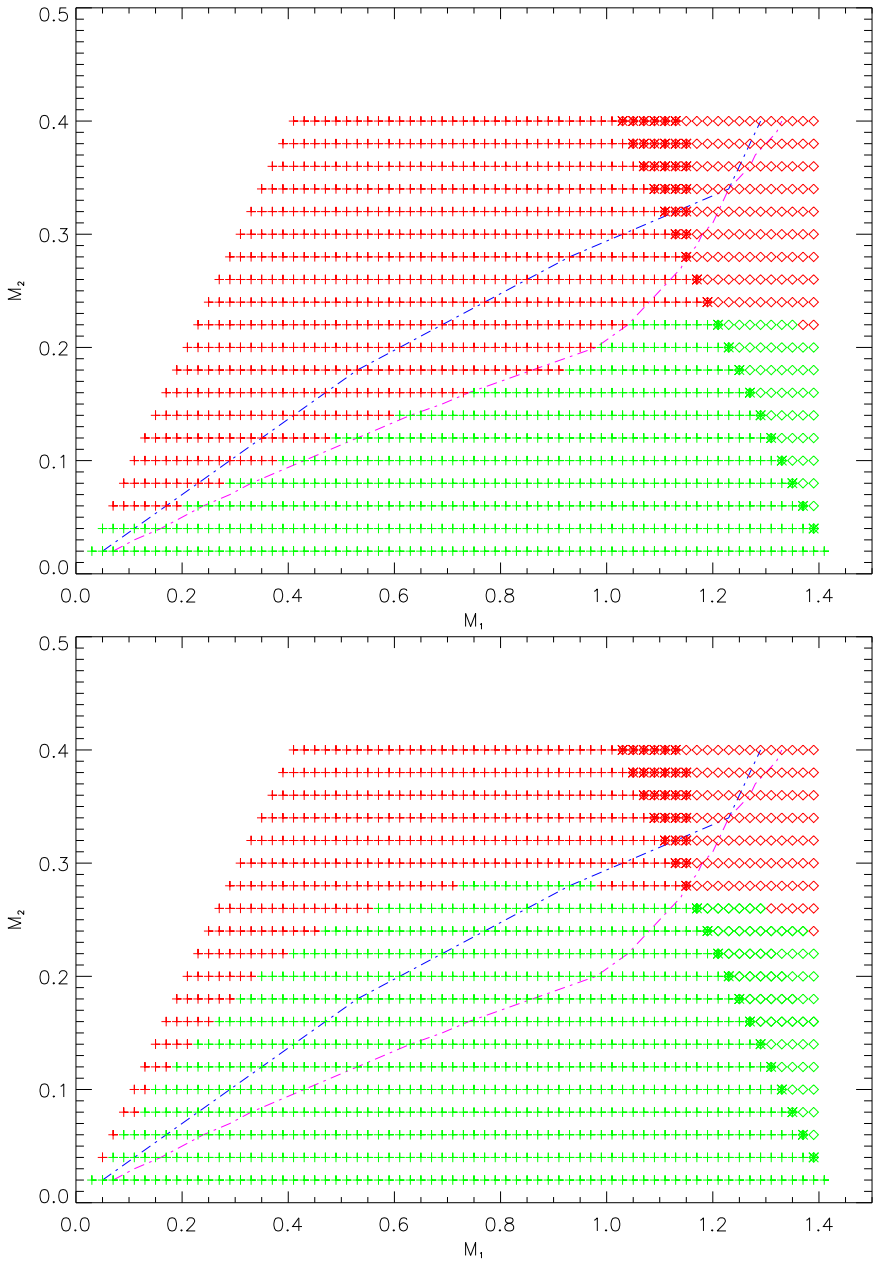

FIGURE 5.7. Behavior of systems across the parameter space – I. Evolution for 10^9 yrs for an initial τ_{s_1} of 10^{15} yrs (top panel) and for τ_{s_1} of 10 yrs (bottom panel) with the affects of the donor spin ignored. This synchronization time is for the initial configuration and evolves according to Eq. (2.10). The red symbols represent Super-Eddington accretion, the green are Sub-Eddington, the pluses (+) and hollow diamonds ($\Diamond$) represent systems with total mass below and above the Chandrasekhar limit respectively. Among the latter asterisks over diamonds indicate systems in which the accretor does not reach the Chandrasekhar limit in 10^9 yr. The magenta line is the stability boundary without these effects. The blue dash-dot line is the initial stability boundary with all donor effects included shown here for comparison.

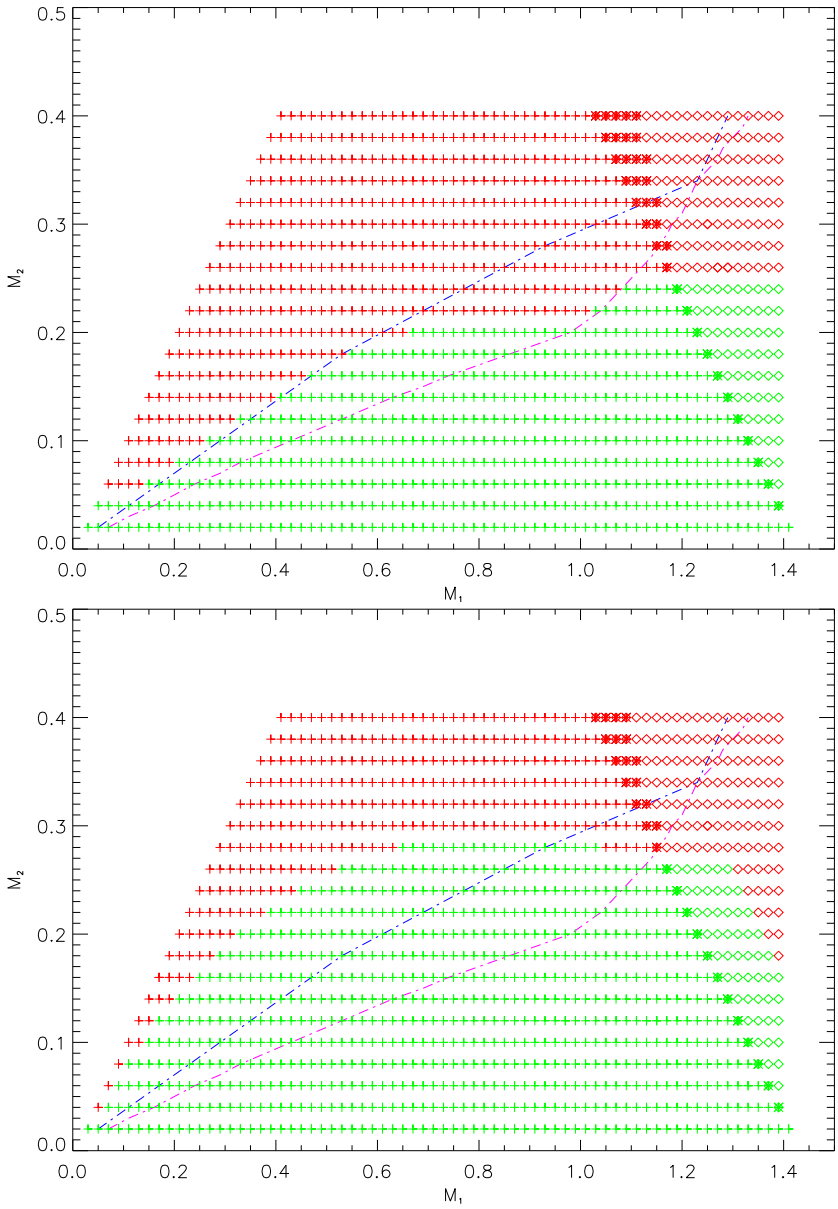

FIGURE 5.8. Behavior of systems across the parameter space – II. Evolution for 10^9 yrs for an initial τ_{s_1} of 10^{15} yrs (top panel) and for τ_{s_1} of 10 yrs (bottom panel). This synchronization time is for the initial configuration and evolves according to Eq. (2.10). τ_{s_2} is calculated based on whatever τ_{s_0} is required to obtain the desired value of τ_{s_1}. The red symbols represent Super-Eddington accretion, the green are Sub-Eddington, the pluses (+) and hollow diamonds ($\Diamond$) represent systems with total mass below and above the Chandrasekhar limit respectively. Among the latter asterisks over diamonds indicate systems in which the accretor does not reach the Chandrasekhar limit in 10^9 yr. The blue dash-dot line is the initial stability boundary with all donor effects included. The magenta line is the stability boundary without these effects, shown here for comparison. Note the transition in the Super and Sub-Eddington accretion rate around an M_2 of 0.2 $M_\odot$ to the latter stability curve.

cretor masses is relatively smaller, and so the threshold for super critical accretion is relatively lower at accretor masses close to the Chandrasekhar limit.

In Fig. 5.9 we show the locus of systems that undergo oscillations in their separation and orbital period. As is described in Section 5.1, when a system first gets into contact and if the mass transfer timescale is much shorter than the tidal synchronization timescale of the accretor, the accretor can spin up appreciably. This is especially so in the case of unstable mass transfer. Eventually, as the separation increases, the mass transfer rate begins to fall and τ_{M_2} increases rapidly (See Fig. 4.1). τ_{s_1} does not evolve as rapidly as the mass transfer rate and eventually, the synchronization timescale (τ_{s_1}) becomes of the order of (or shorter than) the mass transfer timescale (τ_{M_2}). In this situation, the angular momentum stored in the spin of the accretor is efficiently returned to the orbit. If enough asynchronism has been built up in the accretor during the accretion phase, the additional injection of spin angular momentum to the orbit can cause the system to detach. Thus the appropriate matching of timescales is critical for tidally induced detachment to operate, and as a result the oscillations are observed only in a particular domain in the $M_2 - M_1$ parameter space. Since the tidal synchronization timescale is a 'free parameter' not determined from first principles, this domain is also a function of the choice of the tidal timescale. We choose, rather arbitrarily, tidal timescales of 500 yrs, 2500 yrs and 5000 yrs for our study. From Fig. 5.9 we notice firstly that the systems that do undergo oscillations are *less stable* or unstable systems. Almost all the systems lie above the magenta stability curve (See Fig. 5.5 and related discussion) and are almost evenly distributed on either side of the blue stability curve. We also observe that systems with high donor mass ($M_2 > 0.35 M_\odot$) do not undergo oscillations. This is because the mass transfer rates are high in this domain and thus the tidal timescales (considered here) are much higher as compared to the mass transfer timescales. Consequently, the radius of the donor keeps up with the increase in the Roche lobe radius throughout the evolution, and the systems stay in contact. On the other hand, systems to the bottom right, the ones with low donor mass and high accretor mass are stable systems and are more likely to be disc systems. Thus the accretor is not spun up as much as in the case of less stable or unstable systems and consequently these systems do not undergo any oscillations either.

5.3 Comparison with Hydrodynamic Simulations

A class of equilibrium configurations result from a relationship between the pressure (P) and the density (ρ) given by

$$P = K\rho^{n+1/n}, \tag{5.2}$$

is called the "Polytropic" equation of state which is widely used in both, the analytic and numerical studies of stellar models. K is called the polytropic constant

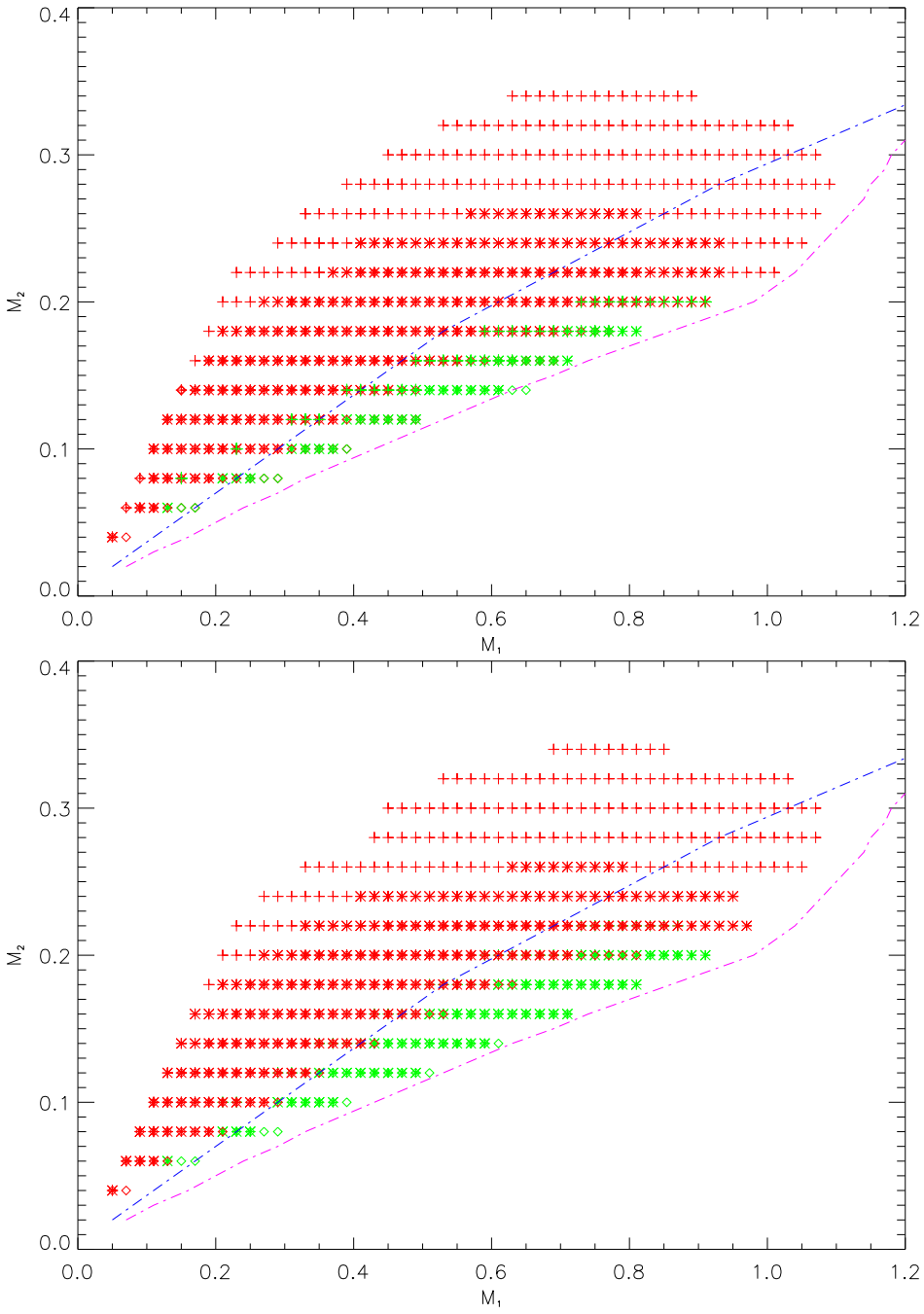

FIGURE 5.9. Tidal effects across the parameter space. *Top Panel:* Systems which undergo 'oscillations' at least once during their evolution for $\tau_{s_1} = 500$ yrs (pluses, +), 2500 yrs (crosses, $\times$) and 5000 yrs (hollow diamonds, $\Diamond$). As before, red indicates super-Eddington transfer during any part of the evolution, whereas green indicates subcritical transfer throughout the 10^9 yr evolution. The magenta and blue lines are the stability limits as in previous figures. τ_{s_2} is held at a constant 10 yrs initially for all the points. *Bottom panel:* The same cases, but with $\tau_{s_2} = 100$ yrs.

TABLE 5.2. Parameter values in code and real units for hydrocode model Q0.5

System Parameter Parameter	Initial SCF value	Initial "real" value
q	0.500	0.500
M_1	3.073×10^{-3}	1.0 $M_\odot$
M_2	6.143×10^{-3}	0.5 $M_\odot$
a	0.8764	0.052 $R_\odot$
Ω	0.1174	0.0655
K_1	0.016	3.12×10^{12}
K_2	0.016	3.12×10^{12}

and n is the polytropic index. In the case of spherical polytropes with uniform entropy in mechanical equilibrium, one can show that (Chandrasekhar, 1939)

$$R_i \propto M_i^{(1-n)/(3-n)} \tag{5.3}$$

Motl, Tohline & Frank (2002) developed a 3-D code comprising of a Self-Consistent Field code which generates synchronous polytropic binaries in circular orbits and a gravitational hydrodynamics code to follow the evolution of such binaries in time. This code was improved upon by D'Souza et al. (2006), and is currently capable of following self-consistently the evolution of model white dwarf binaries through the rapid phases of mass transfer, tracking mass and angular momentum with high accuracy for well over 30 orbital periods. Detached, Semi-detached or contact binaries can be generated using the self-consistent field code. These systems may be driven by either imposing angular momentum loss from the system or by an arbitrary rate of pseudo-thermal expansion of the donor. The resultant evolution is quite complicated, and hence a simpler approach like our OAE helps in understanding some of the aspects of these 3-D hydro-evolutions.

To this end, we apply the same initial conditions to our OAE as have been used in the various runs carried out by D'Souza et al. (2006). In this work, several models are generated and evolved under different conditions. Here, we concentrate on the runs with $q = 0.5$. The initial parameters of the binary are given in Table 5.2 for ready reference. In these runs, the binary was evolved at a constant driving rate of 1% per orbital period for 2.7 orbits (Q0.5-a, blue curve), 5.3 orbits (Q0.5-b, green curve) and throughout the evolution (Q0.5-c, red curve) as shown in Fig. 5.10. In order to compare these runs with the results from our OAE, we apply the same initial conditions as that imposed in D'Souza et al. (2006). We have the tidal normalization factor (τ_{s_0}, see eq. 2.10) and the mass transfer rate scaling ($\mathfrak{m}$) – such that $\dot{M}_2 = -\mathfrak{m}\dot{M}_0 f(\Delta)$ – as 'free parameters', which we adjust so as to obtain as close a match to the hydro-runs as we can. In the particular run shown in Fig. 5.10, $\tau_{s_0} = 0.75$ and $\mathfrak{m} = 35.0$. This choice is not unique – indeed, we get reasonable 'fits' even for other combinations of these 'free parameters'. It should be noted that in the numerical simulations of D'Souza et al. (2006) the minimum

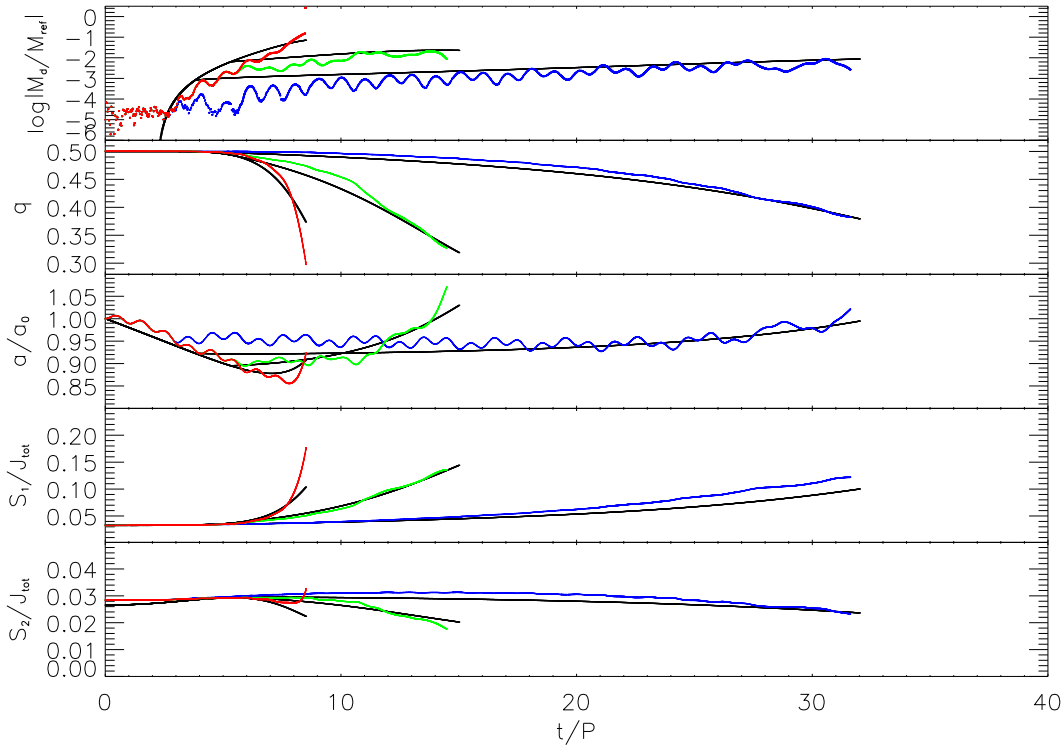

FIGURE 5.10. Comparison of the OAE numerical integrations with some of the numerical simulations ($q = 0.5$ run) in D'Souza et al. (2006). Three simulations were performed for the same initial conditions but the binary was driven by angular momentum losses at the level of 1% per orbit for different times in order to achieve increasing depths of contact: Q0.5-a (blue; driven initially for 2.7 orbits), Q0.5b (green; driven for the first 5.3 orbits) and Q0.5-c (red; driven throughout). The solid black curves show the accretion rate in donor masses per period, the binary mass ratio, the separation normalized to the initial separation, and the spin angular momenta as predicted by the OAEs, while the colored curves show the same quantities as derived from the results of the simulations. We arbitrarily change τ_{s_i} of the donor and accretor to match the Q0.5-a run and then predict the outcomes of the other simulations. Here, $\tau_{s_1} \sim 150P$ and $\tau_{s_2} \sim 3.5P$ initially.

resolvable mass transfer was on the order of $\sim 10^{-5}M/P$, which translates for short period AM CVn binary parameters to $\sim 10^{4}\dot{M}_{\rm Edd}$! Also, in the case of the hydro-runs, one observes severe distortion of the accretor and the formation of an accretion belt around the accretor towards the end of the 3-D simulations. These features cannot be easily incorporated in the OAEs, and so the later stages of evolution especially in the case of Q0.5-c, cannot be properly represented in the OAE. An added complication is that for the hydro-runs, the driving was cut off after the systems were thought to have reached a deep enough contact. Since the effective density levels, especially near the edge of the stars in the 3-D numerical model differs from an ideal n = 3/2 polytrope due to the finite numerical resolution of the code, the depth of contact achieved after a certain amount of driving for a certain period of time is not necessarily the same for the hydro-runs and the OAE runs. This is especially true for Q0.5-a, because it is the one which is most sensitive

to the depth of contact at the instant the driving is cut-off. For runs Q0.5-b and Q0.5-c, the depth achieved is deep enough to make small differences between the hydro-runs and the OAE unimportant. The LSU group (Motl, Tohline & Frank, 2006) is working on another set of runs in which the driving is not cut off and the systems are driven at slightly lower (and more realistic) rates. We hope that this will eliminate another source of discrepancy between the hydro-runs and the OAE.

Despite the above mentioned shortcomings, the OAEs do reproduce reasonably well the behavior of the binaries we have studied. One notices that the hydro-runs have a gentler slope initially which progressively gets steeper as compared to the OAE runs. This, we believe, is a consequence of the complicated fluid flow around the L_1 point and the distortion of the donor star. Moreover, during the initial stages of the evolutions, the 3-D hydrodynamic simulations are subject to numerical noise which is not the case for our numerical integrations. The relative significance of this noise diminishes as the mass transfer rate increases during the evolution. Also, the epicyclic motion that one encounters in the hydro-runs (see D'Souza et al. (2006) for details) cannot be reproduced in our results, since we assume circular orbits. Thus the behavior of the OAE is much smoother than the numerical hydro-runs with no abrupt changes in slopes of the various parameters.

We conclude from the above discussion and Fig. 5.10, that the OAEs confirm that: a) tidal effects play an important role in the numerical simulations of the binary, b) direct impact accretion is an important effect and can lead to significant spin-up of the accretor at the expense of orbital angular momentum, and c) the OAE prediction that systems that are initially unstable can indeed survive mass transfer seems to bear out in the hydro-runs despite the rather extreme conditions the binaries in the hydro-runs are subjected to. Moreover, the tidal timescales that most closely match the behavior observed in the simulations serve as a measure of the numerical dissipation present in the simulations.

5.4 DWD GWR Sources and LISA

As mentioned in the introduction, DWD binaries and AM CVn binaries in particular are *guaranteed* sources for the space based gravitational wave detector LISA (Bender, 1998). Numerous studies are being carried out to generate accurate 'wave templates' for GWR sources, in order to detect and analyze these intrinsically weak signals. The GWR strain, which is the quantity the detector measures, has two polarizations given by

$$h_+ = \frac{2G^2 M_1 M_2}{aDc^4} \cos 2\omega t \tag{5.4}$$

$$h_\times = -\frac{2G^2 M_1 M_2}{aDc^4} \sin 2\omega t \tag{5.5}$$

where, D is the distance of the source from the detector. The GWR luminosity of a binary is given by:

$$L = \frac{2G^4}{5} \left(\frac{M}{ac}\right)^5 \tag{5.6}$$

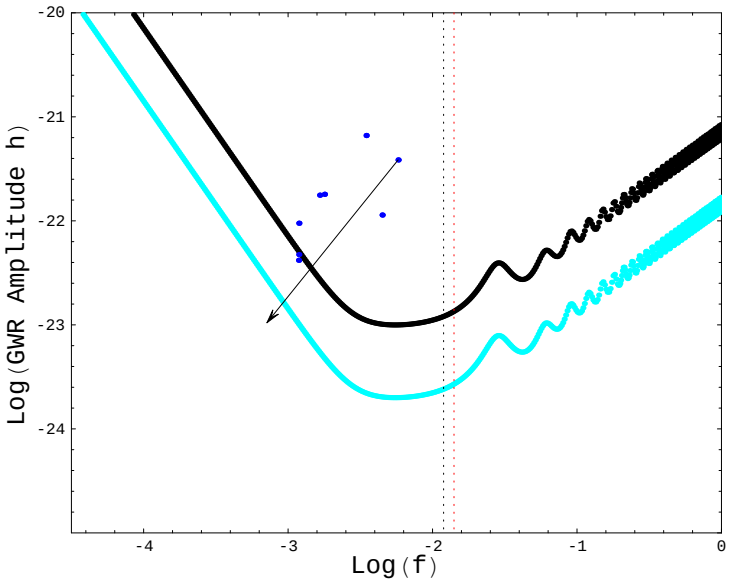

FIGURE 5.11. The LISA sensitivity curve along with the known AM CVn systems for mission time of 1 yr. The cyan curve represents a S/N of 1 and the black curve is a S/N of 5. The arrow represents the direction of evolution of RX J0806, which will end up near the arrowhead in 10^9 yr. The source is assumed to be at a distance of 300 pc, unless the distance is known (See table 1.1). The vertical black (inefficient tidal coupling) and red (efficient tidal coupling) dotted lines are the frequencies corresponding to the initial masses of the donor, above which DWD systems are likely to undergo super-Eddington accretion.

where, M is the total mass of the system. Thus the GWR luminosity is a strong function of the separation a. From our formulation (Chapter 2), it is straightforward to calculate the strain, since it is only a function of the orbital separation a and the mass of the components M_1 and M_2 which we can track self-consistently. Moreover, we can also include the effects of the spin-orbit coupling, direct impact accretion and also mass loss due to super-critical accretion. It is instructive to study the 'strain sensitivity curve' (Hughes et al., 2001), where the height of the source above the sensitive curve is the S/N with which the source will be detected in ideal conditions (perfect template and no background or confusion noise). The sensitivity curve (Fig. 5.11) represents the fractional change in the LISA detector arm length due to various sources of noise, integrated over one year. The sensitivity curve is itself a function of the integration time: the longer the integration time, the more sensitive the instrument and the higher the S/N for a given source. Note that in order to be able to integrate the signal for a period of one year, accurate templates need to be generated for the possible evolution trajectories of the DWD systems.

In general, one can distinguish between two types of sources for LISA – a) sources with evolution slow enough that $\dot{f} \approx 0$ through the integration time, and b) sources for which $\dot{f} \neq 0$. In the first case, since the systems are not evolving very rapidly, in principle one can use a sine-wave as a template. But for the systems

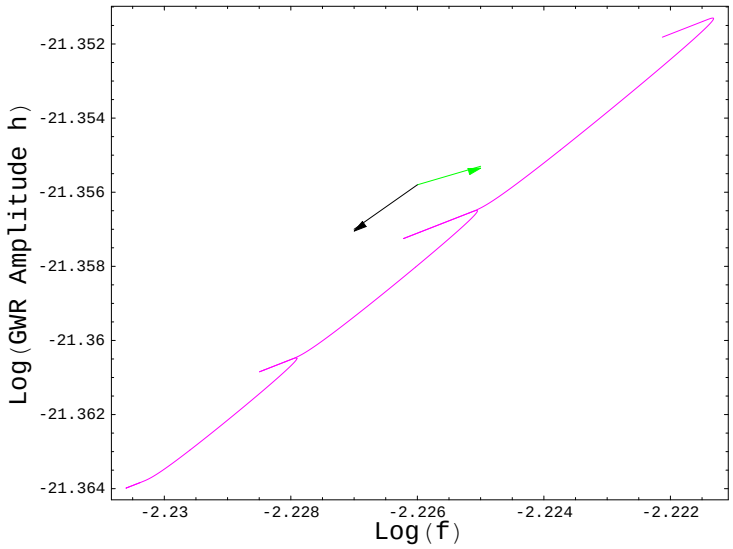

FIGURE 5.12. Oscillation cycles and the sensitivity curve. Short term evolution of a DWD binary undergoing oscillation cycles on the LISA strain curve. The binary is assumed to be at a distance of 300 pc. The green arrow represents the approximate direction of evolution of a detached system, whilst the black arrow represents the direction of evolution of a system undergoing conservative mass transfer.

that evolve rapidly, one needs proper templates in order to integrate the signal over the observational timescale. Strictly speaking, one needs to develop detailed 3-D models of mass transferring binaries in order to generate accurate templates for these objects. This is however, a time and resource consuming option. Though our orbit averaged equations do a reasonable job in tracking the evolution of the 3-D hydro-dynamic simulation (Section 5.1), we shall not present the strain curves for individual systems, but instead concentrate on the overall evolution of the system in the $\log(f) - \log(h)$ domain. In Fig. 5.11, we show the LISA sensitivity curve, along with the known AM CVn systems from Table 1.1. The arrow points in the direction of evolution – as a given system transfers mass, its orbital separation increases and consequently, the amplitude and the frequency decrease. Also, we have seen in Section 5.2 that for inefficient tidal coupling all the systems with a donor mass $M_2 \gtrsim 0.25\ M_\odot$ (0.28 $M_\odot$ in the case of efficient tidal coupling) undergo super-Eddington accretion. Since the orbital period, and hence the GWR frequency, for a system in contact is a strong function of the donor mass (Eq. 4.12) this corresponds to a particular frequency above which the systems will tend to accrete super-critically, at least for a brief phase in its evolution. Note that this frequency is *independent of the distance of the object*, but depends strongly on the mass-radius relationship and the consequential angular momentum loss mechanisms from the system (which determine the stability properties of the system and hence the mass transfer rate).

We now translate the results from Sections 5.1 & 5.2 displayed in Figs. 5.7, 5.8 & 5.9 onto the LISA sensitivity curve.

Short Term Evolution

DWD systems with intermediate tidal synchronization timescales with mass ratio's $q \sim q_{\rm stable}$ which are undergoing direct impact accretion tend to undergo oscillation cycles (Gokhale et al., 2006). As we have seen in Section 5.1, the oscillation cycles tend to last for $\sim 10^5$ years after the system initially gets into contact. This should be reflected in the short-term behavior of DWD systems on the LISA sensitivity curve. In Fig. 5.12 we plot the evolution of a system ($M_2 = 0.125\ M_\odot$, $q = 0.28$, $\tau_{s_1} = 2500$ yr) over 20,000 yr as it evolves on the $\log(f)$ - $\log(h)$ plane. Initially (top right corner of Fig. 5.12), the system evolves towards the top right (indicated by the green arrow): to higher amplitudes and frequencies, since the separation decreases due to loss of angular momentum by GWR. Once the system gets into contact, and sufficient depth of contact is achieved, the system begins to separate, leading to a decrease in amplitude and frequency (indicated by the black arrow in Fig. 5.12). This persists until the system detaches and the GWR term dominates again in Eq. 2.17. Once this happens, the system evolves again along the direction depicted by the green arrow until it gets into contact again. After this the system follows, as before, the trajectory toward the bottom left of the figure. Thus, due to the tidal oscillations, the amplitude and the frequency of the GWR signal also oscillates – increasing whenever the system is detached and decreasing whenever it is in contact and the separation is increasing. This example illustrates an added complication in the generation of accurate templates; for example, if the system is undergoing oscillations, the same point on the $\log(f)$ - $\log(h)$ plane can be traversed by the same system multiple times, at least for a few years after initial contact.

Long Term Evolution

We start with a uniformly distributed grid of initial component masses, and let the systems evolve for 10^9 yrs and plot the strain at the initial and final times on the sensitivity curve. We start with a uniform distribution of masses in the M_2 - M_1 parameter space, just as we did in section 5.2, and determine the gravitational wave strain and frequency at the point of contact for each of these systems. These are shown in Fig. 5.13 by the red (super-Eddington systems) and green dots (sub-Eddington systems). Systems with the same donor masses lie almost parallel to the abscissa since the orbital period at contact is a strong function of the donor mass alone (Eq. 4.12). The top panel in Fig. 5.13 represents the case of inefficient tidal coupling whilst the bottom panel represents efficient tidal coupling. As we have seen in Fig. 5.8, the direct impact systems with inefficient coupling tend to accrete supercritically and so many more systems in the top panel undergo super-Eddington accretion. We notice that systems above a particular frequency ($\log(f_{\rm Edd}) \sim$ -2 in the top panel and $\log(f_{\rm Edd}) \sim$ -1.8 in the bottom panel) always undergo super-Eddington accretion, irrespective of the mass ratio q as was described earlier. There are systems below these frequencies that also undergo super-Eddington accretion – these are usually systems with mass ratio's $q \gtrsim q_{\rm stable}$.

The systems tend to evolve (as denoted by the arrow in Fig. 5.11) towards lower frequencies and lower values of the GWR strain. We notice that all systems, irrespective of their initial masses tend to collect in a small area towards the

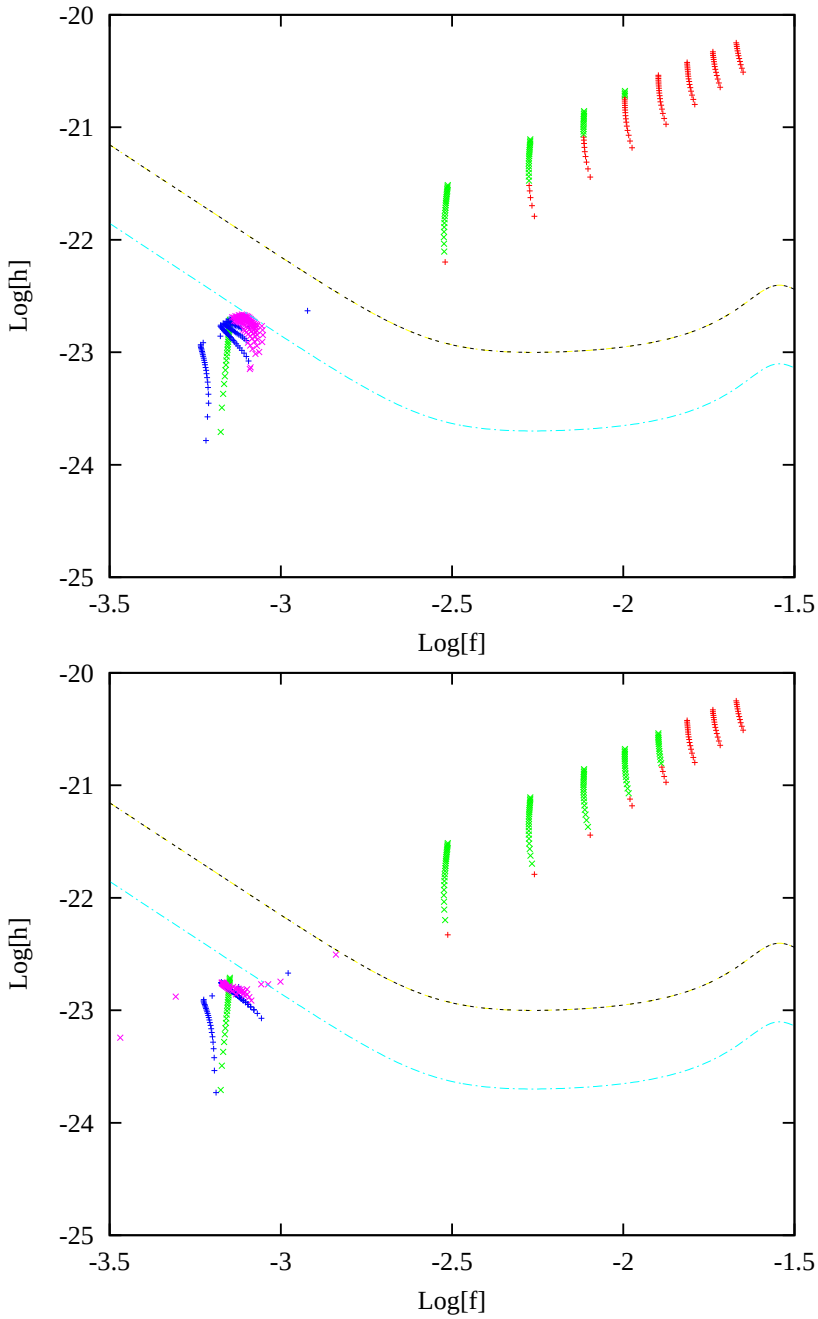

FIGURE 5.13. Evolution of DWD systems on the sensitivity curve. The initial and final location of DWD systems on the LISA sensitivity curve for inefficient spin-orbit coupling ($\tau_{s_1} \sim 10^{10}$ yrs, top panel) and extremely efficient coupling ($\tau_{s_1} \sim 10$ yrs, bottom panel). All systems are assumed to be at a distance of 300 pc. The green and red points running parallel to the abscissa represent sub and super-Eddington systems at the initial state, just as they become semi-detached. We have chosen a uniform initial distribution of donor mass with M_2 ranging from 0.01 $M_\odot$ to $M_2 = 0.41$ $M_\odot$ in steps of 0.05 $M_\odot$. The initial accretor mass is also changed in steps of 0.05 $M_\odot$ from 0.05 to 1.4 $M_\odot$ for systems having total mass $M < M_{\rm ch}$. The final state represents the state of the system after 10^9 yrs, the blue points being the sub-Eddington and the magenta being the super-Eddington systems. The cyan and black lines indicate the LISA sensitivity curves with a S/N of 1 and 5 respectively.

bottom left of the plots. This is because the GWR timescale ($\tau_{\rm GR}$) approaches our integration timescale of 10^9 yrs as the systems evolve to higher separations. In effect then, the systems stall and the evolution timescale is much higher than the Hubble timescale. The systems which undergo super-Eddington accretion at some point in their evolutions have a larger spread in their final distribution since mass loss from the system alters their evolutionary tracks.

Kopparapu & Tohline (2006) present population boundaries in the $\log(f)-\log(h)$ plane, which represent limits on the domain in which one would expect to 'see' GWR signals from mass transferring AM CVn systems. The GWR frequency $f_{\rm Edd}$, which corresponds to the maximum donor mass that a AM CVn system can have in order to undergo sub-Eddington accretion, serves as another such 'boundary'. Above this boundary, we expect that the evolution of the binary will be influenced by mass loss from the system, and in extreme cases (higher frequencies), by the formation of a common envelope.

The next logical step in this type of analysis is to incorporate the above results in a population synthesis study. For this, an appropriate initial mass function is required which specifies the initial distributions of the total mass, mass ratio, orbital periods and so on. Then, treating for example, the tidal synchronization timescale as a free parameter, one can study the evolutionary outcomes of the entire population of DWD systems in the galaxy. Stroeer et al. (2005) and others have done such studies, but without incorporating the effects of intermediate tidal timescales and the advective donor spin term.

Part II: Extensions to Accretion Disk Theory

6. Accretion Disks: Theory

6.1 Background

Accretion refers to the phenomenon of accumulation of matter onto a massive central body. In nature, one encounters accretion processes at different scales, ranging from planets to the centers of galaxies. Kuiper (1941) was one of the first modern scientists to consider the accretion of matter onto a massive object during his study of contact binaries. He immediately realized that as matter was transferred from one star to the other, it invariably formed a ring around the central star. Despite this early insight, Kuiper's work remained rather obscure and it was Salpeter (1964) & Prendergast & Burbridge (1968) who resurrected the idea of an "accretion disk" to explain the details of the mass transfer in massive compact objects like black holes and X-ray binaries. It was, however, the seminal paper by Lynden-Bell (1969) that firmly entrenched the paradigm that accretion disks were indeed the central power houses of quasars along with the central black hole. This paper by Lynden-Bell (1969) and those by Shakura & Sunyaev (1973) and Lynden-Bell & Pringle (1974) laid the foundations of accretion disk theory as we know it today.

The basic concept involved in accretion and the formation of a disk is simple to understand. As an example, consider the formation of a star out of a tenuous gas cloud. As the cloud collapses under its own self-gravity, the internal energy generated is promptly radiated away, but the gas does not have the opportunity to rid itself of angular momentum. As a consequence, an initially spherical blob of gas tends to rotate faster and flatten in the plane to form a disk. The disk thus acts as a repository for the excess angular momentum as the gas contracts under its own weight. Thus, an originally spherically symmetric distribution, in the presence of a small amount of rotation, is transformed into a disk with most of the matter moving inwards and a small amount of matter carrying away the excess angular momentum outward to infinity.

Accretion disks are a common phenomenon in astrophysics. As mentioned in Chapter 1, they are of significance in mass transferring binary systems, active galactic nuclei, protoplanetary disks and so on. In what follows, we shall concentrate on disks found in binary systems though our treatment is quite general, as we shall see in Section 7.2. As we have seen in Section 2.2, a binary is driven into contact either by the loss of angular momentum or the evolution of one the components, so that the donor fills up its Roche lobe. Matter begins to leak through the L_1 point, and is attracted towards the accretor due to gravity. These parcels of gas have high specific angular momentum, and if the accretor is a compact object, the gas swirls around the accretor. As we have seen in Section 2.2, to a good approximation, we can assume the stream to follow a ballistic trajectory (Fig. 2.2).

Thus, we expect the stream to follow an elliptical orbit in the plane of the binary. The potential around the accretor is not a pure $1/r$ potential, but is a perturbed potential due to the presence of the donor. As a consequence, the ballistic trajectory does not close on itself, but is instead rosette shaped. If we have a continuous stream of parcels of gas instead of a single test particle, the stream would interacts with itself, resulting in dissipation of energy via shocks (Frank et al., 2002). However, the stream does not have the means to lose angular momentum and so it forms a circular (lowest energy) orbit around the accretor. Shocks and viscous dissipation result in the conversion of the energy in the bulk motion of the gas into heat energy, which is radiated away. As the gas loses more and more energy, it tends to circularize since for a gas with fixed amount of angular momentum, a circular orbit is the orbit with least energy. Now, the gas has to sink deeper into the potential well because it is loosing energy, but it can only do so if it can rid itself of some of its angular momentum. In the absence of external torques, this can occur only if angular momentum is transferred outwards by the internal torques in the "disk". Thus, the initial configuration with a ring of gas at $R = R_{\rm circ}$, spreads out into a disk in the plane of the orbit, with the bulk of the gas spiralling in and a small amount of material spiralling outwards, carrying away the excess angular momentum.

6.2 Basic Equations

In this section, we develop the basic equations which govern the structure and evolution of accretion disks, concentrating on disks in binary systems for concreteness. Our treatment is quite general, though, and can easily be extended to disks in other scenarios. We have outlined above, how the material leaking out of the L_1 point settles into an accretion disk. In most cases, the disk is confined close to the orbital plane and to a good approximation, one can consider the disk to be a two-dimensional flow. This is called the *thin disk approximation*, and for the most part it is quite successful in accounting for many of the observational characteristics of binary systems with accretion disks.

Consider the orbital plane of a binary to lie in the z=0 plane of an $(R,\ \phi,\ z)$ co-ordinate system centered on the primary star with mass M_1 and radius R_1. The gas has a circular velocity (v_ϕ) given by

$$v_\phi = R\Omega(R) \tag{6.1}$$

where, Ω is the angular velocity of the disk given by

$$\Omega(R)^2 = \frac{1}{R}\frac{\partial \Phi}{\partial R} \tag{6.2}$$

In most cases of interest when a compact object is at the origin, the potential $(\Phi(R))$ near the origin is dominated by the central mass. Also note that the specific angular momentum (the angular momentum per unit mass) is given by $h = R^2\Omega(R)$. Apart from the circular velocity v_ϕ, the gas also has a small radial velocity v_R. The disk itself is characterized by a surface density $\Sigma(R,t)$, which is

obtained by integrating the gas density ρ along the z-direction. We now use the conservation of mass and angular momentum to obtain the transport equations for the accretion disk due to the radial motion (Frank et al., 2002). Consider an annulus of the disk lying between a radius R and $R + \Delta R$. The total mass in this annulus is $2\pi R\Delta R\Sigma$, and the rate at which the mass in this annulus changes is given by the net flow across its boundaries from the neighboring annuli. Thus

$$\begin{aligned}\frac{\partial}{\partial t}(2\pi R\Delta R\Sigma) &= v_R(R,t)2\pi R\Sigma(R,t) - v_R(R+\Delta R,t) \\ &\quad \times 2\pi(R+\Delta R)\Sigma(R+\Delta R,t) \\ &\simeq -2\pi\Delta R\frac{\partial}{\partial R}(R\Sigma v_R)\end{aligned}$$

In the limit that $\Delta R \to 0$, we obtain the mass conservation equation

$$\begin{aligned}R\frac{\partial\Sigma}{\partial t} + \frac{\partial}{\partial R}(R\Sigma v_R) &= 0, \\ \therefore 2\pi R\frac{\partial\Sigma}{\partial t} + \frac{\partial\dot{M}}{\partial R} &= 0 \end{aligned} \tag{6.3}$$

where, $\dot{M} = 2\pi R\Sigma v_R$ is the vertically and azimuthally integrated outward mass transfer through the disk. Similarly, the amount of angular momentum in an annulus lying between R and $R + \Delta R$ is given by $2\pi R\Delta R\Sigma R^2\Omega$, and the rate of change of angular momentum in this annulus is also given by the net flow across the boundaries of the annulus. This leads to an equation for the conservation of angular momentum in the disk:

$$\begin{aligned}R\frac{\partial}{\partial t}(\Sigma R^2\Omega) + \frac{\partial}{\partial R}(R\Sigma v_R R^2\Omega) &= \frac{1}{2\pi}\frac{\partial G}{\partial R} \\ \therefore 2\pi R\frac{\partial}{\partial t}(\Sigma h) + \frac{\partial}{\partial R}(\dot{M}h) &= \frac{\partial G}{\partial R}\end{aligned} \tag{6.4}$$

Here, $G(R,t)$ represents the total viscous torque exerted in the disk by the stuff outside of R *on* the stuff inside of R. On combining Eqs. 6.3 & 6.4, we obtain

$$\dot{M}(R,t) = \frac{\partial G(R,t)}{\partial h}\ . \tag{6.5}$$

Using this last result in the second term on the left-hand side of equation (6.3), we get:

$$2\pi R\frac{\partial\Sigma}{\partial t} = -\frac{\partial}{\partial R}\frac{\partial G}{\partial h}\ . \tag{6.6}$$

The above form was used by Lyubarskij & Shakura (1987) for their treatment of non-stationary disk accretion in the Keplerian case, but in fact it is valid also in the more general case considered here. Eq. 6.6 can be written in a more familiar form as

$$\frac{\partial\Sigma}{\partial t} = -\frac{1}{2\pi R}\frac{\partial}{\partial R}\Big[\frac{1}{(R^2\Omega)'}\frac{\partial G}{\partial R}\Big]\ . \tag{6.7}$$

In the case of a Keplerian disk, the angular frequency is given by

$$\Omega_K(R) = \left(\frac{GM}{R^3}\right)^{1/2} \tag{6.8}$$

and so using Eq. 6.8, Eq. 6.6 reduces to the well-known diffusion equation:

$$\frac{\partial \Sigma}{\partial t} = \frac{3}{R}\frac{\partial}{\partial R}\Big\{R^{1/2}\frac{\partial}{\partial R}(\nu \Sigma R^{1/2})\Big\} \tag{6.9}$$

6.3 The Role of Viscous Torques

Viscosity plays an important role in the formation and evolution of the accretion disk. Theoretically, the origin of viscosity in a disk was not well understood for a long time even though it was invoked in the standard theory of disks right from the beginning. Balbus & Hawley (1991) discovered that magnetohydrodynamic (MHD) turbulence results in a viscosity of the right magnitude and sign. In fact, the weak-field instability which leads to the turbulence was already known to Velikhov (1959) & Chandrasekhar (1961). In any case, we shall see below that the detailed knowledge of the origin of viscosity is not critical in understanding the evolution of disks.

The gas in the disk rotates differentially, for example in a Keplerian disk. This leads to a shear in the gas given by $A = Rd\Omega/dR$. The presence of any viscosity, whatever its origin, leads to viscous dissipation in the disk that damps out the shearing stresses. This results in the conversion of the kinetic energy of the gas in the disk to heat energy which is radiated away. Thus the gas loses energy and has to sink deeper into the potential well, which it can do only by ridding itself of some angular momentum. This is achieved by the spreading of the disk both inward and outward from the initial ring – most of the mass moves inward, but a small amount of material moves outward, carrying with it the excess angular momentum. The local viscous timescale which is of the order $t_{\rm visc} \sim \frac{R^2}{\nu}$, is the timescale over which the disk spreads. In general, this timescale is much longer than the timescale over which the gas loses energy. As a result, even though the gas spirals in – it follows a near circular orbit which is the lowest energy configuration for gas with a specified amount of angular momentum.

The viscous force per unit length is given in terms of the rate of shearing as $\nu\Sigma A$ and hence the torque exerted by an annulus at $R + dR$ on an annulus centered at R is given by

$$\begin{aligned} G(R,t) &= 2\pi R\nu\Sigma AR \\ &= 2\pi R\nu\Sigma R^2\Omega' \end{aligned} \tag{6.10}$$

where, $\Omega' = d\Omega/dR$ and ν is the kinematic viscosity.

Since we are not in a position to derive an expression for the viscosity from first principles, we utilize a parametrization following Shakura & Sunyaev (1973). Quite

generally, one can assume that the primary mechanism for redistribution of angular momentum within the disk is turbulent motion of some kind. The *kinematic* viscosity is then given by (Pringle, 1981)

$$\nu \sim \lambda \tilde{v} \tag{6.11}$$

where λ is scale and $\tilde{v}$ is the velocity of the turbulence. In an accretion disk, the maximum scale of the turbulence has to be of order H, the scale height of the disk. Also, the turbulence cannot be supersonic since that would lead to shocks that would damp out the turbulence efficiently. Hence we can write

$$\nu = \alpha c_{\rm s} H \tag{6.12}$$

with $\alpha \leq 1$. This is the famous α-prescription (Shakura & Sunyaev, 1973), which allows us to model disks despite our ignorance about the origin of the viscosity. The parameter α is usually a *free parameter* in disk modeling, though it is somewhat constrained by observations. Semi-empirical studies usually assign $\alpha \sim 0.1$-0.01.

Apart from driving the angular momentum transport within the disk, the viscous torques also are responsible for converting rotational energy into heat energy at a rate $G\Omega' dR$ per ring of width dR within the disk. This heat energy is eventually radiated away from the upper and lower faces of the disk. Thus, the rate of energy dissipation per unit area in the disk is given by

$$D(R) = \frac{G\Omega'}{4\pi R} \tag{6.13}$$

and thus the total disc luminosity is

$$L_{\rm disk} = 2 \int_{R_\star}^{\infty} D(R) 2\pi R dR \tag{6.14}$$

where $R_\star$ represents the surface of the central star and hence the inner edge of the disk. In the Keplerian case, it is easy to show that (Pringle, 1981)

$$L_{\rm disk} = \frac{1}{2} \frac{GM\dot{M}}{R_\star} \tag{6.15}$$

Note that the amount of energy available is approximately equal to the total potential drop from infinity to the surface of the star at $R_\star$, and is simply $GM/R_\star$. We see that the disk luminosity accounts for only one-half the amount of energy available. The rest of the energy is emitted by the boundary layer, and in general, the contribution from the boundary layer to the overall luminosity of the disk is just as significant as the rest of the disk (See Section 6.4.2).

Turning back to the viscosity ν, we expect ν to be a function of both the local surface density $\Sigma(R)$ and the temperature $T(R)$ (the sound speed is a function of T). Thus $\nu \equiv \nu(T, \Sigma)$ and if $T(R)$ is known, one can write $\nu \equiv \nu(R, \Sigma)$. We shall deal with general solutions to the disk equation in Section 6.5. In the next section we deal with the simpler time-independent case, especially in the case of the Keplerian potential to obtain explicit expressions for the temperature, surface density and viscosity within the disk.

6.4 The Steady State

To obtain a steady state, we set the time derivative in (6.6) to zero and we obtain immediately the equilibrium torque in terms of h:

$$G(R) - G_0 = \dot{M}(h(R) - h_0)\,, \tag{6.16}$$

where R_0 is some reference radius at which the torque $G_0 = G(R_0)$ is known, $h_0 = h(R_0)$, and $\dot{M}$ is the constant mass transfer rate. Substituting the general expression for the viscous torque (6.10) in the above equation, we can solve for the combination $\nu\Sigma$:

$$\nu\Sigma = \frac{\dot{M}(R^2\Omega - h_0) + G_0}{2\pi R^3 \Omega'} = \frac{1}{2\pi}\frac{\mathrm{d}\ln R}{\mathrm{d}\ln\Omega}\left[\dot{M}\left(1 - \frac{h_0}{h}\right) + \frac{G_0}{h}\right]\,. \tag{6.17}$$

This is a convenient starting point for the complete solution for the structure of the steady state disk if the viscosity is known. It has to be supplemented by the vertical pressure balance equation, the vertical radiative transfer equation and the required opacities. While this may not be trivial in every case since ν in general may depend on Σ, the problem is solved in principle as we shall see in the following sections. Presently, we will obtain below a few explicit examples of steady disks, some already well-known, to illustrate the insight that can be gained from equation (6.17).

6.4.1 The Standard Keplerian Disk

In the standard treatments of the accretion disk around a white dwarf rotating slower than break-up velocity, the viscous torque vanishes at the inner boundary of the thin disk near the stellar radius R_*. Our equations neglect any radial pressure gradients and thus cannot be used in the above form to solve for the structure of the boundary layer (See however Section 6.4.2 below). Setting $\Omega = \Omega_\mathrm{K}$, $R_0 = R_*$, and $G_0 = 0$, we obtain from equation (6.17) the well-known result

$$\nu\Sigma = -\frac{\dot{M}}{3\pi}\left(1 - \sqrt{\frac{R_*}{R}}\right)\,, \tag{6.18}$$

where $\dot{M}$ is negative for accretion. Note that this solution explicitly requires the presence of a large negative torque at the outer boundary, usually assumed to originate from tidal forces.

Near the outer boundary of the disk a rapid transition from viscous to tidal torques takes place and the stream material, which carries the specific angular momentum h_circ of the circularization radius, is mixed and accelerated up to the local Keplerian angular velocity (see Fig. 6.1). A simple model of this tidal dissipation and stream mixing region can be formulated as follows. Let h_out denote the largest specific angular momentum of the disk for which equation (6.16) is valid. At some slightly larger radius the disk is truncated by tides and thus the viscous torque

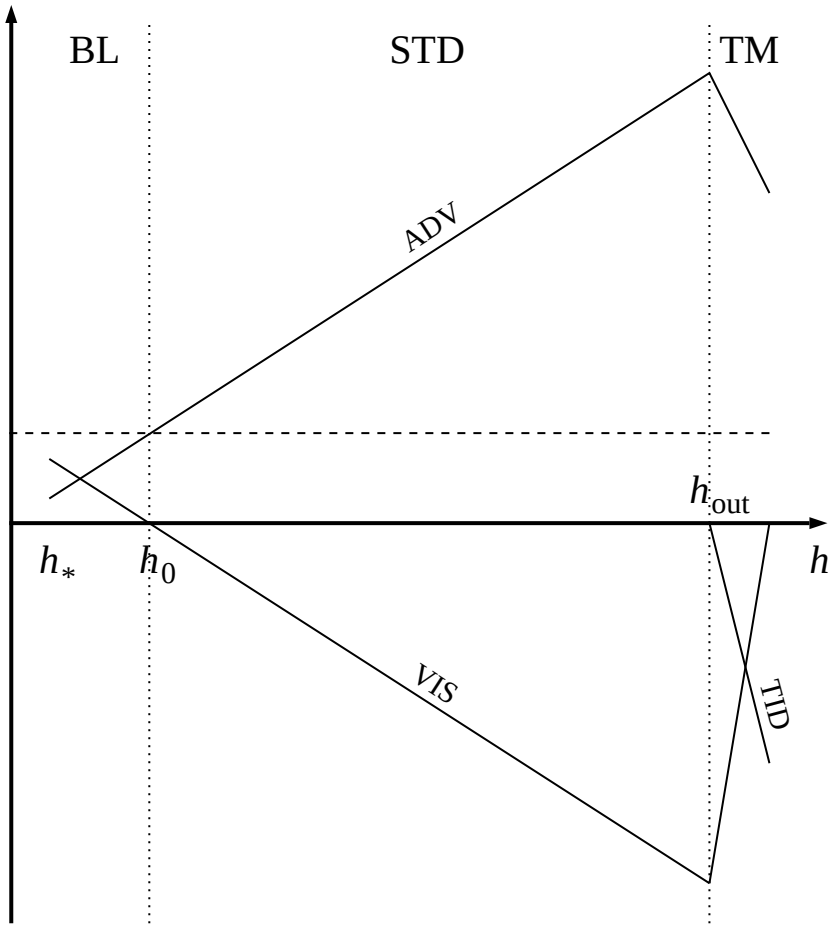

FIGURE 6.1. Angular momentum fluxes and torques shown schematically as functions of the specific angular momentum h. The regions labeled BL, STD and TM indicate respectively the boundary layer, the standard thin disk, and the tidal truncation and stream mixing region at the outer boundary.

must vanish there since there is no material beyond this radius. In steady state the total angular momentum of this outer layer must remain constant, therefore

$$-\dot{M}(h_{\rm out} - h_0) - \dot{M}h_{\rm circ} + \dot{M}h_{\rm out} + G_{\rm tides} = 0\,. \tag{6.19}$$

The first term in the above equation is the viscous torque exerted by the disk on the inner boundary of the layer, $G_{\rm tides}$ is the total tidal torque, and the other two terms represent the advection of angular momentum in and out of the layer respectively. This yields the physically reasonable result $G_{\rm tides} = \dot{M}(h_{\rm circ} - h_0)$, showing that tides simply remove the excess angular momentum from the disk while viscous torques transport this excess to the outer boundary.

6.4.2 Boundary Layer

Radial pressure gradients become important in the boundary layer (BL) and are important in determining the structure of this layer as mentioned above. However, as long as no significant azimuthal pressure gradients develop, we can extend our treatment of the angular momentum flux through the BL. This will enable us to derive an expression for the viscous dissipation in the BL based on energy and angular momentum conservation alone. In a narrow layer whose width b is determined by pressure gradients (Pringle, 1981; Frank et al., 2002), the angular velocity in the disk drops from a nearly Keplerian value to the stellar rotation rate. Let the specific angular momentum at the surface be h_*, then the BL satisfies $h_* < h < h_0$. While the radial extent of the BL is usually much less than the thickness of the disk, $b \ll H$, the difference $h_0 - h_*$ is not negligible unless the star is spinning near break up speed.

Since the torque vanishes at $h = h_0$, the net angular momentum flux into the star in steady state is $-\dot{M}h_0$. In fact this must be the *net* angular momentum flux at all radii in steady state. In the standard thin disk region h is Keplerian, or more generally given by equation (6.2), but becomes sub-Keplerian in the BL. The advected angular momentum is at all radii given by $-\dot{M}h$, even in the BL, where we do not know the radial variation of h with R until we solve for its structure. Thus the viscous torque, given by equation (6.16) in the standard disk region (STD), must be such in the BL that the net angular momentum flux is $-\dot{M}h_0$. Consequently the viscous torque in the BL has the same form in terms of h given by equation (6.16) and is shown schematically on Fig. 6.1. As the angular velocity decreases in the BL to match the stellar surface value, the advective flux falls while the viscous stress rises contributing to the spin up of the star, in such a way that the net flux of angular momentum remains equal to $-\dot{M}h_0$.

The rate of dissipation of energy in the BL can now be computed as the difference between energy fluxes at the top, where $\Omega \approx \Omega_{\rm K}(R_*)$ and the bottom where $\Omega = \Omega_*$, plus any work done by torques at these boundaries. The torque at the top vanishes while the viscous torque at the stellar surface is $G_* = \dot{M}(h_* - h_0)$. To first order in b/R_* we take $h_0 \approx R_*^2\Omega_{\rm K}$, and the rate of energy dissipation in the BL to the same order is given by

$$L_{\rm BL} = \frac{1}{2}(-\dot{M})(\Omega_{\rm K}^2 - \Omega_*^2) - \dot{M}(h_* - h_0)\Omega_* = \frac{GM(-\dot{M})}{2R_*}\left(1 - \frac{\Omega_*}{\Omega_{\rm K}}\right)^2 . \quad (6.20)$$

This is always less than the commonly adopted expression

$$L_{\rm BL} = \frac{GM(-\dot{M})}{2R_*}\left(1 - \frac{\Omega_*^2}{\Omega_{\rm K}^2}\right) , \quad (6.21)$$

which ignores the work done by viscous torques at the stellar surface (King, priv. comm.; Frank et al. (2002)), except at both extremes when either the star does not spin at all, or when it spins at break up. Note also that the our treatment holds even if the star were spinning in a retrograde sense, in which case the BL would

dissipate more than in the zero spin case, an effect not captured by the incorrect expression (6.21).

6.4.3 Temperature Distributions in Accreting and Passive Disks

A disk that is subject to torques at the boundaries such that no accretion is taking place, i.e. $\dot{M} = 0$, carries a constant torque $G = G_0$, and thus from Eq. 6.17 we get

$$\nu\Sigma = \frac{1}{2\pi}\frac{\mathrm{d}\ln R}{\mathrm{d}\ln\Omega}\frac{G_0}{h}\,, \tag{6.22}$$

Such *passive* disks are unlikely in astrophysical settings, but hold some academic interest. The surface temperature distribution of a disk is obtained by equating the outward vertical radiative flux to the local viscous dissipation rate given by

$$D(R) = \frac{1}{2}\nu\Sigma(R\Omega')^2 \tag{6.23}$$

For example, in the optically thick case one obtains generally, for both passive and accreting disks

$$\sigma T(r)^4 = \frac{1}{4\pi}\Omega^2\left|\frac{\mathrm{d}\ln R}{\mathrm{d}\ln\Omega}\right|\left[|\dot{M}|\left(1-\frac{h_0}{h}\right)+\frac{|G_0|}{h}\right] \tag{6.24}$$

As an example let us consider the case when $\dot{M} = 0$, which is the case of a passive accretion disk. For a Keplerian disk, we obtain from Eqs. 6.10 & 6.23:

$$\begin{aligned} G_0 &= -3\pi(GMR)^{1/2}\nu\Sigma \quad \text{and,} \\ D(R) &= \frac{9}{8}GM(\nu\Sigma R^{1/2})R^{-7/2} \end{aligned} \tag{6.25}$$

Now, using the α prescription for the viscosity, and using the fact that for a thin, Keplerian disk we must have $c_s = (kT/m_p)^{1/2}$ and $H = (c_s/v_K)\ R$ where v_K is the Keplerian velocity, we can write

$$\nu = \frac{\alpha k}{m_p(GM)^{1/2}}T(R)R^{3/2} \tag{6.26}$$

where, m_p is the mass of a proton and k is the Boltzmann constant. Using Eqs. 6.24, 6.25 & 6.26 one obtains the following set of equations for the disk parameters

$$\begin{aligned} T(R) &= \left[\frac{3}{8\pi\sigma}(GM)^{1/2}(-G_0)\right]^{1/4}R^{-7/8} \\ \nu(R) &= \frac{\alpha k_b}{m_p}\frac{1}{(GM)^{1/2}}\left[\frac{3}{8\pi\sigma}(GM)^{1/2}(-G_0)\right]^{1/4}R^{5/8} \\ \Sigma(R) &= \frac{(-G_0)m_p}{3\pi\alpha k}\left[\frac{3}{8\pi\sigma}(GM)^{1/2}(-G_0)\right]^{-1/4}R^{-9/8} \end{aligned} \tag{6.27}$$

Note that the quantity in the square bracket is always positive since G_0 itself is negative (Eq. 6.25).In the case of optically thin disks, one needs to specify the optical depth τ as well, since

$$D(R) = \sigma T^4 \tau \tag{6.28}$$

in this case. Usually, one assumes the Rosseland mean opacity (κ) such that $\tau = \kappa\Sigma$. In this case, the disk parameters turn out to be

$$\begin{aligned} T(R) &= \Big[\frac{3}{8\pi\sigma\kappa}(GM)^{1/2}(-G_0)\Big]^{1/4}\Sigma(R)^{-1/4}R^{-7/8} \\ \nu(R) &= \frac{\alpha k}{m}\frac{1}{(GM)^{1/2}}\Big[\frac{3}{8\pi\sigma\kappa}(GM)^{1/2}(-G_0)\Big]^{1/4}\Sigma(R)^{-1/4}R^{5/8}, \\ \Sigma(R) &= \Big[\frac{(-G_0)m}{3\pi\alpha k}\Big]^{4/3}\Big[\frac{3}{8\pi\sigma\kappa}(GM)^{1/2}(-G_0)\Big]^{-1/3}R^{-3/2} \end{aligned} \tag{6.29}$$

where, κ itself can be a function of Σ and T.

As mentioned before, setting $G_0 = 0$ in Eq. 6.17, yields the well-known surface density and temperature distributions for accreting Keplerian disks (Frank et al., 2002).

6.5 Time Dependent Solutions

In the most general case, it is not possible to find analytic solutions for the diffusion Eq. 6.7 unless some simplifying assumptions are made. Here, we consider some special cases for which it is possible to reduce Eq. 6.7 to a simple diffusion equation which has known analytic solutions, which help us in understanding the evolution of the disk when the proper boundary conditions are applied.

Using Eqs. 6.7 & 6.10, we can write quite generally

$$\frac{\partial\Sigma}{\partial t} = -\frac{1}{2\pi R}\frac{\partial}{\partial R}\Big[\frac{1}{(R^2\Omega)'}\frac{\partial G}{\partial R}\Big] \tag{6.30}$$

$$= -\frac{1}{R}\frac{\partial}{\partial R}\Big\{\frac{1}{(R^2\Omega)'}\frac{\partial}{\partial R}(\nu\Sigma R^3\Omega')\Big\} \tag{6.31}$$

Here we have made no assumption about the central potential and hence the orbital frequency Ω can be non-Keplerian. We now assume the angular velocity to be a power-law in R: $\Omega = \Omega_0(R/R_0)^a$, and change the variable R via the substitution, $x \rightarrow (R/R_0)^{(a+2)}$. On substitution and some algebra, one obtains:

$$\frac{\partial\Sigma}{\partial t} = -\frac{a(a+2)}{R_0^2}\; x^{\frac{a}{a+2}}\; \frac{\partial^2}{\partial x^2}(\nu\Sigma x) \tag{6.32}$$

Now, we also assume a power law dependance for the viscosity:

$$\nu = \nu_0(R/R_0)^n(\Sigma/\Sigma_0)^m = \nu_0\;(\Sigma/\Sigma_0)^m\; x^{n(a+1)} \tag{6.33}$$

and so,

$$\frac{\partial \Sigma}{\partial t} = -\frac{a(a+2)\nu_0}{R_0^2}\, x^{\frac{a}{a+2}} \frac{\partial^2}{\partial x^2}\Big[\Big(\frac{\Sigma}{\Sigma_0}\Big)^m \Big(\frac{x}{x_0}\Big)^{n(a+1)} \Sigma\, x\Big]$$

Defining

$$S = \frac{\Sigma}{\Sigma_0}\Big(\frac{R}{R_0}\Big)^{-a/2(a+2)} \quad \& \quad \tau = -\frac{a(a+2)\nu_0}{R_0^2}\ \ t \equiv \frac{t}{t_{vi}},$$

where $t_{\rm vi} = R_0^2/(-a(a+2)\nu_0)$, we have

$$\frac{\partial S}{\partial \tau} = \frac{\partial^2}{\partial x^2}\Big[S^{m+1} x^{\frac{a}{a+2}(m+1)+2n+1}\Big] \tag{6.34}$$

This is the general form of the non-linear diffusion equation that governs the evolution of the accretion disk. In the Keplerian case, when a = -3/2, we have

$$\frac{\partial S}{\partial \tau} = \frac{\partial^2}{\partial x^2}\Big[S^{m+1} x^{2n-3m-2}\Big] \tag{6.35}$$

which is the form used by Pringle (1991) to obtain self-similar solutions to an "external accretion disk". We shall review some of those results later, but for now we consider the simple case when the viscosity is just a function of R and is independent of Σ ($m = 0$).

6.5.1 Special Cases

Let us set $a = -3/2$ to represent the Keplerian case and $m = 0$. Then Eq. 6.35 reduces to

$$\frac{\partial S}{\partial \tau} = \frac{\partial^2}{\partial x^2}\Big[S\ x^{2(n-1)}\Big] \tag{6.36}$$

It is useful to re-write the above equation by rearranging the terms. Firstly note that for $m = 0$, we have $\nu = \nu_0(R/R_0)^n = \nu_0 x^{2n}$. Multiplying by ν on both sides we obtain after some algebra

$$\frac{\partial}{\partial \tau}(\nu\Sigma x) \ \ = \ \ x^{2n-2}\frac{\partial^2}{\partial x^2}(\nu\Sigma x)$$

and so,

$$\frac{\partial \sigma}{\partial \tau} \ \ = \ \ x^{2n-2}\frac{\partial^2 \sigma}{\partial x^2} \tag{6.37}$$

where, $\sigma(x,\tau) = \nu\Sigma x$. Though the above equation does not have a general solution, it is possible to obtain analytic solutions for different values of n. For example let us consider the case when $n = 0$, which represents a constant viscosity throughout the disk (Frank et al., 2002). The evolution equation for the disk then reduces to

$$\frac{\partial}{\partial \tau}(x\ \Sigma) = \frac{1}{x^2}\frac{\partial^2}{\partial x^2}(x\ \Sigma)$$

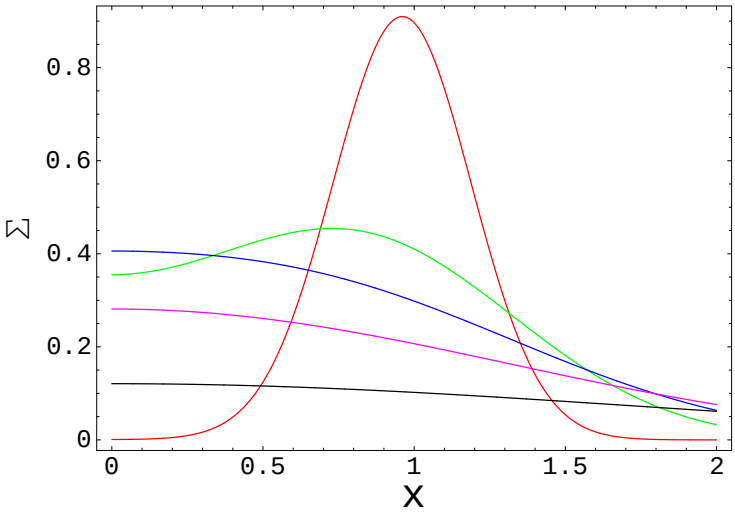

FIGURE 6.2. The evolution of surface density for ν = constant. The surface density Σ (in arbitrary units) as a function of the dimensionless radial coordinate x for different times ($\tau = 0.1$ (red), 0.5 (green), 1.0 (blue), 2 (magenta) & 5 (black)).

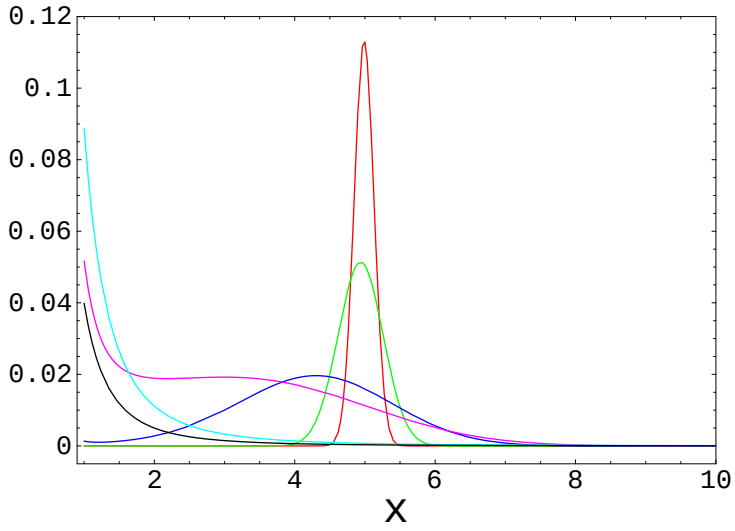

FIGURE 6.3. Evolution of Surface Density for $\nu \propto R$. The surface density Σ (in arbitrary units) as a function of the dimensionless radial coordinate x for different times ($\tau = 0.01$ (red), 0.05 (green), 0.5 (blue), 1.0 (magenta) , 1000 (cyan) & 5000 (black)). In the initial stages, the disk evolves oblivious to the inner boundary condition, until it reaches the inner edge. Once it reaches a peak surface density at the inner edge, corresponding to the maximum torque at the inner edge, it then evolves to ever decreasing Σ (and the torque) in a self-similar fashion.

For concreteness, let us assume that initially, we have a ring of matter at R_0 around the binary –

$$\Sigma(R,0) = \frac{m}{2\pi R_0}\delta(R - R_0) \tag{6.38}$$

where $\delta(R - R_0)$ is the Dirac-delta function. Thus the solution for the surface density $\Sigma(x,\tau)$ is given by

$$\Sigma(x,\tau) = \frac{m}{\pi R_0^2}\ \tau^{-1}x^{-1/4}\exp\Big[-\frac{(1+x^2)}{\tau}\Big]I_{1/4}(2x/\tau) \tag{6.39}$$

The solution given by Eq. 6.39 is plotted in Fig. 6.2 for different values of τ. We notice that the initial configuration spreads into a disk due to the viscous torques in the disk. The disk spreads out on a *viscous timescale* defined as $t_{\rm visc} \sim R/v_R$ where v_R is the effective radial velocity of the annulus centered at R.

Another straight-forward illustrative example is the case when the viscosity is a linear function of the radial co-ordinate R (Pringle, 1991). In this case, the evolution equation reduces to

$$\frac{\partial}{\partial\tau}\Sigma x^3 = \frac{\partial^2}{\partial x^2}\Sigma x^3 \tag{6.40}$$

which on separation of variables leads to the general solution

$$\sigma(x,\tau) = \int_{-\infty}^{\infty}(A_\lambda\cos\ \lambda x + B_\lambda\sin\ \lambda x)\ e^{-\lambda^2\tau}\ d\lambda \tag{6.41}$$

Here $\sigma(x,t) = \Sigma x^3$, and A_λ & B_λ are constants of integration to be determined by the initial and boundary conditions. For a particular solution, consider the boundary condition $\partial\sigma/\partial x = 0$ at $x = x_{\rm in}$. We obtain

$$\sigma(x,\tau) = \int_{-\infty}^{\infty} A_\lambda\frac{\cos\lambda(x - x_{\rm in})}{\cos\lambda x_{\rm in}}\ e^{-\lambda^2\tau}\ d\lambda$$

As for the previous example, consider an initial ring of mass at some radius x_1,

$$\sigma(x,0) = \sigma_0\delta(x - x_1) \tag{6.42}$$

where σ_0 is a constant, and $\delta(x - x_1)$ is a delta function centered at x_1. On substitution and a bit of algebra one arrives at the solution

$$\sigma(x,\tau) = \frac{\sigma_0\tau^{-1/2}}{4\pi^{1/2}}\Big[e^{-(x-x_1)^2/4\tau} + e^{-(x+x_1-2x_{\rm in})^2/4\tau}\Big] \tag{6.43}$$

Since $\nu \propto R$, the above solution also shows how the surface density Σ varies as x and τ, and we have plotted Σ as a function of x at different τ in Fig. 6.3. The boundary condition for this solution implies that the disk mass is constant and a finite torque is applied at the inner edge of the disk. The initial 'ring' of matter

at first evolves oblivious to the inner boundary condition, and spreads into a disk due to its inherent diffusive nature. On reaching the inner edge, the disk builds up sufficient surface density at the inner edge to match the required torque. At later times, it evolves to lower surface densities as the viscous torques carry mass out to infinity as a result of gaining angular momentum at the inner edge.

The solutions to both the cases considered above show similar characteristics which can be summarized as follows:

1. The disk evolves and spreads inwards till it reaches the inner boundary. This inner edge is determined by the torque being applied by the central object at that location.

2. A *quasi-stationary* accretion stage in which the disk gradually spreads outwards. Here the mass accretion rate is practically constant or increases slowly.

3. After a long time, the disk enters a new stage of equilibrium. The accretion may cease at this stage and the disk gradually spreads outward (especially in the case of circumbinary disks) with the surface density falling continuously.

The first stage occurs on relatively short timescales, and is the transient stage in the entire evolution of the disk. The second and third stages occur on long timescales and are independent of the initial conditions. These stages can be modeled by quasi-stationary solutions. In fact, if accretion ceases, i.e. if $\dot{M}_{acc} \to 0$, as in the third stage, the solution is steady stage as mentioned above. These characteristics are not unique to the cases considered above, and indeed other values of n also yield solutions that show similar behavior. In fact, the solutions at later times already resemble what is called "Self-Similar" behavior, i.e. at later times, the solutions have lost memory of the initial conditions and the solutions preserve their functional form or shape.

6.5.2 Self-Similar Solutions

In general, as mentioned above, the viscosity is a function of both R and Σ, and thus we have a non-linear diffusion equation for the evolution of the accretion disk; the solutions to which have to be obtained numerically. However, if we let ν be a power law in R and Σ, it is possible to solve the resulting equation (Eq. 6.35) using the method of similarity variables. Even in this case, strictly speaking, the solutions can be obtained only when it is possible to set the inner edge of the disk $R_{\rm in} = 0$. This can be done for the case $\nu \propto R$, but in general not when ν varies as a higher power of R. The reason for this is that one can obtain a self-similar solution only when the equation under consideration does not have any explicit length or timescales. If one can transform the inner boundary condition to the origin, only then does the equation not have any explicit length scale; and if the mass transfer is constant, there is no timescale either (Spruit & Taam, 2001). The solutions are still asymptotically self-similar though, and as $t \to \infty$ the length scale $\Sigma_{\rm in}/\partial_r \Sigma_{\rm in} \gg R$. One can then replace the inner edge at $R_{\rm in}$ to 0 without causing too much error.

The general solution to Eq. 6.35 has been derived by Pringle (1991) and we shall not reproduce it here. Instead, we illustrate how the self-similar solution obtained for a simpler case matches that obtained above by using the separation of variables. We again assume that $\nu \propto R$ and is independent of the surface density Σ for this purpose, noting that the most general solution is obtained in a similar fashion, albeit requiring more elaborate algebra. We have again, from Eq. 6.37

$$\frac{\partial \sigma}{\partial \tau} = \frac{\partial^2 \sigma}{\partial x^2}$$

for $n = 1$. We now define the *similarity variable* $\xi = x\tau^{\lambda}$ and look for solutions of the form (Zeldovich & Raizer, 1986)

$$\sigma = \tau^{\mu} f(\xi) \tag{6.44}$$

The parameters λ and μ are determined by substituting the solution into the equations and the boundary conditions. The boundary conditions are set by the particular case in hand. Since we shall consider circumbinary disks (CBDs) in the next chapter, we choose the boundary conditions: $\sigma \to 0$ as $x \to \infty$ and that the mass input rate at the inner edge of the disk $R_{\rm in}$ is given by

$$\left(\frac{\partial \sigma}{\partial x}\right)_{\rm in} = -\delta \dot{M}_2 \tag{6.45}$$

where $\delta = \epsilon(1-\beta)$ is the fraction of the mass which settles into the CBD [1]. Under these conditions, we obtain on substitution $\lambda = -1/2$ and $\mu = 1/2$. Thus Eq. 6.37 reduces to an ordinary differential equation for f:

$$f''(\xi) + \frac{1}{2}\xi f'(\xi) - \frac{1}{2} f(\xi) = 0 \tag{6.46}$$

subject to the condition $f'(0) = -1$. Note that in the linear case, we can simply translate the x co-ordinate by the transformation $x \to x - 1$ without loss of generality and thus the inner boundary condition at $x = x_{\rm in}$ is replaced by the condition at $x = 0$. The solution for Eq. 6.46 can be written as

$$f(\xi) = -\xi + \frac{2}{\sqrt{\pi}} e^{-\xi^2/4} + \xi {\rm Erf}\left(\frac{\xi}{2}\right) \tag{6.47}$$

where ${\rm Erf}(\xi/2)$ is the error function. Asymptotically, one expects ${\rm Erf}(\xi/2) \to 1$ and so $f(\xi) \to 2/\sqrt{\pi} e^{-\xi^2/4}$. Writing this in terms of the physical variables Σ and ν we obtain

$$\Sigma = \left(\frac{t}{t_{\rm vi}}\right)^{1/2} \frac{(-\delta \dot{M}_2)}{3\pi\nu_0} \left(\frac{R}{R_0}\right)^{-3/2} e^{-\xi^2/4} \tag{6.48}$$

[1] $1-\beta$ represents the fraction of mass lost from the system as a result of super-Eddington mass transfer, see Section 4.2

Thus, asymptotically, the surface density Σ goes as $e^{-\xi^2/4}$. Also, at large times, Σ increases as $t^{1/2}$ and within the disk, the surface density decreases with distance as $R^{-3/2}$.

We shall use this form of the solution in the next section to illustrate the effects of a CBD on the evolution of a binary system. As mentioned earlier, it is possible to obtain approximate self similar solutions for the case when the viscosity is non-linear and also depends on the surface density Σ (Pringle, 1991).

7. Accretion Disks: Extensions to the Standard Theory

7.1 Circumbinary Disks and Binary Evolution

In Part I of this work, we have noted that the evolution of binary systems is strongly influenced by the angular momentum redistribution in, and angular momentum loss from the system. We have studied the effects of tides, mass transfer & loss and GWR loss in different regimes and also alluded to other effects (section 2.1.4) such as magnetic breaking and circumbinary disks (CBDs). Having reviewed some of the properties of disks in the previous chapter, we are now in a position to study the influence of a CBD on the central binary system, and also the effect of the binary on the evolution of the CBD. In the case of the CBD, the orbit of the binary provides the central angular momentum source which is fed to the CBD by tidal torques. Thus angular momentum is drained out of the orbit and fed to the disk, whose outer edge spreads outward due to viscous torques within the disk.

One can envision a disk formed from the remnant debris left around at the time of the formation of the binary itself. For example, it can be formed out of the material from a common envelope phase during the formation of DWD systems or cataclysmic variables (CVs). Moreover, stellar winds or material being ejected during super-Eddington accretion can settle into a disk around the binary and exert appreciable torques on the orbit once sufficient surface density has been built up in the disk.

The physics of the CBD and its influence on the binary has been studied in the case of cataclysmic variables in a series of papers by Spruit & Tamm, and Dubus, Spruit & Tamm (hereafter DST) (Spruit & Taam, 2001; Taam & Spruit, 2001; Dubus, Taam & Spruit, 2002; Taam, Sandquist & Dubus, 2003). Cataclysmic variable stars are widely studied observationally, and many models have been proposed to explain the observations. One of the problems that has beset the models is the observed spread in the inferred mass transfer rates for a given orbital period. For CVs, the mass transfer rate is related to the orbital period of the binary, if one assumes that the system is undergoing stable mass transfer (See Eq. 4.12 for the corresponding relation for DWDs). As a possible explanation for this discrepancy, DST proposed that an additional mechanism might be in play leading to the different mass transfer rates – and proposed that the presence of a CBD can account for the spread in the mass transfer rates, and also account for other unexplained observations like excess IR radiation from the CVs, presence of emission lines and so on. While they have shown that it is possible to account for some of the discrepancies, other problems surface; like the presence of the CBD will effectively lead to the disappearance of the 'period gap' that is observed in CVs. Moreover, if the CBDs are ubiquitous, they are bound to have a detectable observational signature, but not many systems seem to even suggest that they have CBDs around them.

At the very least, this puts a limit on the amount of mass a CBD can contain, and consequently on how much it can influence the binary.

In the following, we use some of the tools developed by DST, and it is our aim to eventually employ them in the context of the DWD systems we studied in Part-I. As we have seen, DWDs are formed via common envelope evolution and are also prone to super-Eddington accretion, both of which imply that there is a possibility of mass being expelled to condense into a disk around the binary. Though we are not in a position to model in any detail either the disk, or its effect on the binary, we present some preliminary results of the coupling between the CBD and the binary at the end of this chapter. Eventually, our aim is to carry out calculations for DWDs, analogous to what DST have carried out in the case of CVs. The observational properties of the CBD and dynamic effects of the CBD on the central DWD can then be carried out, which is likely to have an impact on both traditional astronomy and GWR astronomy.

7.1.1 Effect of a CBD on Binary Evolution

The presence of a CBD results is an additional angular momentum loss from the binary, as the inner edge of the disk exerts a torque on it. Thus,

$$\dot{J}_{\rm orb} = \dot{J}_{\rm tot} - \dot{J}_1 - \dot{J}_2 - \dot{J}_{\rm cbd} \tag{7.1}$$

where, J_1 and J_2 are the spins of the component stars. In the case of CVs above the *period gap*, $\dot{J}_{\rm tot}$ is given by the magnetic breaking rate whilst in the case of DWD binaries and CVs below the *period gap*, it is given by the GWR rate. For the moment, let us assume that the spins are synchronized with the orbits. Then the term which dominates on the right hand side of the above equation determines the evolution of the binary. Now, the tidal torque exerted by the disk on the binary can be given by

$$\dot{J}_{\rm cbd} = 3\pi\nu_{\rm in}\Sigma_{\rm in}(GMR_{\rm in})^{1/2} \tag{7.2}$$

We concentrate on disks that are fed mass from the inner binary due to mass loss associated with super-Eddington accretion. The term $3\pi\nu_{\rm in}\Sigma_{\rm in}$ in the equation above then represents the mass flow at the inner edge of the disk, whilst the term $(GMR_{\rm in})^{1/2}$ represents the specific angular momentum of the material at the inner edge of the disk. In writing Eq. 7.2, we have assumed that the tidal interaction torque between the disk and the binary is localized at the inner edge. This is a good assumption in the case of CBDs that are fed by mass loss from the binary, since we expect a build-up of mass near the inner edge. Moreover, Eq. 6.48 implies that the surface density falls as $R^{-3/2}$.

Having specified the form of the CBD torque, we include this term in our evolution equations for the binary from Part I. Firstly, we make the assumption that as the mass is lost from the binary, it is decoupled from the orbit, i.e., the outgoing mass does not exert any torque on the binary. This mass wind then settles into the disk near its inner edge. As and when the disk has accumulated a large enough

mass and a high enough surface density, it can exert appreciable tidal torques on the binary. Thus the CBD torque term is a *consequential* term, since its magnitude depends on the presence of mass loss associated with the mass transfer. The surface density of the disk (and hence the torque) are proportional to the mass transfer rate. The mass transfer rate itself depends on the rate at which the CBD torques the binary orbit – thus there exists a positive feedback between the mass-fed disk and the mass transfer rate. In terms of the equilibrium mass transfer rate from Part I, the CBD torque term (Eq. 7.2) appears in the denominator of Eq. 2.37, and affects the stability properties of the binary.

It is possible that the CBD is formed out of material not associated with mass transfer, for example, from the remnants of a common envelope evolution. The disk would still influence the binary via tidal torques until the disk dissipates away. In this case, the CBD torque acts as a *driving* term, and appears in the numerator of Eq. 2.37.

In general, the boundary condition at the inner edge of the disk should contain contributions from both the consequential and the tidal terms. The gravitational torque we are concerned with here is not of viscous origin, and so it would be unphysical to impose it as a boundary condition for the evolution equation for the viscous torques. To circumvent this problem, one can assume that there exists a thin boundary (inside the inner edge of the original disk) over which the tidal torques operate and that one can have both an advective term ($\propto \dot{M}$) and a tidal term ($G_{\rm tides}$ c.f. Eq. 6.19, Fig. 6.1) at the inner edge of the original "standard disk". It is important to correctly classify the consequential and the secular terms because, as we have seen in Section 2.3, the consequential terms can significantly affect the value of $q_{\rm stable}$ and change the evolutionary fate of a binary with a given mass ratio q.

As a simple illustration of the above arguments, we present the case of a DWD binary undergoing super-Eddington accretion for a certain phase in its evolution, in which a fraction of the mass lost from the binary settles into a circumbinary disk at some radius $R_{\rm in}$. In this case, Eq. 4.8 has an additional term

$$\dot{J}_{\rm orb} \;=\; \dot{J}_{\rm sys} - \Big(-\dot{M}_2[\beta j_1 - j_2 + (1-\beta)j_{\rm w} + j_{\rm cbd}] + \dot{J}_{\rm 1,tid} + \dot{J}_{\rm 2,tid}\Big) \;, \quad (7.3)$$

where $j_{\rm cbd} = \delta(GMR_{\rm in})^{1/2}$ is the specific angular momentum of the material at the inner edge of the disk. Following the same treatment as in Section 2.3, we can write

$$\Big(\frac{\dot{M}_2}{M_2}\Big)_{\rm eq} = \frac{\nu_{\rm L} - \nu_2}{\zeta_2 - \zeta_{\rm L}} \quad (7.4)$$

with $\zeta_{\rm L}$ is given by Eq. 2.22 but with q_a defined as

$$q_a \equiv 1 + (1-\beta)q - \frac{1-\beta}{2(1+q)} - M_2\frac{j_1 - j_2 + j_{\rm cbd}}{J_{\rm orb}} \quad (7.5)$$

Note that as far as the binary evolution is concerned, we need only follow the evolution of the inner edge of the disk since the binary is coupled only to the inner

edge by construction. For simplicity, we also ignore the tidal terms implying that the spins and the orbit are decoupled. We assume also that $\delta = \epsilon(1-\beta)$ is the fraction of the mass lost $(1-\beta)$ that is accreted onto the inner edge of the CBD and the rest is lost from the system without further influencing the binary or the disk in any way. In Fig. 7.1 we plot the evolution of two systems (the same as Fig. 4.4) which are coupled to the CBD according to the prescription described above. For comparison, the red curve in Fig. 7.1 represents the same cases as Fig. 4.4, i.e., effectively there is no CBD, since we do not couple the disk to the binary orbit. The green curve corresponds to an ϵ =0.1, i.e., we let 10% of the mass ejected due to super-Eddington accretion settle into the disk at the inner edge, whilst the blue curve represents the same for $\epsilon = 0.15$. The values of ϵ chosen here are arbitrary, since we are not in a position to determine how much mass that is lost from the binary due to super-Eddington accretion can settle into the disk. However, it is clear from Fig. 7.1, that if a CBD is present and has a sufficient surface density, it can exert appreciable torques on the central binary and lead to accelerated evolution. The greater the value of ϵ, the greater is the instability induced by the positive feedback between the surface density of the disk, the corresponding torque and the mass transfer rate in the binary. This is because the greater the value of ϵ, the greater is the value of $j_{\rm cbd}$ in Eq. 7.5. In fact, it is even possible that $q_a < 0$ for certain extreme cases of mass loss – at least for short phases during the evolution of the binary. $q_a < 0$ is a situation of extreme instability because any value of $q_a < 1/3$ implies that the binary is unstable (c.f. Eq. 2.38). Thus the overall effect of the coupling of the CBD fueled by mass loss from the binary during mass transfer and the binary can be extremely destabilizing, and could lead to rapid merger or tidal disruption of the binary.

In Fig. 7.1, we have also shown the surface density at the inner edge of the disk as a function of time. We note that the surface density rises to a high value in a relatively short time after super-Eddington accretion commences in the binary. In the first case, where we have not coupled the binary to the disk, we notice that the surface density remains constant as long as super-Eddington accretion occurs in the binary. On the other hand, for the other two cases, Σ rises, and then rises even more. This is because of the positive feedback between the disk and the binary – this lasts until the super-Eddington accretion ceases. Note that since the evolution is accelerated, the binary separation increases at a faster rate, and the net driving falls more rapidly. This leads to a shorter duration of super-Eddington transfer when the disk and the binary are coupled, but to higher net loss of mass from the binary, due to the enhanced mass transfer rate. The positive nature of the feedback between the disk and the binary is also apparent from the plots of β. Note that in the cases where the disk and the binary are coupled, $1-\beta$ increases to an even higher value (top panel in Fig. 7.1) after the initial phase. It falls rapidly to zero (i.e., $\beta \rightarrow 0$) only when the system begins to recover, which happens when the q value has fallen sufficiently and the driving has decreased sufficiently to allow sub-Eddington mass transfer to occur.

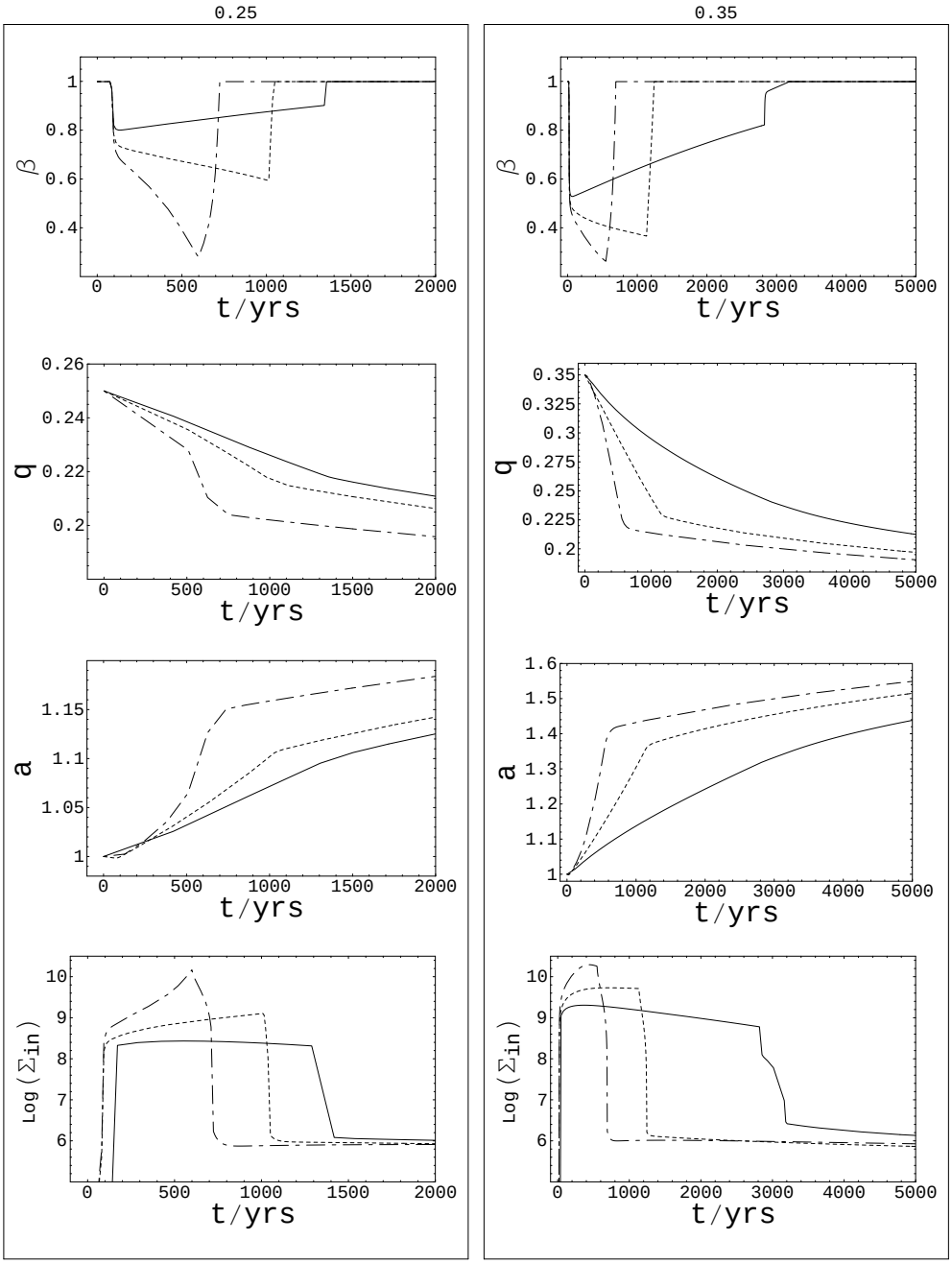

FIGURE 7.1. The evolution of two DWD systems with initial mass ratios $q = 0.25$ (left panel) and $q = 0.35$ (right panel). The three curves represent no coupling with the CBD (solid curves), CBD coupled to the binary with $\epsilon = 0.1$ (dashed curves) and with $\epsilon = 0.15$ (dot-dashed curves). Note the accelerated evolution when the binary and the CBD are coupled, and also the increased rate of evolution when the surface density of the disk is higher (greater ϵ).

The above illustration is highly artificial, in that several of the parameters can have values wildly different from what we have assumed. Even if super-Eddington accretion were to occur in a system, there is no guarantee that a CBD would form,

or how much mass it would contain. Moreover in our numerical integrations, we have assumed that the disk evolves according to the solution corresponding to $\nu \propto R$, an ad-hoc assumption made for the sake of simplicity. We have ignored the detailed evolution of the disk itself, and assumed that only the inner edge of the disk and the binary interact, and that the rest of the disk has no influence on the binary evolution. Nonetheless, the above illustration gives us an idea of the destabilizing influence of a CBD replenished by the mass loss from a binary undergoing mass transfer.

7.2 Non-Keplerian Potentials

In this section, we review some of the work done in the field of disks around *active galactic nuclei* (AGNs), which are thought to contain supermassive black holes ($M_{\rm bh} \sim 10^8 M_\odot$) surrounded by a disk, which fuels the central black hole. The high luminosity's ($\sim 10^{44}$ erg s^{-1}) of AGNs implies very high accretion rates ($\dot{M} \sim 1.0\ M_\odot {\rm yr}^{-1}$). We first show that the disk equations from Chapter 6 can be generalized to include non-Keplerian potentials, and that the profiles of the global parameters like the torque and the angular momentum distribution in the disk are consistent with more rigorous treatments. This treatment can also be applied to stellar mass black holes and as Paczyński & Wiita (1982) and Paczyński (1998) have shown, can be extended to geometrically thick disks, which also have non-Keplerian profiles. We then consider the case of a particular AGN; NGC 1068, which is one of the most studied Seyfert galaxies.

7.2.1 Paczynski's Toy Model

As we have mentioned before, the formalism we use for describing the evolution of an accretion disk, is quite general and can be used also when the potential in which the disk finds itself is non-Keplerian. For example, Paczyński & Wiita (1982) devised an approximate way of treating thin and thick disks around a Schwarzschild black hole by introducing a pseudo-Newtonian potential ($\Phi_{\rm PW}$, hereafter PW potential) which reproduces the most important features of the geodesic motion on circular orbits. In fact, they use explicitly the integrated torque Eq. 6.16 to obtain their disk solutions. The pseudo-Newtonian potential is given by

$$\Phi_{\rm PW}(R) = -\frac{GM}{r - r_{\rm s}} \tag{7.6}$$

with $r_s = 2\ GM/c^2$ being the Schwarzschild radius. Here $r = (R^2 + z^2)^{1/2}$ is the spherical radius with the cylindrical coordinates (R, z, ϕ) fixed at the center of the black hole. This way of representing the potential has the property that the last marginally stable orbit around the black hole is at $r_{\rm ms} = 3\ r_{\rm s}$ and the marginally bound orbit is at $r_{\rm mb} = 2\ r_{\rm s}$, which is a faithful representation of particles orbiting a Schwarzschild black hole (Paczyński & Wiita, 1982). As in the case of the Keplerian potential, one can write the specific angular momentum of the material orbiting

the black hole at a distance R as

$$j = (GMR)^{1/2}\Big(\frac{R}{R - R_{\rm s}}\Big) \tag{7.7}$$

Following Paczyński (1998), we can then write the general form for thin as well as thick disks in the steady state, and the form is similar to Eq. 6.16. Note that in the case of black hole accretion disks the inner edge is at the innermost marginally stable orbit $r_{\rm ms}$ and so

$$G = G_{\rm ms} + (-\dot{M})(j - j_{\rm ms}) \tag{7.8}$$

is the corresponding torque equation. The 'no torque' condition at the inner edge usually applies to disks around black holes, and so $G_{\rm ms} = 0$. This is because, as Paczyński (2000) points out, "no information could propagate upstream in the supersonic region inward of $r_{\rm ms}$". Paczyński (1998) goes on to apply this toy model to thick, advection dominated disks and study its properties. We shall not pursue this further, but instead proceed to show that the torque and angular momentum distribution throughout the disk in the PW potential almost exactly matches the exact values calculated relativistically.

7.2.2 Relativistic Torque and Angular Momentum

The theory of geometrically thin accretion disks was generalized to the relativistic case by Novikov & Thorne (1973). We first begin by defining the viscous stress tensor, which in the case of thin disks where the azimuthal component of the velocity v_ϕ dominates, is given by

$$T_{R\phi} = \rho\nu\Big(\frac{\partial v_\phi}{\partial R} - \frac{v_\phi}{R}\Big) = \rho\nu R\frac{\partial\Omega}{\partial R} \tag{7.9}$$

and the torque between two adjacent rings is

$$G = \int d\phi\ R \int dz\ R\ T_{r\phi} \tag{7.10}$$

and so we have

$$\frac{\dot{M}\Omega}{2\pi} f(R) \ = \ -\int dz\ T_{r\phi} \tag{7.11}$$

which is completely equivalent to the Keplerian case with

$$f(R) = 1 - \Big(\frac{R_{\rm in}}{R}\Big)^2 \frac{\Omega(R_{\rm in})}{\Omega(R)} \ = \ 1 - \frac{h_{\rm in}}{h} \tag{7.12}$$

where the subscript 'in' refers to the inner edge of the disk. Thus on determining $\Omega^2 = 1/R\ \partial\Phi/\partial R$ in various potentials, we can determine the torque profile in the disk.

Now, it is possible (Krolik, 1999) to write the equation for the stress, and hence the torque in the same form as Eq. 7.11, by explicitly replacing Ω by the Keplerian angular velocity, Ω_K

$$\frac{\dot{M}\Omega_K}{2\pi} R_T(x) = -\int dz\ T_{r\phi} \tag{7.13}$$

and replacing $f(r)$ by the *relativistic reduction factor* $R_T(x)$ which is given by:

$$R_T(x) = \frac{C(x)}{A(x)} \tag{7.14}$$

$x = r/r_g$, $r_g = GM/c^2$ is the gravitational radius. The functions $C(x)$ and $A(x)$ are given by:

$$A(x) = 1 - \frac{2}{x} + \frac{a_*^2}{x^2} \tag{7.15}$$

$$\begin{aligned} C(x) = 1 - \frac{y_{\rm ms}}{y} - \frac{3a_*}{2y}\ln\Big(\frac{y}{y_{\rm ms}}\Big) - \frac{3(y_1-a_*)^2}{yy_1(y_1-y_2)(y_1-y_3)}\ln\Big(\frac{y-y_1}{y_{\rm ms}-y_1}\Big) \\ - \frac{3(y_2-a_*)^2}{yy_2(y_2-y_1)(y_2-y_3)}\ln\Big(\frac{y-y_2}{y_{\rm ms}-y_2}\Big) \\ - \frac{3(y_3-a_*)^2}{yy_3(y_3-y_1)(y_3-y_2)}\ln\Big(\frac{y-y_3}{y_{\rm ms}-y_3}\Big) \end{aligned} \tag{7.16}$$

with $y = x^{1/2}$. Also, $y_{\rm ms}$ is the value of y at the marginally stable orbit, and $y_{1,2,3}$ are the three roots of $y^3 - 3y + 2a_* = 0$. The parameter a is the spin of the black hole and a_* is the black hole spin a normalized to GM/c. For a Schwarzschild (non-spinning) black hole, $a = 0$.

Thus, the torque is given by:

$$\begin{aligned} G(R) &= \int d\phi\ R \int dz\ R\ T_{R\phi} \\ &= 2\pi R^2\Big(\dot{M}\Omega + \frac{G_{\rm ms}}{R^2}\Big) R_T(R) \\ &= \Big(\dot{M}h(R) + G_{\rm ms}\Big) R_T(R) \end{aligned} \tag{7.17}$$

From Fig. 7.2 we plot the torque according to Eq. 7.8, with j calculated in a Keplerian potential, PW potential and Eq. 7.17. For the sake of concreteness, we take the mass of the Schwarzschild black hole to be $1.5 \times 10^6 M_\odot$, and a luminosity of $\sim 5 \times 10^{44} L_\odot$, which sets the accretion rate. We see that the relativistic and PW torques match almost exactly. We have set the torque $G_{\rm ms}$ at the inner boundary, which is pegged at the marginally stable orbit ($r_{\rm ms} = 6r_g$ in the Schwarzschild case), to zero. Similarly, the specific angular momentum profile across the disk is identical for the PW and relativistic case, both of which deviate from the Keplerian profile near the inner edge of the disk. As we have seen before, the inner boundary contributes to almost half of the luminosity of the disk, and hence it is important

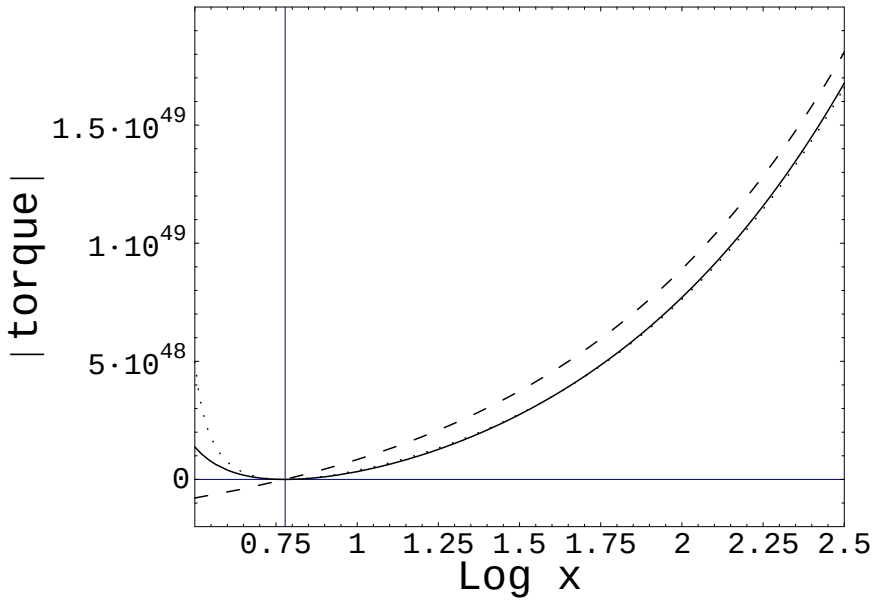

FIGURE 7.2. The torque profile in a non-Keplerian potential. Keplerian (dashed), PW (solid) and the relativistic-torque (dotted curve). The latter two overlap almost exactly beyond the inner edge of the disk, which in these units is at $x = 6$.

to follow the distribution of the viscous dissipation and hence also the torque accurately. We have shown the the PW potential, despite is simple form, faithfully represents the relativistic correction terms in the case of Schwarzschild black holes. Of course, far away from the inner edge (R $\gg R_{\rm ms}$) it is reasonable to neglect the effects of the black hole, and one can assume that the potential is purely Keplerian.

7.2.3 NGC 1068

The nucleus of NGC 1068 is known to host a supermassive black hole, striking evidence for which is provided by the study of the Doppler shifts of the *water maser lines* (Greenhill & Gwinn, 1997). This method is unique in that it provides some of the most reliable information about the mass of the central object, since it probes the gravitational potential to very small distances ($<$ 1 parsec). In the case of NGC 1068, the water maser emission is seen from the center of the nucleus to a radius of about 1 pc, and is believed to be emitted from gas rotating in an accretion disk which happens to be edge-on along our line of sight (See Maloney (2002) for an excellent review of masers in AGNs). The rotation profile obtained by the maser observations suggests strongly that the rotational velocity in the disk falls off as $R^{-0.31}$ (Greenhill et al., 1996) instead of $R^{-0.5}$, which is what one would expect for a Keplerian disk [1]. Many models have been proposed to explain this sub-Keplerian rotation, see for example, Kumar (1999), Pier & Krolik (1992) and Lodato & Bertin (2003). Kumar (1999) for example, proposes a "clumpy disk

[1]The rotation profile of another such AGN, NGC 4258, is consistent with a Keplerian disk (See Miyoshi et al. (1995))

model" to explain the observed rotation profile for NGC 1068, whilst Pier & Krolik (1992) argue that radiation pressure may reduce the rotational velocity in the disk. Here, we consider a simple model for NGC 1068 which consists of a central black

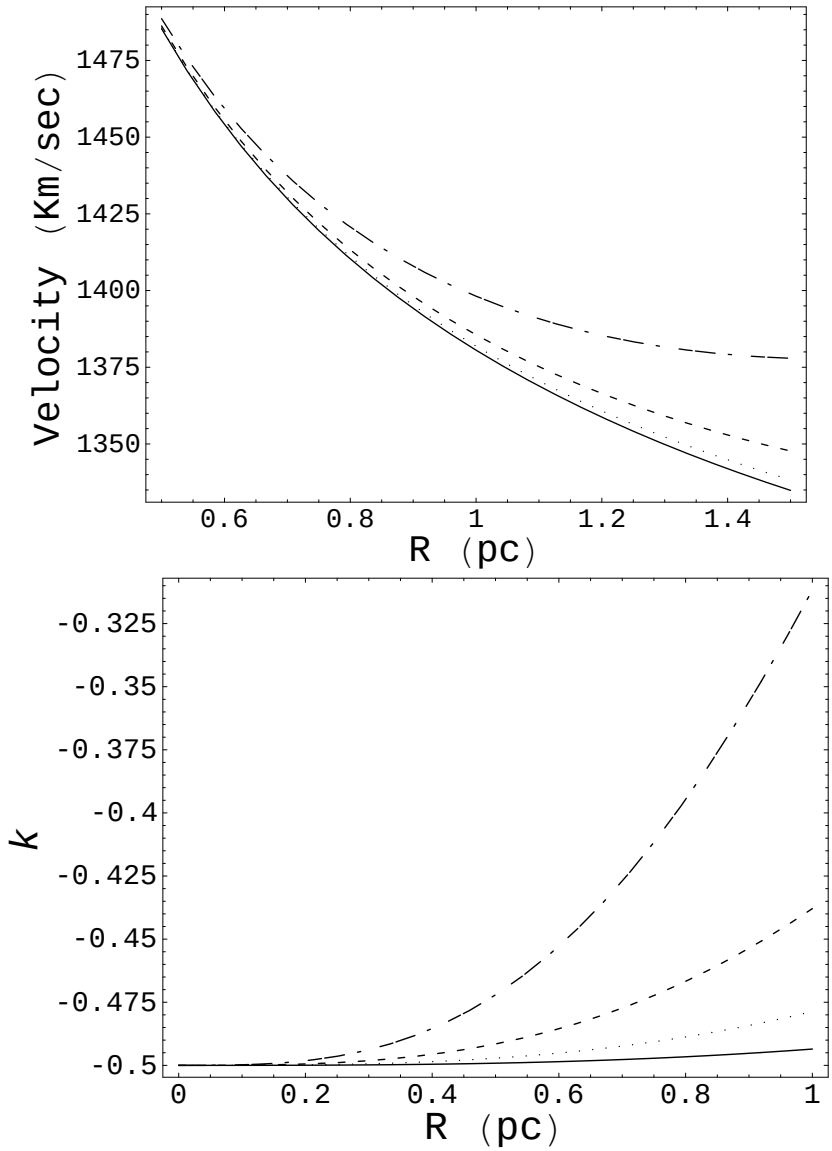

FIGURE 7.3. The Rotation curves and the corresponding velocity exponent k for NGC 1068. The black curve corresponds to a central black hole of mass $1.5 \times 10^7 M_\odot$ and a stellar cluster of mass $M_{\rm sc} = 1.5 \times 10^7 M_\odot$. The dotted line is for $M_{\rm sc} = 5 \times 10^7 M_\odot$, the dashed curve corresponds to $M_{\rm sc} = 1.5 \times 10^8 M_\odot$ and the dot-dashed curve is for $M_{\rm sc} = 5 \times 10^8 M_\odot$. The parameter b is set to 10 pc. Also note that the systemic velocity of 1126 Km/sec is added to the velocity plotted here.

hole and a dense cluster of stars surrounded by a massive, but thin accretion disk. The star cluster is modeled by using a 'Plummer sphere', the potential of which is

given by

$$\Phi_{\rm sc} = -\frac{GM_{\rm sc}}{\sqrt{r^2+b^2}} \tag{7.18}$$

where, $M_{\rm sc}$ is the mass of the cluster and b is a free parameter which represents the extent over which the mass is distributed (Binney & Tremaine, 1988). We now define the velocity exponent k as

$$k = \frac{\partial \ln v_\phi}{\partial \ln R} = 1 + \frac{d \ln \Omega}{d \ln R} \tag{7.19}$$

where $\Omega^2 = 1/R\ \partial\Phi/\partial R$ and $\Phi = \Phi_{\rm bh} + \Phi_{\rm sc}$ is the potential due to the central black hole and the star cluster. Note that in the Keplerian case, as expected, we obtain $k = -0.5$. In the presence of the star cluster, k will deviate from -0.5 and is a function of R and b.

In Fig. 7.3, we plot the rotation curve for the water maser curve for our model, with and without the star cluster. We notice that when the stellar cluster has to be much more massive that the central black hole itself in order to have an appreciable effect on the potential and hence the rotation curve of the disk. Kumar (1999) notes that the mass contained in the central 50 pc of the disk is about $5 \times 10^8 M_\odot$. Setting the parameter $b = 10$ pc in our calculations, implies that the inner 10 pc contains almost half this mass. We have noted that the presence of the cluster affects the velocity exponent k, which we plot in the bottom panel of Fig. 7.3. We note that the presence of the cluster does lead to sub-Keplerian rotation and $k \sim -0.31$ around a parsec.

There are several problems with this picture. Firstly, the cluster density needed to make k consistent with observations is much higher than what is suggested observationally (Kumar, 1999), unless the cluster consists of low luminosity objects. Also, one has to take into account the interactions between the stars at such high densities (Goodman, 2003) and also the observational signatures of such a cluster. Moreover, it is possible the disk becomes massive enough and becomes unstable to axisymmetric perturbations, leading to its fragmentation (Goodman, 2003).

8. Discussion and Conclusions

We have presented a simple, semi-analytic approach to describe the evolution of binary star systems in which we track the mass of each component, the total mass of the system, the orbital angular momentum and the spin angular momenta of each component. We have included the effects of mass and angular momentum loss from the system and also the exchange of mass and angular momentum between the components of the binary. We have generalized the orbit-averaged equations (OAE) that describe the evolution of the binary to include both the advective and tidal exchange of angular momentum between the components and the orbit.

We find that the material flowing across the L_1 point has two effects on the internal redistribution of angular momentum in the binary: a) it spins up the accretor by transferring a specific angular momentum $j_{\rm circ}$ to the spin at the expense of the orbital angular momentum and, b) it reduces the spin angular momentum of the donor by an amount $\sim R_2^2\omega_2$. This second effect has not been accounted for in previous studies of DWD binary systems, and we find that it has a mildly stabilizing effect on the binary evolution.

We have presented analytic solutions for the evolution of binary systems, generalizing the results of Webbink & Iben (1987) to binaries with any polytropic index and to binaries with isothermal atmospheres. We have also studied the effects of letting the binary parameters evolve in a self-consistent fashion; rather than keeping them fixed as in the analytic case. The analytic solutions always predict that if a binary attains contact when the mass ratio q is such that the ensuing mass transfer is unstable, the binary merges in a finite time. On the other hand, the numerical integrations of the OAE always predict that a binary that undergoes unstable mass transfer at initial contact can evolve to a state of stable mass transfer, survive and evolve into an AM CVn type system.

For systems with the mass ratio q much greater than $q_{\rm stable}$, the mass transfer rate can reach arbitrarily high values, but the amount of matter the accretor can accrete is limited by radiation pressure. To account for this, we have included the effects of super-Eddington mass transfer (Han & Webbink, 1999). We find that when tides are inefficient, almost all the systems with an unstable mass ratio ($q > q_{\rm stable}$) undergo super-Eddington accretion. Stable systems with donor masses $\gtrsim 0.25\ M_\odot$ also tend to undergo super-Eddington accretion, irrespective of the mass ratio. We have assumed that the mass lost from the system is expelled from the system without further interacting with the binary. This assumption breaks down when the mass loss rate is so high that it results in the formation of an optically thick envelope, which is likely to cause the merger of the binary due to frictional angular momentum loss. Nevertheless, we have shown that the systems tend to return to stability, and so we suspect that many of the systems previously believed to merge as a result of this effect would survive provided that the peak

mass transfer rate, and the corresponding mass loss rate, is not too high. Further investigation using 3-D hydrodynamic simulations which include radiative effects is required to fully understand this possibility.

An interesting consequence of efficient tidal coupling is that the domain over which mass transfer is sub-Eddington is significantly enhanced, thus increasing the possibility of survival of these systems. Another interesting consequence of the tidal coupling is that for intermediate tidal synchronization timescales, we observe mass transfer oscillation cycles. These cycles occur for a relatively short duration after 'first contact'. They tend to occur in systems around the stability boundary, where the mass transfer rates are high or rise to a high value rapidly. We find that direct impact systems around the stability boundary are more likely to undergo these oscillation cycles whereas none of the disk systems we studied show the cycles.

The extremely short period DWD binaries listed in Table 1.1, RX J0806+15 and V407 Vul, are considered to be progenitors of AM CVn type binaries. Observations suggest that the orbital period in these systems is decreasing, which is at odds with the expectation that the orbital period of mass transferring DWD systems should increase. We have shown that it is possible, at least for a short duration after 'initial contact', that the systems undergo oscillation cycles which implies an enhanced probability for observing one of these systems with a negative $\dot{P}$, even as it is transferring mass. Recently, however, D'Antona et al. (2006) have proposed that if these systems are very young and contain a donor with a significant non-degenerate atmosphere, then it is possible that the donor star actually contracts, and so does the orbital period. The advantage of this model is that if nuclear reactions help in keeping that donor star warm and hence non-degenerate, the atmosphere can be sustained for timescales $> 10^7$ yrs. We are in the process of studying the implications of this model on the general population of close DWD systems.

We have used the OAEs with suitably adjusted tidal coupling time scales to analyze and interpret the results of some of the simulations described by D'Souza et al. (2006). The mass transfer rates that these hydrodynamic simulations can resolve are much higher than the Eddington critical rate and probably much higher than the rates likely to arise during the onset of mass transfer in most realistic cases. Nevertheless they describe correctly the dynamical aspects of the mass transfer and tidal interactions under these conditions. These simulations did not include enough physics to tackle common envelope evolution, but they should be viewed as the first steps toward that goal. In the meantime, we have used the OAEs to analyze and interpret the results of the 3-D simulations. Comparing the predictions of the OAEs with the simulations, we have been pleased to find that they predict the outcome of the simulations reasonably well. It is only in the final stages of the hydro-simulations when the components (especially the donor) get severely distorted that the OAEs, which assume spherically symmetric components, fail to reproduce the behavior of the simulations.

DWD systems are some of the most common compact systems in the Galaxy and are of particular importance for the space based GWR detector LISA. AM

CVn systems are guaranteed sources for LISA and the knowledge of possible evolutionary trajectories is valuable. The framework we have outlined in this paper can be used to generate templates for short period DWD's in general and AM CVn systems in particular. Similar work has been done already (see for example, Kopparapu & Tohline (2006) and Stroeer et al. (2005)); but the effects of the tidal coupling, the advective term associated with the donor spin and so on, which we have introduced here, need to be incorporated into these studies.

Mass lost from a system undergoing super-Eddington mass transfer can settle into a disk around the binary to form a circumbinary disk. In the second part of the thesis, we present a simple toy model for the evolution of accretion disks in general. We investigate the flow of angular momentum and energy in the disk, especially near the boundary layer, and derive a expression for the energy dissipated at the boundary layer. We apply the formalism to develop steady, time-dependent, active and passive disks as well as to circumbinary disks. From our preliminary studies, we find that if the mass lost from a DWD system during super-Eddington accretion settles into a circumbinary disk, the evolution of the DWD is accelerated. The effect of the disk which is fed mass as a consequence of mass transfer is destabilizing and is a function of the amount of mass that settles into the disk. Our results suggest that it is possible that in certain extreme cases, the formation of a circumbinary disk can lead to rapid disruption of the binary. Further work is required to accurately follow the evolution of both the disk and the binary in a self-consistent way, in order to fully appreciate the effects of such a disk on DWD binary evolution.

Bibliography

Abbott B., et al. 2005, Phys. Rev. D, 72, 8

Andronov, N., Pinsonneault, M. & Sills, A., 2003, ApJ, 582, 358

Balbus, S & Hawley, J., 1991, ApJ, 467, 76

Bender P. L. et al., *LISA Pre-Phase A Report*, 1998.

Binney, J. & Tremaine, S., 1988, Galactic Dynamics (Princeton: Princeton University Press)

Campbell, C.G. 1984, MNRAS, 207, 433

Carroll, B.W. & Ostlie, D.A., 1996, An Introduction to Modern Astrophysics (Addison-Wesley)

Chandrasekhar, S., 1939, An Introduction to the Study of Stellar Structure (Chicago: Univ. Chicago Press)

Chandrasekhar, S., 1961, Hydrodynamics and Hydrodynamic Stability (Dover Publications: Oxford University Press)

Cropper, M., Harrop-Allin, M.K., Mason, K.O. et al., 1998, MNRAS, 293, L57

Cropper, M., Ramsay, G. & Wu, K., 2003, ASP Conf. Ser. 315: IAU Colloq. 190: Magnetic Cataclysmic Variables, p. 324

D'Antona, F., Ventura,P., Burderi, L. & Teodorescu, A., 2006, preprint (astro-ph/0606577)

D'Souza, M., Motl, P., Tohline, J. & Frank, J., 2006, ApJ, 643, 381

Dubus, G., Tamm, R. & Spruit, H., 1989, ApJ, 569, 395

Eggleton, P., 1983, ApJ, 268, 368

Espaillat C., Patterson, J., Warner, B. & Wouldt, P., 2005, PASP, 117, 189

Frank, J., King, A. R., & Raine, D. J., 2002, Accretion Power in Astrophysics (3d ed; Cambridge: Cambridge Univ. Press)

Gokhale V.M., Peng, X.M. & Frank, J., 2006, *Submitted to ApJ*

Goodman, J., 2003, MNRAS, 339, 937

Greenhill, L., Gwinn, C. ,Antonucci, R. & Barvainis, R., 1996, ApJL, 472, L21

Greenhill, L. & Gwinn, C., 1997, CfA preprint 4508

Hakala, P. and Ramsay, G. and Wu, K. and Hjalmarsdotter, L. and Järvinen, S. and Järvinen, A. and Cropper, M., 2003, MNRAS, 343, L10-L14

Han Z. 1998, MNRAS, 296, 1019

Han, Z. & Webbink, R.F. 1999, A&A 349, L17

Hughes, S.A. and Marka, S. and Bender, P.L. & Hogan, C. J., *astro-ph/0110349*

Hulse, R. A., Taylor, J. H. 1975, ApJ, 195L, 51

Iben, I. Jr, Tutukov, A. V. 1984, ApJS, 54, 335

Iben, I. Jr, Tutukov, A. V. 1986, ApJ, 311, 753

Jędrzejec, E. 1969, MS thesis, Warsaw University

Kallrath, J. & Milone, E., 1999, Eclipsing Binary Stars (New York : Springer)

King, A., 1988, Q. Jl. Astr. Soc , 29, 1

Kopal, Zdenek, 1955, Ann. Astrophys., 18, 379

Kopal, Zdenek, 1977, Dynamics of Close Binary Systems (Boston: D Reidel Publishing)

Kopparapu, R. & Tohline J.E., 2006, *Submitted to ApJ*

Krolik, J., 1999, Active Galactic Nuclei (Princeton: Princeton University Press), 147

Kuiper, G., 1941, ApJ, 93, 133

Kumar, P., 1999, ApJ, 519, 599

Lodato, G., & Bertin, G., 2003, A&A, 398, 517

Lai, D., Rasio, F.A., & Shapiro, S.L., 1993, ApJL, 406, 63

Lai, D., Rasio, F.A., & Shapiro, S.L., 1993, ApJS, 88, 205

Lai, D., Rasio, F.A., & Shapiro, S.L., 1993, ApJ, 420, 811

Lai, D., Rasio, F.A., & Shapiro, S.L., 1993, ApJ, 423, 344

Lai, D., Rasio, F.A., & Shapiro, S.L., 1993, ApJ, 437, 742

Landau, L.D. & Lifshitz, E.M., 1975, The Classical Theory of Fields, Pergamon Press, Oxford

Lubow, S.H. & Shu, F.H., 1975, ApJ, 198, 383

Lynden-Bell, D., 1969, Nature, 223, 690

Lynden-Bell, D. & Pringle, J.E., 1974, MNRAS, 168, 603

Lyubarskij, Y.E. & Shakura, N.I., 1987, Soviet Astronomy Letters, 13, 386

Maloney, P., 2002, Publications of the Astronomical Society of Australia,, 19, 401

Marsh, T.R., Nelemans, G. & Steeghs, D., 2004, MNRAS 350, 113

Marsh, T.R. & Nelemans, G., 2005, MNRAS, 363, 581

Marsh, T.R. & Steeghs, D., 2002, MNRAS, 331, L7

Miyoshi, M, Moran, J., Herrnstein, J. et al., 1995, Nature, 373, 127

Motl, P., Tohline, J. & Frank, J., 2002, ApJS, 138, 121

Motl, P., Tohline, J. & Frank, J., 2006, *In preparation*

Novikov, I. & Thorne, K., 1973, In Black Holes – Les Astres Occulus, ed. C. De Witt & B.S. De Witt (New York: Gordon & Breach), 343

Nelemans, G., Yungelson, L.R., Portegies Zwart, S.F. & Verbunt, F., 2001, A&A, 491 (Nelemans 2001a)

Nelemans, G., Portegies Zwart, S.F., Verbunt, F. & Yungelson, L.R., 2001, A&A, 939 (Nelemans 2001b)

Nelemans, G., Yungelson, L.R. & Portegies Zwart, S.F., 2001, A&A, 375, 890 (Nelemans 2001c)

Nelemans, G., preprint (astroph/0409676)

Paczyński, B., 1971, Ann. Rev. Astron. Astrophys., 9, 183

Paczyński, B., 1998, preprint (astroph/9812047)

Paczyński, B., 2000, preprint (astroph/0004129)

Paczynski B. & Sienkiewicz R., 1972, Acta Astr., 22, 73

Paczynski B. & Wiita, P, 1982, A & A, 88, 23

Patterson, J., 1984, ApJS, 54, 443

Pier, E. & Krloik, J., 1992, ApJ, 399, 23L

Plavec, M. & Kratochvil, P., 1964, Bull. Astron. Isnt. Czechoslovakia, 15, 165

Prendergast, K.H., Burbridge, G.R., 1968, ApJ, 151, L83

Pringle, J.E., 1991, MNRAS, 248, 754

Pringle, J.E., 1981, ARAA, 19, 137

Ramsay, G., Cropper, M., Hakala, P., 2006, MNRAS, 367, L62

Rasio, F. A. & Shapiro, S. L. 1992, ApJ, 401, 226 (RS92)

Rasio, F. A. & Shapiro, S. L. 1994, ApJ, 432, 242 (RS94)

Rasio, F. A. & Shapiro, S. L. 1995, ApJ, 438, 887 (RS95)

Rasio, F. A., 1995, 444, L41

Ritter H., 1988, A&A, 202, 93

Salpeter, E., 1964, ApJ, 140, 796

Savonije, G.J., 1978, A&A, 62, 317

Shakura, N.I. & Sunayev, R.A., 1973, A&A, 24, 337

Shore, S.N., Livio, M. & van den Heuvel, E.P.J., 1992, Interacting Binaries (Springer-Verlag)

Spruit, H.C. & Taam, R.E., 2001, ApJ, 548, 900

Stroeer A., Vecchio, A. & Nelemans G. 2005, ApJ, 633, L33

Strohmayer, T.E., 2002, ApJ, 581, 577

Taam, R. & Spruit, H., 1989, ApJ, 345, 972

Taam, R. & Spruit, H., 2001, ApJ, 561, 329

Taam, R., Sandquist, E.L., & Dubus, G., 2003, ApJ, 592, 1124

Tsugawa, M. & Osaki, Y., 1997, PASJ, 49, 75

Tutukov, A. V. & Yungelson, L. R., 1994, MNRAS, 268, 871

Velikhov, E., 1959, Sov. Phys. JETP, 9, 995

Verbunt, F. & Rappaport, S., 1988, ApJ, 332, 193

Verbunt, F. & Zwaan, C., 1981, A&A, 100, L7

Webbink, R.F., & Iben, I., Jr., 1987, Proceedings of the 2nd Conference on Faint Blue Stars, p. 445

Webbink, R.F., 2003, preprint (astro-ph/0304420)

Willems, B. & Kalogera, V., 2005, preprint (astro-ph/0508218)

Wu, K., Cropper, M., Ramsay, G., Sekiguchi, K., 2002, MNRAS, 331, 221

Yungelson, L.R., Livio, M., Tutkov, A.V. & Saffer, R.A., 1994, ApJ, 420, 336

Zeldovich, Y.B. & Raizer, Y.B., 1986, Physics of Shock Waves and High Temperature Hydrodynamic Phenomena (London: Academic Press)

Appendix A: The Binary Evolution Equations

We summarize here, the basic evolution equations first introduced in Chapter 2 for ready reference and convenience. The evolution of a mass transferring binary system depends primarily on two factors: a) the loss and redistribution of angular momentum and b) the loss and redistribution of mass. Another factor that can influence the evolution of such a system is the evolution of one of the components itself: for example, a main sequence star can evolve off the main sequence and fill up its Roche lobe, thus altering the evolution of the system.

The mass transfer rate is a strong function of the depth of contact, and thus we write

$$\boxed{\dot{M}_2 = -\dot{M}_0(M_1, M_2, a) f(\Delta R_2) = \begin{cases} -\dot{M}_0 (\Delta R_2/R_2)^{n+3/2} & \text{polytropic donors,} \\ -\dot{M}_0 \exp\left(\Delta R_2/H\right) & \text{isothermal atmospheres.} \end{cases}} \quad (1)$$

where $\dot{M}_0$ is a relatively gentle function of the binary parameters and f is a strong function of the depth of contact, $\Delta R_2 = R_2 - R_{\rm L}$. The depth of contact can vary because of a change in the radius of the either the donor star or the Roche lobe. Symbolically, we can write the logarithmic time derivative of the donor radius as

$$\boxed{\frac{\dot{R}_2}{R_2} = \nu_2 + \zeta_2 \frac{\dot{M}_2}{M_2}} \quad (2)$$

where ν_2 represents the rate of change of the donor radius due to intrinsic processes such as thermal relaxation and nuclear evolution, whereas $\zeta_2 = d\ln R_2/d\ln M_2 \approx -1/3$ (for white dwarf donors) usually describes changes resulting from adiabatic variations of M_2. Similarly, one can write for the Roche lobe radius

$$\boxed{\frac{\dot{R}_{\rm L}}{R_{\rm L}} = \nu_{\rm L} + \zeta_{\rm L} \frac{\dot{M}_2}{M_2}} \quad (3)$$

where,

$$\begin{aligned} \zeta_{\rm L} &= \frac{d\ln R_{\rm L}}{d\ln M_2} \\ &= \frac{2(1+q)}{3} \frac{\ln(1+q^{1/3}) - q^{1/3}/(1+q^{1/3})}{0.6q^{2/3} + \ln(1+q^{1/3})} + 2((1+q)r_h)^{1/2} - 2(1-q) \end{aligned}$$

and,

$$\nu_{\rm L} = \frac{2\dot{J}_{\rm sys}}{J_{\rm orb}} - 2\frac{\dot{J}_{1,\rm tid} + \dot{J}_{2,\rm tid}}{J_{\rm orb}}$$

The first term in $\nu_{\rm L}$ represents systemic angular momentum loss, whilst the second term represents the effect due to tides. The systemic term usually represents angular momentum loss either by gravitational wave radiation or by magnetic braking

(Section 2.1). The tidal torque, in its simplest form, is a function of the degree of asynchronism ($\Omega - \omega_i$) and of the tidal synchronization timescale ($\tau_{\rm s_i}$) and is given by

$$\boxed{\dot{J}_{i,\rm tid} = \frac{k_i M_i R_i^2}{\tau_{s_i}}(\Omega - \omega_i)} \tag{4}$$

Here k_i represents the dimensionless moment of inertia of the i^{th} component. In our case, the synchronization time cannot be calculated from first principles, and hence is a free parameter. The evolution of the tidal timescale however, is followed using the prescription given by Campbell (1984).

Finally, one can also write the rate of the change of the orbital separation in terms of the mass and angular momentum loss & redistribution terms. For this we rearrange Eq. 2.17 and use the definition of $\nu_{\rm L}$ to write

$$\boxed{\frac{\dot{a}}{a} = \nu_{\rm L} - \frac{2\dot{M}_2}{M_2}[q_a - q]} \tag{5}$$

where

$$q_a \equiv 1 + (1-\beta)q - \frac{1-\beta}{2(1+q)} - M_2\frac{\beta j_1 - j_2 + (1-\beta)j_{\rm w}}{J_{\rm orb}}.$$

where, β represents the fraction of mass accreted by the primary, and is calculated following Han & Webbink (1999) in the case of Super-Eddington accretion. Setting β to 1 above implies conservative mass transfer. Also, j_1 and j_2 represent the specific angular momenta of the stream near the surface of the accretor and the surface of the donor respectively whilst $j_{\rm w}$ is the specific angular momentum of any wind emanating from the binary (See discussion in Section 2.2.1). Once the mass radius relationship is specified, the terms in Eq. 2 can be determined. Similarly, the terms in Eq. 3 can be calculated under the assumption of Roche geometry and once the angular momentum loss and redistribution mechanisms are specified. This information is then used to calculate the rate of change of the orbital separation (Eq. 5). Once mass transfer commences, Eq. 1 is non-zero and is calculated self-consistently as the radii and the separation evolve. Thus the set of linear, coupled equations 1, 2, 3, 4 & 5 completely specify the evolution of the binary system.

These equations are integrated using the following logic: At every time-step, we know the mass, radii and Roche lobe radii of the components along with the orbital separation. Initially, we assume the components to be synchronized with the orbit, and specify some value for the tidal synchronization time ($\tau_{\rm s_i}$). We calculate the intrinsic change in the donor radius (ν_2), GWR driving rate ($\nu_{\rm L}$) and the mass transfer rate ($\dot{M}_2$) at every time-step. We also check if the mass transfer rate exceeds the Eddington limit, and if it does, a certain fraction of the mass being transferred is lost from the system (as described by Han & Webbink (1999)). This information is then used to calculate the new masses, radii and orbital separation for the next time-step. The driving rate, mass transfer rate and so on are calculated with the new values of the radii, orbital separation, tidal timescales etc. and the integration continues.

Appendix B: Permission to Reproduce Figure 1.3

Vayujeet

From: "Icko Iben" <icko@astro.uiuc.edu>
To: <gokhale@theory.phys.lsu.edu>
Sent: Thursday, October 19, 2006 3:23 PM

10/19/06

Dear Varyujeet,

By all means include any figure I've ever published.
The whole point of publishing is to provide information
that other folks might find useful and/or interesting.
Best wishes for constructing a useful and interesting
thesis.

Cheers, Icko Iben, Jr.

Appendix C: Permission to Reproduce Figure 1.4

Vayujeet

From: "Gijs Nelemans" <Nelemans@astro.ru.nl>
To: "Gokhale Vayujeet" <gokhale@theory.phys.lsu.edu>
Sent: Thursday, October 12, 2006 3:37 PM
Subject: Re: permission to use figure...

Dear Vayujeet,

Of course you can use that figure, at least if you refer to the original paper.

Best wishes,

Gijs

> i am a graduate student at the Louisiana State University, Physics &
> Astronomy dept. i would like to include a figure from one of your
> publications in the introductory chapter of my thesis titled "Mass
> Transfer and Evolution of Compact Binaries". The said figure is fig. 1
> from astroph/0409676v2, outlining the various channels of AM CVn
> formation.
>
> i would greatly appreciate it if you could grant me permission to include
> this figure in my thesis. It succintly outlines the different
> possibilities for the formation of such systems, which greatly helps the
> narrative.
>
> thanking you very much in advance,
>
> - Vayujeet.
>

Vita

Vayujeet M. Gokhale was born on September 15^{th} 1976, in Bombay, India. He finished his undergraduate studies at SIES college, Bombay, in 1996. He earned a Master of Science degree in nuclear physics from the University of Bombay in 1998. From 1998 to 2000, he worked as a doctoral candidate at the Nuclear Research Laboratory (NRL) at the Bhabha Atomic Research Center, Trombay, in gamma ray astronomy. He is currently a candidate for the degree of Doctor of Philosophy in physics, which will be awarded in May 2007.